

REGULATION OF GLYCEROLIPID METABOLISM IN *ARABIDOPSIS THALIANA*

By

Anastasiya Lavell

A DISSERTATION

Submitted to
Michigan State University
in partial fulfillment of the requirements
for the degree of

Biochemistry and Molecular Biology – Doctor of Philosophy

2019

ABSTRACT

REGULATION OF GLYCEROLIPID METABOLISM IN *ARABIDOPSIS THALIANA*

By

Anastasiya Lavell

Chloroplast membranes house the photosynthetic machinery and have a distinct lipid composition, with characteristically abundant galactolipids mono- and digalactosyldiacylglycerol (MGDG and DGDG). Both galactolipids are synthesized through both plastid and ER pathways in Arabidopsis, resulting in distinguishable molecular species. Phosphatidic acid (PA) is the first key intermediate formed by the plastid galactolipid biosynthetic pathway. It is further dephosphorylated to diacylglycerol (DAG), which is a substrate for MGDG Synthase (MGD1). MGD1 further adds a galactose to DAG from UDP-Gal. The enzymatic reactions yielding these galactolipids are known, but regulatory factors controlling this process are largely unknown. We identified a predicted rhomboid-like protease 10 (RBL10), located in plastids of Arabidopsis thaliana, that affects galactolipid biosynthesis likely through intramembrane proteolysis. Plants with T-DNA disruptions in RBL10 have greatly decreased 16:3 (acyl carbons : double bonds) and increased 18:3 acyl chain abundance in MGDG of leaves. Additionally, *rb10-1* mutant chloroplasts show reduced [¹⁴C]-acetate incorporation into MGDG during pulse-chase labeling, indicating a reduced flux through the plastid galactolipid biosynthesis pathway. While plastid MGDG biosynthesis is blocked in *rb10-1* mutants, they are capable of synthesizing PA, as well as producing normal amounts of total MGDG by compensating with ER-derived lipid precursors. These findings link this predicted protease to the utilization or transport of PA for plastid galactolipid biosynthesis potentially

revealing a regulatory mechanism for galactolipid biosynthesis in chloroplasts. In addition to serving as a key metabolite, PA also has signaling roles in the cell, making its trafficking important to understanding plant cell metabolism. The substrate(s) of RBL10 are not yet known, but Blue-Native PAGE and FPLC analysis showed that RBL10 is part of a large molecular weight complex (>660kDa). The protein interactors of RBL10 are currently being probed by using co-immunoprecipitation and split-ubiquitin yeast two-hybrid approaches. Additionally, RBL10 seems to be autoproteolytic toward its own carboxy-terminal domain (CTD). The role of complex residency and autolytic activity of RBL10 is not currently clear, but these findings could help uncover the identity of a new transporter of PA in the chloroplast as well as a regulatory mechanism of its activity.

ACKNOWLEDGEMENTS

The journey to becoming a scientist was not trivial or quick, however, I could not see it happening any other way. Through the challenges of doctoral research, coursework, and the more bureaucratic aspects of belonging to a branch of science, I have gained an appreciation for the institution of academic research. On my way, I have encountered many individuals who deserve a sincere thank you, for their help, support, and guidance. I thank my advisor, Christoph Benning, who has given me not only the training to become a skilled researcher but also the room to grow and develop my own ideas. I always felt that Christoph truly cares for his students, and for that I am forever grateful. An unexpected way that Christoph helped me, was through having a lab full of great people. I want to thank all Benning lab members and I have to say a special thanks to Patrick Horn, Anna Hurlock, Yang Yang, and Kun Wang for answering a million questions, discussing my project endlessly, and making lab life fun. I want to recognize and thank my committee members, Jian Hu, Gregg Howe, Lee Kroos, and Danny Schnell. They have been insightful, constructive, and supportive throughout my career as a graduate student. I have immense gratitude for being a part of the Biochemistry and Molecular Biology department, and being supported by wonderful individuals like Jessica Lawrence, Ashley Parks, and Billy Yang. I have had the pleasure of working with Jon Kaguni and David Arnosti as graduate student directors and the honor of serving on the BMB Graduate Student Council. Doug Whitten has been instrumental for my doctoral work. In my future, I am not certain that I will ever find a collective of scientists as amazing as I did at the MSU-DOE Plant Research Laboratory. The PRL has been my home for the last

four years and I will think fondly to my time here. I would not have been able to accomplish my work without the help of John Froehlich. I want to thank the PRL office staff for all their help and making my graduate experience a smooth one. I owe an immense thank you to all the undergraduate and high school students I have had the distinct pleasure of working with. In the hopes of teaching them I seemed to learn the most. For their mentorship and inspiration to teach, I thank Joyce Parker and Jon Stoltzfus. The Plant Biotechnology for Health Sustainability Training program greatly enriched my graduate life in numerous ways, and I have to thank Rob Last for making all that possible for me and many others. I cannot express my gratitude enough to my family and loved ones. The love and support from my family has been instrumental for my success. To my best friend and partner in life, Jonathan, I owe a huge thank you, I could not have done this without him. Last but not least, I want to thank my friends, those who have not wavered in their support of me. No challenge is too great when you have the love of your friends and family as well as the guidance and support from your mentors.

TABLE OF CONTENTS

LIST OF TABLES.....	ix
LIST OF FIGURES.....	x
KEY TO ABBREVIATIONS	xii
CHAPTER 1 Rhomboids: Regulation from the Membrane	1
Introduction	2
iRhoms Play Regulatory Roles Through Non-Proteolytic Mechanisms	3
Prokaryotic Rhomboids.....	4
Eukaryotic Rhomboids	5
Modulating the Activity of Rhomboids.....	10
REFERENCES.....	13
CHAPTER 2 Cellular Organization and Regulation of Plant Glycerolipid Metabolism ...	19
Abstract.....	20
Introduction	20
Lipid Transport Mechanisms.....	23
Regulation of Lipid Metabolism.....	27
Lipid Signaling and Response to Stress	30
Spatial Arrangement and Complexes of Lipid Biosynthetic Enzymes	32
APPENDIX	35
REFERENCES.....	38
CHAPTER 3 A Predicted Plastid Rhomboid Protease Involved in Phosphatidic Acid Metabolism in <i>Arabidopsis thaliana</i>	48
Abstract.....	49
Introduction	50
Results and Discussion	53
<i>Discovery of a Role for RBL10 in Chloroplast Lipid Metabolism</i>	53
<i>JA and JA-Ile Levels are Affected in rbl10</i>	54
<i>RBL10 is Located in the Inner Envelope Membrane of Chloroplasts</i>	55
<i>ER-Assembled Lipids Serve as Primary Precursors for MGDG Biosynthesis in the rbl10-1 Mutant</i>	56
<i>PA Synthesized in Chloroplasts is Used for PG Biosynthesis but not MGDG</i>	57
<i>MGD1 Activity is not Affected by Loss of RBL10</i>	58
<i>PA Plastid Phosphatase Activity is Increased in rbl10-1 Mutants</i>	58
<i>A Refined Model of PA Metabolism in Arabidopsis Chloroplasts</i>	59
Materials and Methods	61
<i>T-DNA Lines</i>	61
<i>Plant Growth Conditions</i>	61
<i>DNA Constructs and Complementation</i>	62

<i>Homology Modeling</i>	62
<i>Intact Chloroplast Isolation</i>	63
<i>In Vitro Translation of Precursor Proteins</i>	64
<i>Import and Protease Protection Assays</i>	64
<i>Fractionation of Imported RBL10</i>	65
<i>Lipid Analysis</i>	65
<i>Radiolabeling</i>	66
Acknowledgement	67
APPENDICES	68
Appendix 3A Main Text Figures	69
Appendix 3B Supplementary Figures	76
REFERENCES	81
CHAPTER 4 RBL10 Protein Properties and Oligomeric State	87
Abstract	88
Introduction	88
Results and Discussion	90
<i>The Oligomeric State of RBL10 Indicates Stable Protein Interactors</i>	90
<i>Co-Immunoprecipitation of RBL10 Yields Putative Protein Interactors</i>	91
<i>RBL10 is Autolytic Towards its Carboxy-Terminal Domain</i>	93
<i>Catalytic Mutant Constructs of RBL10 Cannot be Stably Transformed into the rbl10-1 Mutant Background</i>	95
Materials and Methods	97
<i>Plant Growing Conditions and Chloroplast Isolation</i>	97
<i>SDS-PAGE and Immunoblot Analysis</i>	97
<i>Blue Native PAGE</i>	98
<i>Size Exclusion Chromatography</i>	100
<i>Co-Immunoprecipitation</i>	101
<i>Protein Production in E. coli</i>	103
Acknowledgement	105
APPENDIX	106
REFERENCES	112
CHAPTER 5 Arabidopsis DGD1 SUPPRESSOR 1 is a Subunit of the Mitochondrial Contact Site and Cristae Organizing System and Affects Mitochondrial Biogenesis ...	116
Abstract	117
Introduction	117
Results	121
<i>DGS1 is present in a multi-subunit protein complex with MIC60, TOM40, TOM20s and RISP</i>	121
<i>The dgs1-1 mutation alters the multi-subunit complex</i>	122
<i>The dgs1-1 mutation alters mitochondrial size</i>	126
<i>The dgs1-1 mutation alters mitochondrial lipid composition</i>	128
<i>The dgs1-1 mutation affects mitochondrial protein abundance, protein import and alternative respiratory capacity</i>	130
<i>Higher drought stress tolerance in dgs1-1 mutant plant lines</i>	132

<i>Phylogenetic and co-expression networks of DGS1 putative orthologs</i>	136
Discussion.....	137
Materials and Methods	142
<i>Plant Materials</i>	142
<i>Plant Growth and Treatments</i>	143
<i>Isolation of mitochondria, chloroplast and ER</i>	143
<i>Blue-native PAGE</i>	144
<i>Immunoprecipitation (IP)</i>	144
<i>Cross-Link Assay</i>	144
<i>Generation of the DGS1 antibody</i>	145
<i>Immunoblot Analysis</i>	146
<i>Outer membrane ruptured mitochondria preparation and protease treatment</i> ..	146
<i>Protoplast Preparation and Fluorescence Microscopy</i>	147
<i>Electron Microscopy</i>	147
<i>Lipid Extractions and Analysis</i>	148
<i>Measurements of Respiratory Parameters on Plant Mitochondria</i>	148
<i>In Vitro Mitochondrial Protein Import</i>	149
<i>In Situ Detection of Reactive Oxidative Species (ROS)</i>	150
<i>Dark-induced Senescence</i>	150
<i>Quantification of H₂O₂</i>	150
<i>Relative Water Content Analysis</i>	151
<i>Chlorophyll analysis and fluorescence</i>	151
<i>Gas Exchange</i>	152
<i>Total RNA Preparation and cDNA Synthesis</i>	152
<i>Global Transcript Analysis</i>	152
<i>Mass Spectrometry</i>	155
<i>Phylogenetic analysis</i>	155
<i>Co-expression analysis</i>	156
<i>Accession Numbers</i>	156
<i>Supplemental Data Sets</i>	156
Acknowledgement	157
Author Contribution	158
APPENDICES	159
Appendix 5A Main Text Figures	160
Appendix 5B Supplemental Figures	175
REFERENCES.....	182
CHAPTER 6 Future Perspectives	190
Introduction	191
Role of Proteolysis in Lipid Homeostasis.....	191
RBL10 and its Protein Interactome	193
Role for Autocatalysis of RBL10	195
Responses to Stress and Lipid Remodeling	197
Concluding Remarks	198
REFERENCES.....	199

LIST OF TABLES

TABLE 4.1. Co-Immunoprecipitation with RBL10-YFP-HA using isolated chloroplast protein lysate, results in recurring appearance of select proteins	107
---	-----

LIST OF FIGURES

Figure 2.1. Scheme of phosphatidic acid (PA) synthesis in the plastid and the endoplasmic reticulum (ER)	36
Figure 2.2. Proposed movement of galactolipids after synthesis from diacylglycerol (DAG)	37
Figure 3.1. Structure and phenotypes of <i>rb10</i> mutant alleles.....	70
Figure 3.2. Localization of RBL10 to the Inner Envelope Membrane of Chloroplast	71
Figure 3.3. Radiolabeled pulse chase of detached leaves using ¹⁴ C-acetic acid.....	72
Figure 3.4. Labeling of isolated chloroplasts of <i>rb10-1</i> mutant and WT with ¹⁴ C-acetate	73
Figure 3.5. Probing PA metabolism in <i>rb10-1</i>	74
Figure 3.6. Proposed model of PA metabolism in the chloroplast envelope membranes..	75
Figure 3.S1. Full lipid analysis of wild-type (WT) and <i>rb10</i> leaves	77
Figure 3.S2. Acyl composition of <i>rb11</i> total leaf lipids and MGDG.....	78
Figure 3.S3. Changes in oxylipin levels in the <i>rb10</i> mutants.....	79
Figure 3.S4. Seed phenotypes of <i>rb10</i> plants	80
Figure 4.1. Blue Native PAGE of solubilized chloroplasts from WT, <i>rb10-1</i> mutant, and <i>rb10-1</i> complemented lines producing RBL10-YFP-HA protein.....	108
Figure 4.2. Size Exclusion Chromatography of protein standards and solubilized chloroplasts of <i>rb10-1:RBL10-YFP-HA</i> line show that RBL10 migrates in a complex at a high MW	109
Figure 4.3. Production of C-Terminally tagged RBL10-T in <i>E. coli</i>	110
Figure 4.4. The fusion protein of MBP-RBL10 WT and single catalytic mutant can be detected with anti-MBP antibody	111

Figure 5.1. DGS1 is present in a large multi-subunit protein complex with MIC60, TOM40, TOM20s and RISP	161
Figure 5.2. A single point mutation in DGS1 alters the multi-subunit complex	162
Figure 5.3. The <i>dgs1-1</i> mutation alters mitochondrial size	164
Figure 5.4. The <i>dgs1-1</i> mutation alters mitochondrial lipid composition	166
Figure 5.5. The <i>dgs1-1</i> mutation affects mitochondrial protein abundance, protein import and alternative respiratory capacity	168
Figure 5.6. The <i>dgs1-1</i> mutation imparts higher drought stress tolerance.....	170
Figure 5.7. Transcriptome analysis of <i>dgs1</i> mutants	171
Figure 5.8. Phylogenetic analysis of DGS1- and NCA2-related proteins.....	173
Figure 5.S1. The intramitochondrial localization of TOM20-2 and TOM40 in Col-0 and <i>dgs1</i> mutant lines	176
Figure 5.S2. Related to Figure 4A and 4B. Leaf lipid analysis of wild type and mutant lines	177
Figure 5.S3. The defective growth phenotype of mutants producing the DGS1-1 protein.	179
Figure 5.S4. Analyses of hydrogen peroxide in <i>dgs1-1</i> lines	181

KEY TO ABBREVIATIONS

ATS1 – glycerol-3-phosphate acyltransferase

DAG – diacylglycerol

DGD1 – digalactosyldiacylglycerol synthase 1

DGDG - digalactosyldiacylglycerol

DGS1 – suppressor of DGD1

ER – endoplasmic reticulum

FA – fatty acid

GlpG – *E. coli* rhomboid

JA – jasmonic acid

JA-Ile – jasmonic acid isoleucine

MGD1 – monogalactosyldiacylglycerol synthase 1

MGDG – monogalactosyldiacylglycerol

PC – phosphatidylcholine

RBL10 – rhomboid-like protein 10

TAG – triacylglycerol

PA – phosphatidic acid

PARL – presenilin-associated rhomboid-like protein

PG – phosphatidylglycerol

TeGDG – tertragalactosyldiacylglycerol

TGD1 – TRIGALACTOSYLDIACYLGLYCEROL 1

TGDG – trigalactosyldiacylglycerol

CHAPTER 1

Rhomboids: Regulation from the Membrane

Introduction

Found in nearly all organisms, a superfamily of rhomboid proteases carries out regulated intramembrane proteolysis. These serine-type endopeptidases utilize a serine-histidine catalytic dyad to cleave transmembrane segments of peptides in the hydrophobic environment of the membrane. The founding member of this family was originally discovered in *Drosophila melanogaster* where it cleaves the factor Spitz from the Golgi membrane and initiates the epidermal growth factor signaling pathway (Lee *et al.*, 2001, Urban *et al.*, 2001, Urban *et al.*, 2002). Since the discovery of this family, rhomboid-like proteins have been predicted across nearly all organisms including animals, plants, bacteria, protozoa, and fungi. With more available genomic data, subclasses of rhomboid or rhomboid-like proteins were identified, creating subtypes with and without the catalytic residues as well as varied amino and carboxy-terminal sequences (Lemberg and Freeman, 2007). Although one of the first characterized rhomboids was in *D. melanogaster*, the origin of the superfamily is hypothesized to date back to a bacterial ancestor with multiple horizontal gene transfer events giving rise to the RHO subfamily and then separately the Presenilin-associated rhomboid-like protein (PARL) subfamily (Koonin *et al.*, 2003). Major strides have been made in the characterization of rhomboid family proteins in diverse organisms, yet with so many predicted rhomboid encoding genes yet to be investigated, a lot of opportunities remain for new and unique regulatory examples. This chapter presents examples of rhomboids and their biological roles from representative organisms across kingdoms and highlights the gaps in knowledge on rhomboid function in plants.

iRhoms Play Regulatory Roles Through Non-Proteolytic Mechanisms

There are two main types of rhomboid-like proteins, active proteases and inactive iRhoms. Though inactive, iRhom proteins possess many of the characteristics of active rhomboids and display the rhomboid transmembrane architecture. However, they have lost the conserved serine and histidine residues which confer proteolytic activity. (Lemberg and Freeman, 2007). Despite a lack of enzymatic activity, there is growing evidence that iRhoms play important roles in metabolism. In flies and mammals, iRhoms seem to participate in ER-associated degradation of EGF and EGF-like ligands, contrary to the effects of active rhomboid-1 on promoting the EFG signaling pathway in *Drosophila* (Zettl *et al.*, 2011). In mice, the roles of iRhom1 and 2 were shown to determine the trafficking of a shedding protease TACE/ADAM17 in macrophages, where proper iRhom mediated trafficking through the ER results in the processing and release of tumor necrosis factor (TNF) (Christova *et al.*, 2013). Though the relationship between iRhom1, iRhom 2, and TACE is well supported, knock-out (KO) mice of iRhom1 fail to create white fat deposits and die (Christova *et al.*, 2013), where iRhom2 KO mice appear to exhibit inflammatory defects only (Adrain *et al.*, 2012). These varied phenotypes of homozygous KOs of iRhom1 and 2, suggest possible differences in expression or additional functions beyond TACE trafficking. The effects on lipid deposition in mice was further investigated in relation to iRhom2, where possible therapeutic strategies for myocardial inflammation resulting from obesity were found by inhibiting endoplasmic reticulum stress (ERS) and iRhom2 signaling pathways (Ge *et al.*, 2019). With a large number of iRhoms predicted alongside active rhomboids, their biological roles remain an open field of research.

Prokaryotic Rhomboids

Bacteria - In the microorganism, *Providencia stuartii*, the rhomboid AarA has been shown to play a role in the oligomerization of the twin-arginine translocase complex. The complex is made up of several Tat proteins, of which one serves as the recruiting factor, TatA. This small peptide has a single pass transmembrane helix which is a substrate for AarA. Upon cleavage, the processed TatA recruits the other Tat proteins and the twin-arginine translocase complex is oligomerized (Stevenson *et al.*, 2007). The *AarA* gene was first discovered through a mutagenesis screen searching for regulatory components of aminoglycoside acetyltransferase, which is involved in resistance to the respective broad-spectrum antibiotic. The resultant *aarA* mutants had increased resistance to gentamicin as well as changes in cell morphology (Rather and Orosz, 1994). Contrary to the AarA, the natural substrate of the *Escherichia coli* rhomboid GlpG and its endogenous role has not yet been identified. Though bacteria lacking GlpG don't share all the phenotypes as the *aarA* mutants, introducing the *GlpG* gene rescues the *aarA* mutants (Clemmer *et al.*, 2006). Despite our lack of understanding of its biological function, the numerous crystal structures, models, (Wang *et al.*, 2006, Wang *et al.*, 2007, Ha *et al.*, 2013, Vinothkumar *et al.*, 2013) and kinetic assays of GlpG (Maegawa *et al.*, 2005, Xue and Ha, 2012, Cho *et al.*, 2016, Guo *et al.*, 2016), led to a better understanding of substrate recognition mechanisms of rhomboid proteases as well as substrate cleavage. Another bacterial rhomboid, GluP in *Bacillus subtilis*, has been implicated in glucose transport as well as cell division. However, the mechanism of action and its natural substrate remains to be discovered (Mesak *et al.*, 2004).

The ability to study the kinetics and structure of GlpG generated a lot of knowledge about the catalytic mechanisms of rhomboids. However, with the emerging diversity of these proteases in eukaryotic organisms a diversity in molecular action might be expected as well.

Eukaryotic Rhomboids

Animals – Following the discovery of the *Drosophila* rhomboid-1, evidence became available that a human rhomboid RHBDL2 is capable of activating EGF ligands and EGFR signaling, though, since there are other parallel pathways to EGF activation, the significance of this finding still remains to be clarified (Adrain *et al.*, 2011). In mitochondria of human neuron cells, a PARL type rhomboid performs an important role in determining the trafficking of a factor called PINK1. The processing of the single transmembrane domain of PINK1 can alter its subcellular location, where the non-cleaved form is targeted to the outer membrane of the mitochondrion and the cleaved form of Pink1 is targeted to the inner envelope membrane of the mitochondrion (Meissner *et al.*, 2011). In the outer membrane location, Pink1 recruits Parkin, a ubiquitin ligase, and initiates mitophagy. In this instance, unhealthy mitochondria are turned over through Pink1/Parkin directed mitophagy. When Pink1 is cleaved and targeted to the inner membrane, it is ultimately degraded by the 26S proteasome. The determining factor for PARL cleavage is the phosphorylation status of the amino-terminal domain (NTD) of PARL. Under normal ATP levels in the mitochondrion matrix, a kinase, PDK2, will phosphorylate PARL, thereby preventing PARL from self-processing to a less active form PACT (Jeyaraju *et al.*, 2006). Under reduced ATP conditions, PARL will not be phosphorylated to the same extent and

will auto-catalytically remove its own NTD, resulting in reduced Pink1 cleavage and ultimately initiation of mitophagy (Meissner *et al.*, 2015, Shi and McQuibban, 2017). The autolytic activity of PARL (β -cleavage) occurs after the initial removal of mitochondrial targeting peptide (α -cleavage) and generates a peptide that is targeted to the nucleus (Sik *et al.*, 2004). This knowledge on proteolytic control of PINK1 trafficking and its influence on initiation of mitophagy provides insight on the key roles of rhomboid-like proteins in complex biological pathways. The change in phosphorylation status of PARL and the subsequent autolytic β -cleavage to the less active form PACT is one example of the self-regulation of rhomboid function. More importantly, these studies demonstrate a mechanism by which rhomboids may act as transducers of metabolic status in the cell or organelle.

Protozoa – The genome of the apicomplexan *Plasmodium falciparum*, implicated in the human disease malaria, also encodes active rhomboid proteases. Proteases PfROM1 and PfROM4 exhibit sheddase activity and cleave a diverse array of adhesin proteins present on the surface of the pathogen; this shedding of adhesins is important during completion of host cell invasion and membrane fusion (Baker *et al.*, 2006). Furthermore, PfROM4 exhibits high specificity for particular adhesins such as EBA-175. Performing mutagenesis of the adhesin protein leads to an inhibition of cleavage by PfROM4 and thereby compromises host cell invasion (O'Donnell *et al.*, 2006). In similar fashion, the rhomboids of *Toxoplasma gondii* are important for the shedding of adhesins during invasion of host cells. Five rhomboid-like proteins and a single PARL-type protein were predicted in *T. gondii*, where proteolytically active TgROM5 appeared to be a spatially and temporally fitting candidate to aid in invasion (Brossier *et al.*, 2005). Further

work showed that TgROM4 also aids in invasion by processing adhesins on the cell surface of *T. gondii* (Buguliskis *et al.*, 2010). Rhomboids in other protozoans have been predicted and understanding the role of rhomboids in host cell invasion creates exciting opportunities for novel drug targets in cases of disease-implicated protozoa such as *Plasmodium*.

Fungi - A pathogenic mold, *Aspergillus fumigatus*, is responsible for over 90% of pulmonary mycosis and can colonize the lung tissues of immunocompromised humans through not yet well established molecular mechanisms (Latge, 2001). During colonization of lung tissue, *Aspergillus* must adapt to lower levels of oxygen than that of the atmosphere. A key protein in the *Aspergillus* genome, identified in mediating this adaptation, is a sterol regulatory element-binding protein (SREBP) homolog SrbA, without which the pathogen was unable to grow under hypoxic (Willger *et al.*, 2008). It was later identified that SrbA is likely a substrate of an *Aspergillus* rhomboid protease RbdA. Under hypoxic conditions, the *rbdA* mutant can be rescued by overexpression of a truncated N-terminal fragment of SrbA in the nucleus (Vaknin *et al.*, 2016). The regulation of adaptability and virulence of a pathogenic mold that is in part controlled by a rhomboid protease, creates yet another potential drug target, in this case for treating immunocompromised individuals infected with *Aspergillus*.

Work in fission yeast described a rhomboid Rbd2 which interacts with the AAA-ATPase Cdc48 in order to identify its ubiquitinated substrate, a SREBP. The Cdc48/Rbd2 interaction is important in the processing of SREBPs and disrupting the binding of Cdc48 to the C-terminus of Rbd2 results in degradation of the ubiquitinated SREBP (Hwang *et al.*, 2016). In both fission yeast and mold, there seem to be additional, diverse terminal

domains that mediate protein-rhomboid interactions. The necessity of Cdc48 for substrate identification by Rbd2 is uniquely different from the presumed rhomboid-substrate interaction within the membrane by virtue of “scanning” the membrane. Though it has been proposed that scanning by a rhomboid in the membrane may be occurring at biologically relevant rates (Kreutzberger *et al.*, 2019), with the diversity of rhomboid mechanisms found so far, it’s likely that more rhomboid chaperones will soon emerge.

Plants - Though an appreciable number of rhomboid mechanisms have been elucidated, there is yet to be a rhomboid and endogenous substrate pair identified in plants. Numerous members of the family have been predicted in model species *Arabidopsis thaliana*, *Populus trichocarpa*, and in *Oryza sativa* (Garcia-Lorenzo *et al.*, 2006). In *Arabidopsis*, 20 rhomboid-encoding genes were predicted and 18 in rice (Tripathi and Sowdhamini, 2006). Though all predicted genes encoded proteins displaying the rhomboid fold, the number of active rhomboids containing the conserved catalytic domains has been refined to 13 in *Arabidopsis* and 12 in rice (Lemberg and Freeman, 2007) with the remaining predicted genes to produce non-catalytic members of the family.

The subcellular distribution of rhomboids in plants has been speculated for some members and demonstrated experimentally for others. Since their function is tied to their membrane location, at least for the process of proteolysis, ascertaining their subcellular distribution is highly important for identifying endogenous substrates. Of the 13 predicted rhomboids in *Arabidopsis*, two are shown to be Golgi-associated (Kanaoka *et al.*, 2005), two are associated with the chloroplast (Knopf *et al.*, 2012, Thompson *et al.*, 2012), one mitochondrial PARL member is confirmed (Knopf *et al.*, 2012), two rhomboids are

predicted at the plasma membrane (Benschop *et al.*, 2007, Inze *et al.*, 2012), and the others have mixed predictions and lack experimental evidence to support their locations at this time.

So far, only one rhomboid in plants has been shown to possess regulated intermembrane proteolysis. The Golgi localized *AtRBL2* can process the *Drosophila* RHO-1 substrates Spitz and Keren; this finding was in contrast to another Golgi resident, *AtRBL1*, which could not process either Spitz or Keren despite its sequence similarity to *DmRHO-1* (Kanaoka *et al.*, 2005). Though the catalytic activity of these two rhomboids has been shown, there are no current hypotheses on what their endogenous substrates are nor what their overall physiological role is. However, this analysis does confirm that rhomboid-like proteins can in fact carry out intramembrane proteolysis in plants.

For the biological importance of plant rhomboids, the best studied member is *RBL10* (At1g25290). Knock-out mutants of *RBL10* were first characterized for their developmental defects, showing irregular flower formation, abnormal pollen morphology, and reduced number of seeds per silique formed (Thompson *et al.*, 2012). The overall mechanism of how *RBL10* influenced these developmental processes was not further elucidated. However, there was a hypothesized disruption of the plant hormone jasmonic acid (JA) signaling in this mutant, which could potentially explain the phenotypes. Further evidence was provided through a proteomic approach, where levels of allene oxide synthase (AOS), an enzyme catalyzing a key step in JA production, were reduced in *rbl10/rbl11* double mutants compared to wild type (Knopf *et al.*, 2012). However, due to the use of a double knock-out mutant for the proteomic analysis, it was unclear which rhomboid actually influenced the levels of AOS. Though redundancy is possible, it was

recently shown that RBL10 participates in lipid homeostasis of Arabidopsis while RBL11 does not. Knock-out mutants of *rb110* show an impaired ability to utilize chloroplast synthesized phosphatidic acid (PA), a key intermediate in lipid biosynthesis, for the formation of galactolipids such as monogalactosyldiacylglycerol (MGDG) (Lavell *et al.*, 2019) (see Chapter 2). This led to the hypothesis that RBL10 may affect trafficking of PA across the inner envelope membrane of the chloroplast. Though the relationship between the reproductive phenotypes and lipid metabolism does not seem immediately clear, the bridge between the two may after all be JA. Since JA is synthesized from chloroplast lipid derived fatty acids, and *rb110* mutant shows a slightly attenuated JA response after wounding (Lavell *et al.*, 2019), it is possible that reduced JA supply during the dynamic process of flower and pollen tube expansion could lead to the developmental phenotypes previously observed.

While many of the rhomboids studied in other organisms seem to play important roles in disease development, the rhomboids in plants are poised to potentially be of importance to plant growth and development.

Modulating the Activity of Rhomboids

As roles of rhomboids are uncovered in various human diseases, the ability to modulate their activity has become an important area of research. The regulation of rhomboid activity is varied; an interesting example is found in human cells where RHBDL4, an ER localized rhomboid-like protein, binds cholesterol and appears to be modulated in activity by the levels of cholesterol present (Paschkowsky *et al.*, 2018). Aside from self-regulation

through autolytic activity as seen in the human PARL, rhomboid catalysis can be inhibited by a limited number of chemical protease inhibitors.

Due to the hydrophobic nature of the active site of rhomboids, not all serine-type protease inhibitors are effective. An inhibitor class derived from natural rhomboid substrates, peptidyl-chloromethylketones (CMK) has been shown to inhibit GlpG through in vivo and in vitro assays (Zoll *et al.*, 2014). A group of compounds called β -lactams was identified to be effective in inhibiting AarA and GlpG. However, interestingly there was some enhanced inhibition of GlpG compared to AarA, raising the exciting possibility of selective inhibition of individual rhomboids (Pierrat *et al.*, 2011). A related class of compounds called β -lactones has also been classified as inhibitors of rhomboid activity (Wolf *et al.*, 2015). Two more compounds, 3,4-dichloroisocoumarin (DCI) and diisopropyl fluorophosphonate (DFP), were shown to be effective in inhibiting GlpG in in vitro assays, with DFP being more potent and causing irreversible inhibition of GlpG (Xue and Ha, 2012). Despite the discovery of potential inhibitors of rhomboids, many of the compounds do not lead to complete ablation of activity and are reversible over time. Even for the more effective compounds, cross reactivity with other vital serine endopeptidases has not been well investigated and remains a hurdle to overcome. Aside from medical implications of rhomboid inhibitors, the discovery and use of inhibitors has provided details about the way rhomboids interact with substrate-like compounds, giving insights into their catalytic mechanisms. For a more detailed overview on rhomboid inhibitors, the reader is directed to an article by Kvido Strisovsky (Strisovsky, 2016).

Overall, understanding the molecular action and biological roles of rhomboids could lead to novel targets for treatments of human disease. Furthermore, understanding

rhomboids in plants could help identify novel regulatory mechanisms for growth and development as well as stress response. These research areas will likely be important for human health and agricultural productivity. Further research on the involvement of rhomboids in lipid metabolism is needed to understand how they may impact plant oil accumulation as well as photosynthetic efficiency of Arabidopsis but ultimately how this may translate to other agriculturally valuable crops. RBL10 is a first step to uncovering novel regulatory mechanisms in the complex processes of PA and galactolipid metabolism.

REFERENCES

REFERENCES

- Adrain, C., Strisovsky, K., Zettl, M., Hu, L., Lemberg, M.K. and Freeman, M.** (2011) Mammalian EGF receptor activation by the rhomboid protease RHBDL2. *Embo Rep*, **12**, 421-427.
- Adrain, C., Zettl, M., Christova, Y., Taylor, N. and Freeman, M.** (2012) Tumor necrosis factor signaling requires iRhom2 to promote trafficking and activation of TACE. *Science*, **335**, 225-228.
- Baker, R.P., Wijetilaka, R. and Urban, S.** (2006) Two Plasmodium rhomboid proteases preferentially cleave different adhesins implicated in all invasive stages of malaria. *Plos Pathog*, **2**, 922-932.
- Benschop, J.J., Mohammed, S., O'Flaherty, M., Heck, A.J., Slijper, M. and Menke, F.L.** (2007) Quantitative phosphoproteomics of early elicitor signaling in Arabidopsis. *Mol Cell Proteomics*, **6**, 1198-1214.
- Brossier, F., Jewett, T.J., Sibley, L.D. and Urban, S.** (2005) A spatially localized rhomboid protease cleaves cell surface adhesins essential for invasion by Toxoplasma. *P Natl Acad Sci USA*, **102**, 4146-4151.
- Buguliskis, J.S., Brossier, F., Shuman, J. and Sibley, L.D.** (2010) Rhomboid 4 (ROM4) affects the processing of surface adhesins and facilitates host cell invasion by Toxoplasma gondii. *Plos Pathog*, **6**, e1000858.
- Cho, S., Dickey, S.W. and Urban, S.** (2016) Crystal Structures and Inhibition Kinetics Reveal a Two-Stage Catalytic Mechanism with Drug Design Implications for Rhomboid Proteolysis. *Mol Cell*, **61**, 329-340.
- Christova, Y., Adrain, C., Bambrough, P., Ibrahim, A. and Freeman, M.** (2013) Mammalian iRhoms have distinct physiological functions including an essential role in TACE regulation. *EMBO Rep*, **14**, 884-890.
- Clemmer, K.M., Sturgill, G.M., Veenstra, A. and Rather, P.N.** (2006) Functional characterization of Escherichia coli GlpG and additional rhomboid proteins using an aarA mutant of Providencia stuartii. *J Bacteriol*, **188**, 3415-3419.
- Garcia-Lorenzo, M., Sjodin, A., Jansson, S. and Funk, C.** (2006) Protease gene families in Populus and Arabidopsis. *Bmc Plant Biol*, **6**, 30.
- Ge, C.X., Xu, M.X., Qin, Y.T., Gu, T.T., Lou, D.S., Li, Q., Hu, L.F., Wang, B.C. and Tan, J.** (2019) Endoplasmic reticulum stress-induced iRhom2 up-regulation promotes macrophage-regulated cardiac inflammation and lipid deposition in high fat diet (HFD)-challenged mice: Intervention of fisetin and metformin. *Free Radic Biol Med*, **141**, 67-83.

- Guo, R., Gaffney, K., Yang, Z., Kim, M., Sungsuwan, S., Huang, X., Hubbell, W.L. and Hong, H.** (2016) Steric trapping reveals a cooperativity network in the intramembrane protease GlpG. *Nat Chem Biol*, **12**, 353-360.
- Ha, Y., Akiyama, Y. and Xue, Y.** (2013) Structure and mechanism of rhomboid protease. *J Biol Chem*, **288**, 15430-15436.
- Hwang, J., Ribbens, D., Raychaudhuri, S., Cairns, L., Gu, H., Frost, A., Urban, S. and Espenshade, P.J.** (2016) A Golgi rhomboid protease Rbd2 recruits Cdc48 to cleave yeast SREBP. *EMBO J*, **35**, 2332-2349.
- Inze, A., Vanderauwera, S., Hoeberichts, F.A., Vandorpe, M., Van Gaever, T. and Van Breusegem, F.** (2012) A subcellular localization compendium of hydrogen peroxide-induced proteins. *Plant Cell Environ*, **35**, 308-320.
- Jeyaraju, D.V., Xu, L., Letellier, M.C., Bandaru, S., Zunino, R., Berg, E.A., McBride, H.M. and Pellegrini, L.** (2006) Phosphorylation and cleavage of presenilin-associated rhomboid-like protein (PARL) promotes changes in mitochondrial morphology. *Proc Natl Acad Sci U S A*, **103**, 18562-18567.
- Kanaoka, M.M., Urban, S., Freeman, M. and Okada, K.** (2005) An Arabidopsis Rhomboid homolog is an intramembrane protease in plants. *FEBS Lett*, **579**, 5723-5728.
- Knopf, R.R., Feder, A., Mayer, K., Lin, A., Rozenberg, M., Schaller, A. and Adam, Z.** (2012) Rhomboid proteins in the chloroplast envelope affect the level of allene oxide synthase in Arabidopsis thaliana. *Plant J*, **72**, 559-571.
- Koonin, E.V., Makarova, K.S., Rogozin, I.B., Davidovic, L., Letellier, M.C. and Pellegrini, L.** (2003) The rhomboids: a nearly ubiquitous family of intramembrane serine proteases that probably evolved by multiple ancient horizontal gene transfers. *Genome Biol*, **4**, R19.
- Kreutzberger, A.J.B., Ji, M., Aaron, J., Mihaljevic, L. and Urban, S.** (2019) Rhomboid distorts lipids to break the viscosity-imposed speed limit of membrane diffusion. *Science*, **363**, 497-504.
- Latge, J.P.** (2001) The pathobiology of *Aspergillus fumigatus*. *Trends Microbiol*, **9**, 382-389.
- Lavell, A., Froehlich, J.E., Baylis, O., Rotondo, A.D. and Benning, C.** (2019) A predicted plastid rhomboid protease affects phosphatidic acid metabolism in Arabidopsis thaliana. *Plant J*, **99**, 978-987.
- Lee, J.R., Urban, S., Garvey, C.F. and Freeman, M.** (2001) Regulated intracellular ligand transport and proteolysis control EGF signal activation in Drosophila. *Cell*, **107**, 161-171.

- Lemberg, M.K. and Freeman, M.** (2007) Functional and evolutionary implications of enhanced genomic analysis of rhomboid intramembrane proteases. *Genome Res*, **17**, 1634-1646.
- Maegawa, S., Ito, K. and Akiyama, Y.** (2005) Proteolytic action of GlpG, a rhomboid protease in the Escherichia coli cytoplasmic membrane. *Biochemistry*, **44**, 13543-13552.
- Meissner, C., Lorenz, H., Hehn, B. and Lemberg, M.K.** (2015) Intramembrane protease PARL defines a negative regulator of PINK1-and PARK2/Parkin-dependent mitophagy. *Autophagy*, **11**, 1484-1498.
- Meissner, C., Lorenz, H., Weihofen, A., Selkoe, D.J. and Lemberg, M.K.** (2011) The mitochondrial intramembrane protease PARL cleaves human Pink1 to regulate Pink1 trafficking. *J Neurochem*, **117**, 856-867.
- Mesak, L.R., Mesak, F.M. and Dahl, M.K.** (2004) Expression of a novel gene, gluP, is essential for normal Bacillus subtilis cell division and contributes to glucose export. *Bmc Microbiol*, **4**, 13.
- O'Donnell, R.A., Hackett, F., Howell, S.A., Treeck, M., Struck, N., Krnajski, Z., Withers-Martinez, C., Gilberger, T.W. and Blackman, M.J.** (2006) Intramembrane proteolysis mediates shedding of a key adhesin during erythrocyte invasion by the malaria parasite. *J Cell Biol*, **174**, 1023-1033.
- Paschkowsky, S., Recinto, S.J., Young, J.C., Bondar, A.N. and Munter, L.M.** (2018) Membrane cholesterol as regulator of human rhomboid protease RHBDL4. *J Biol Chem*, **293**, 15556-15568.
- Pierrat, O.A., Strisovsky, K., Christova, Y., Large, J., Ansell, K., Bouloc, N., Smiljanic, E. and Freeman, M.** (2011) Monocyclic beta-lactams are selective, mechanism-based inhibitors of rhomboid intramembrane proteases. *ACS Chem Biol*, **6**, 325-335.
- Rather, P.N. and Orosz, E.** (1994) Characterization of aarA, a pleiotropic negative regulator of the 2'-N-acetyltransferase in Providencia stuartii. *J Bacteriol*, **176**, 5140-5144.
- Shi, G. and McQuibban, G.A.** (2017) The Mitochondrial Rhomboid Protease PARL Is Regulated by PDK2 to Integrate Mitochondrial Quality Control and Metabolism. *Cell Rep*, **18**, 1458-1472.
- Sik, A., Passer, B.J., Koonin, E.V. and Pellegrini, L.** (2004) Self-regulated cleavage of the mitochondrial intramembrane-cleaving protease PARL yields Pbeta, a nuclear-targeted peptide. *J Biol Chem*, **279**, 15323-15329.
- Stevenson, L.G., Strisovsky, K., Clemmer, K.M., Bhatt, S., Freeman, M. and Rather, P.N.** (2007) Rhomboid protease AarA mediates quorum-sensing in

- Providencia stuartii by activating TatA of the twin-arginine translocase. *Proc Natl Acad Sci U S A*, **104**, 1003-1008.
- Strisovsky, K.** (2016) Rhomboid protease inhibitors: Emerging tools and future therapeutics. *Semin Cell Dev Biol*, **60**, 52-62.
- Thompson, E.P., Smith, S.G. and Glover, B.J.** (2012) An Arabidopsis rhomboid protease has roles in the chloroplast and in flower development. *J Exp Bot*, **63**, 3559-3570.
- Tripathi, L.P. and Sowdhamini, R.** (2006) Cross genome comparisons of serine proteases in Arabidopsis and rice. *Bmc Genomics*, **7**, 200.
- Urban, S., Lee, J.R. and Freeman, M.** (2001) Drosophila Rhomboid-1 defines a family of putative intramembrane serine proteases. *Cell*, **107**, 173-182.
- Urban, S., Lee, J.R. and Freeman, M.** (2002) A family of Rhomboid intramembrane proteases activates all Drosophila membrane-tethered EGF ligands. *Embo J*, **21**, 4277-4286.
- Vaknin, Y., Hillmann, F., Iannitti, R., Ben Baruch, N., Sandovsky-Losica, H., Shadkchan, Y., Romani, L., Brakhage, A., Kniemeyer, O. and Oshero, N.** (2016) Identification and Characterization of a Novel Aspergillus fumigatus Rhomboid Family Putative Protease, RbdA, Involved in Hypoxia Sensing and Virulence. *Infect Immun*, **84**, 1866-1878.
- Vinothkumar, K.R., Pierrat, O.A., Large, J.M. and Freeman, M.** (2013) Structure of rhomboid protease in complex with beta-lactam inhibitors defines the S2' cavity. *Structure*, **21**, 1051-1058.
- Wang, Y., Maegawa, S., Akiyama, Y. and Ha, Y.** (2007) The role of L1 loop in the mechanism of rhomboid intramembrane protease GlpG. *J Mol Biol*, **374**, 1104-1113.
- Wang, Y., Zhang, Y. and Ha, Y.** (2006) Crystal structure of a rhomboid family intramembrane protease. *Nature*, **444**, 179-180.
- Willger, S.D., Puttikamonkul, S., Kim, K.H., Burritt, J.B., Grahl, N., Metzler, L.J., Barbuch, R., Bard, M., Lawrence, C.B. and Cramer, R.A., Jr.** (2008) A sterol-regulatory element binding protein is required for cell polarity, hypoxia adaptation, azole drug resistance, and virulence in Aspergillus fumigatus. *Plos Pathog*, **4**, e1000200.
- Wolf, E.V., Zeissler, A. and Verhelst, S.H.** (2015) Inhibitor Fingerprinting of Rhomboid Proteases by Activity-Based Protein Profiling Reveals Inhibitor Selectivity and Rhomboid Autoprocessing. *Acs Chem Biol*, **10**, 2325-2333.

- Xue, Y. and Ha, Y.** (2012) Catalytic mechanism of rhomboid protease GlpG probed by 3,4-dichloroisocoumarin and diisopropyl fluorophosphonate. *J Biol Chem*, **287**, 3099-3107.
- Zettl, M., Adrain, C., Strisovsky, K., Lastun, V. and Freeman, M.** (2011) Rhomboid family pseudoproteases use the ER quality control machinery to regulate intercellular signaling. *Cell*, **145**, 79-91.
- Zoll, S., Stanchev, S., Began, J., Skerle, J., Lepsik, M., Peclinovska, L., Majer, P. and Strisovsky, K.** (2014) Substrate binding and specificity of rhomboid intramembrane protease revealed by substrate-peptide complex structures. *Embo J*, **33**, 2408-2421.

CHAPTER 2

Cellular Organization and Regulation of Plant Glycerolipid Metabolism

This work has been further edited and is published in Plant and Cell Physiology (<https://academic.oup.com/pcp>)

Lavell, A. and Benning, C. (2019) Cellular Organization and Regulation of Plant Glycerolipid Metabolism. *Plant Cell Physiol*, 60, 1176-1183.

Abstract

Great strides have been made in understanding how membranes and lipid droplets are formed and maintained in land plants, yet much more is to be learned given the complexity of plant lipid metabolism. A complicating factor is the multi-organellar presence of biosynthetic enzymes and unique compositional requirements of different membrane systems. This necessitates a rich network of transporters and transport mechanisms that supply fatty acids, membrane lipids, and storage lipids to their final cellular destination. Though we know a large number of the biosynthetic enzymes involved in lipid biosynthesis and a few transport proteins, the regulatory mechanisms, in particular, coordinating expression and/or activity of the majority remain yet to be described. Plants undergoing stress alter their membranes' compositions, and lipids such as phosphatidic acid have been implicated in stress signaling. Additionally, lipid metabolism in chloroplasts supplies precursors for jasmonic acid (JA) biosynthesis, and perturbations in lipid homeostasis has consequences on JA signaling. In this review, several aspects of plant lipid metabolism are discussed that are currently under investigation: cellular transport of lipids, regulation of lipid biosynthesis, roles of lipids in stress signaling, and lastly the structural and oligomeric states of lipid enzymes.

Introduction

Lipid metabolism in plants is an essential process that provides cells with membranes, a storage form of energy and building blocks, and potent signaling compounds. In this review, we will give some necessary background on plant lipid metabolism and outline the frontiers of our knowledge on plant lipid biosynthesis and transport. In addition, we

will point out the outstanding questions about the biophysical arrangement or topology of lipid biosynthetic enzymes. Plant cells, as any other eukaryotic cell, are composed of many membrane systems and compartments with unique lipid compositions. Here we will focus primarily on land plants and how they carry out lipid biosynthesis in the plastid and the endoplasmic reticulum (ER), and related processes associated with those compartments. Most of the information described here is based on the model plant *Arabidopsis thaliana* (*Arabidopsis*) unless otherwise indicated.

In both the ER and plastid, phosphatidic acid (PA) is the first lipid species formed by de novo complete acylation of glycerol-3-phosphate (glycerol-3-P). During the biosynthesis of PA, the specificity of the acyltransferases associated with the respective compartments determines the length of acyl chains esterified. In the plastid, glycerol-3-P acyl transferase and lysophosphatidic acid acyltransferase (ATS1 and ATS2) produce a PA bearing 18:1 and 16:0 acyl chains (carbon # : double bond #) at the *sn*-1 and *sn*-2 positions of the glycerol backbone, respectively (Bin *et al.*, 2004, Kim and Huang, 2004, Tzafrir *et al.*, 2004, Xu *et al.*, 2006). Meanwhile, the ER acyltransferases produce a PA with predominantly 18-carbon acyl chains at both *sn*-1 and *sn*-2 positions (Kim *et al.*, 2005). This distinction results in two identifiable sets of molecular species of lipids that are, within limitations, representative of the lipid assembly in the respective compartments. Though the fluxes through these two parallel pathways have been estimated based on the 16/18 carbon ratio, or more precisely by positional analysis of membrane lipid acyl composition, there are some caveats on the specificity of acyltransferases and possible lipid reassembly. For example, acyl editing of chloroplast-assembled lipids has recently been observed through in vivo lipid tagging using an ER-

targeted $\Delta 6$ -desaturase from *Physcomitrella patens* (Hurlock *et al.*, 2018). Already, acyl editing of ER lipids has been known for some time for phosphatidylcholine (PC) in plants (Bates *et al.*, 2007). However, if acyl editing of chloroplast lipids contributes significantly to the acyl composition of chloroplast lipids, the reliability of the 16/18 carbon ratio as a simple metric for the origin of plastid lipids needs to be reevaluated. This is particularly true for *Chlamydomonas*, for which a plastid-type lysophosphatidic acid acyltransferase associated with the ER has been discovered (Kim *et al.*, 2018), explaining the unusually high 16/18 ratio of *Chlamydomonas* galactolipids, even though it has been shown to import ER-derived lipid precursors into the plastid (Warakanont *et al.*, 2015).

In addition to differing acyltransferase preferences of the two pathways, the conversion of PA to other lipid classes also differs between the two compartments as the ER produces exclusively phospholipids and triacylglycerols while the plastid synthesizes the phospholipid phosphatidylglycerol (PG), the sulfolipid sulfoquinovosyldiacylglycerol (SQDG), and the two galactolipids mono- and digalactosyldiacylglycerol (MGDG and DGDG).

Though components of both pathways are present in most land plants, not all plants utilize them both or to the same extent. For example, grasses primarily rely on the ER pathway (Petroustos *et al.*, 2014, Yang *et al.*, 2017). However, to understand the interplay between the ER and plastid pathways, *Arabidopsis* provides an excellent starting model due to its near equal utilization of both pathways.

Lipid Transport Mechanisms

As pointed out above, *Arabidopsis* produces glycerolipids through the plastid and ER pathways, also denoted prokaryotic and eukaryotic pathways, respectively (Browse *et al.*, 1986, Kunst *et al.*, 1988, Mongrand *et al.*, 1998). There is also some lipid assembly in the mitochondrion and the reader is directed to the Acyl-Lipid Metabolism chapter of the *Arabidopsis* Book (Li-Beisson *et al.*, 2013) for further information concerning mitochondrial lipid metabolism. Though the assembly of glycerolipids occurs in more than one compartment, with the exception of fatty acids synthesized in the mitochondrion mostly as precursors to lipoic acid (Wada *et al.*, 1997), the plastid is the location where the vast majority of fatty acids are de novo synthesized. In order to supply substrates to the glycerolipid assembly machinery at the ER, acyl groups must be exported from the plastid. In addition, the ER provides glycerolipid precursors to the chloroplast requiring a transport system. The flux of acyl groups from the plastid is substantial especially in seed oil storage tissues, and yet at this time it is still not unambiguously known by which molecular mechanism the acyl groups are exported from the plastid (Fig. 2.1) (Koo *et al.*, 2004). One hypothesis suggests transport of lipids or fatty acids through ER-plastid contact sites, which have been observed (Andersson *et al.*, 2007). An inner chloroplast envelope membrane-spanning protein FAX1 seems to play a role in lipid homeostasis of ER-derived lipids and can complement the *fat1* yeast mutant deficient in fatty acid export (Li *et al.*, 2015). Although FAX1 is likely to aid in the transport of fatty acids across the inner envelope membrane at least in specific tissues, it appears as though not all fatty acid export from chloroplasts is abolished in the *fax1* mutant and other mechanisms may be in play. The necessity of transport channels or other protein-mediated mechanisms to

move fatty acids across the inner envelope membrane as well as the outer envelope leaflets to the ER membranes (Fig. 2.1) makes this an active area of research.

After lipids are assembled at the ER, there are several proposed mechanisms on how those lipids make it back to the plastid. One reported transport mechanism involves the phospholipid transporter ALA10. Mutants of ALA10 have a lowered MGDG/PC ratio and *ALA10* overexpression leads to an increase in MGDG/PC ratio, suggesting a role of ALA10 in maintaining MGDG metabolism in the chloroplast (Botella *et al.*, 2016, Botella *et al.*, 2017). Based on these data it was concluded that this transporter may be important for efficient translocation of PC across the ER membrane and to the plastid either through ER-plastid contact sites or by another mechanism yet to be described.

A means of reimporting ER-assembled lipids into the plastid has been described and a multiprotein ABC transporter complex consisting of three proteins TRIGALACTOSYLDIACYLGLYCEROL1, 2, 3 (TGD1, 2, 3) has been identified. Together with two additional proteins, TGD4 and TGD5, these proteins provide a conduit for lipid transfer that spans the outer and inner envelope membranes of the plastid and coordinates lipid import from the ER in a unidirectional manner (Xu *et al.*, 2003, Xu *et al.*, 2005, Awai *et al.*, 2006, Lu *et al.*, 2007, Lu and Benning, 2009, Xu *et al.*, 2010, Roston *et al.*, 2011, Roston *et al.*, 2012, Fan *et al.*, 2015). TGD4 and TGD5 are located at the outer envelope, where TGD4 contains a PA binding site (Wang *et al.*, 2013) and is hypothesized to facilitate the translocation of ER-assembled PA to the plastid membranes (Wang *et al.*, 2012). This occurs in coordination with the inner envelope subcomplex composed of TGD1, TGD2, and TGD3, which may also assist the translocation of PA through the identified PA-binding site of the TGD2 protein (Awai *et al.*, 2006, Lu and Benning, 2009).

Since PA is also synthesized at the chloroplast stroma side of the inner envelope membrane, there could be an outwards transporting mechanism that translocates plastid PA and inserts it into the same leaflet as the ER-sourced PA. A bacterial ABC transporter of lipopolysaccharide (LPS) precursors resembling the plant TGD complex has been shown to mediate the outwards transport of lipids from the inner membrane to the outer membrane of the cell (Sperandeo *et al.*, 2008). Bacterial lipid transporter systems Mla, Pqi and Yeb, have been structurally analyzed and have intermembrane spanning projections, like the LPS transporter and the TGD complex, which aid in lipid transport from the inner to the outer membrane (Ekiert *et al.*, 2017). It is possible that similar mechanisms exist to move plastid-assembled lipids outwards through the chloroplast to the envelope membranes (Fig. 2.1).

As both eukaryotic and prokaryotic DAG species are galactosylated by monogalactosyldiacylglycerol synthase 1 (MGD1) located at the intermembrane leaflet of the inner envelope membrane, the transport of the product MGDG to the thylakoid membranes needs to be aided by a protein channel or transport mechanism. In addition to MGDG, the product of digalactosyldiacylglycerol synthase 1 (DGD1), digalactosyldiacylglycerol (DGDG), must also be translocated across the outer and inner envelope membranes to be incorporated into the thylakoid membranes. These galactolipid transport mechanisms could share the same machinery or use specific transporters for each lipid (Fig. 2.2). A proposed mechanism by which DGDG moves from the outer envelope to the inner envelope membrane involves the N-terminal extension of DGD1 itself (Kelly *et al.*, 2016) (Fig. 2.2).

Another intriguing area of study is the export of plastid lipids under certain environmental stresses such as phosphate starvation. A study looking for a non-DGD1 dependent pathway of DGDG synthesis led to the discovery of a suppressor mutant *dgs1* which accumulates galactolipids despite lacking the enzyme DGD1 responsible for the bulk synthesis of DGDG (Xu *et al.*, 2008, Moellering and Benning, 2010). Interestingly, the homozygous *dgd1/dgs1* mutant also accumulated oligogalactolipids (Xu *et al.*, 2008) such as trigalactosyldiacylglycerol (TGDG) which are typically induced by freezing stress (Moellering *et al.*, 2010). Under phosphate starvation, Arabidopsis plants substitute phospholipids for galactolipids in order to maintain cellular membranes while reserving phosphate for DNA and protein synthesis (Härtel *et al.*, 2000, Härtel *et al.*, 2001, Kobayashi *et al.*, 2009). During early stages of phosphate starvation, PC abundance, unlike other phospholipids, increases and so does DAG that may be derived from the PC before glycolipid synthesis increases (Jouhet *et al.*, 2003). There is some evidence that a mitochondrial complex containing Mic60 plays a role in the response to phosphate starvation and import of plastid-derived galactolipids to the mitochondrion under phosphate starvation (Michaud *et al.*, 2016). It is also hypothesized that MGDG is important during pollen tube expansion to satisfy the need for lipids for rapidly growing membranes (Kobayashi *et al.*, 2004). Galactolipids like DGDG can be detected by antibody in the plasma membrane and the abundance of MGD synthases 2 and 3 is high in pollen tubes. The use of a synthetic MGD synthase inhibitor galvestine-1 showed reduced pollen tube elongation (Botte *et al.*, 2011). These are a few examples of the presence of galactolipids in extraplastidic membranes requiring export from the plastid.

Presumably, the ER as well as other cellular membranes would acquire galactolipids by mechanisms similar to those apparent during phosphate-deprived conditions.

Regulation of Lipid Metabolism

For an integral process such as membrane biogenesis, there must be tight regulation of the flux through the lipid biosynthetic pathways. However, surprisingly little is known about the means by which lipid-synthesizing enzymes are regulated with regard to their genes' expression or their enzymatic activity. One of the better understood regulatory mechanism of lipid metabolism is the regulation of the heteromeric acetyl-CoA carboxylase (ACCase), the complex initiating fatty acid synthesis within plastids. The expression of ACCase subunit genes is coordinated and it appears that the amount of each subunit is modified post-translationally as subunits oligomerize and excess proteins are degraded (Sasaki and Nagano, 2004) and the protein activity is stimulated by light (Sasaki *et al.*, 1997). Like in animals and yeast, plant ACCase enzymes in Arabidopsis, Nicotiana, as well as Brassica, have been shown to catalyze the committed step of fatty acid synthesis, and respond to feedback inhibition by fatty acids (Shintani and Ohlrogge, 1995, Andre *et al.*, 2012, Bates *et al.*, 2014). Negative regulators of the ACCase in Arabidopsis, BADC1, 2, and 3, have been proposed to function in a competitive manner to inhibit the activity of the heteromeric ACCase (Salie *et al.*, 2016).

Another manner of controlling lipid biosynthesis involves the WRINKLED1 (WRI1) transcription factor, which regulates the rate of acyl chain biosynthesis. Several WRI isoforms have been characterized, but their functions seem dependent on their tissue/cell-specific presence. WRI1 stimulates the production of fatty acids, and ectopic

expression of *WRI1* leads to more oil accumulation in *Arabidopsis* seeds and seedlings grown on sucrose media (Cernac and Benning, 2004). While *WRI1* expression is associated with seeds, *WRI3* and 4 activity was narrowed to floral tissues, where *WRI4* promoter-GUS fusion-staining also appeared to be present in plant nectaries (To *et al.*, 2012). In seed tissues, *WRI1* also controls the expression levels of *BCCP2* and thereby ACCase and fatty acid synthesis (Thelen *et al.*, 2001, Ruuska *et al.*, 2002). *WRI1* orthologues have been found in different oil storing tissues, for example the embryo in maize (*Zea mays*), the mesocarp in oil palm (*Elaeis guineensis*) (Pouvreau *et al.*, 2011, Ma *et al.*, 2013)), castor bean (*Ricinus communis*), rapeseed (*Brassica napus*), nasturtium (*Tropaeolum majus*), the burning bush (*Euonymus alatus*) (Troncoso-Ponce *et al.*, 2011), and non-seed tissues of Chinese tallow (*Triadica sebifera*) (Divi *et al.*, 2016). The regulatory nature of *WRI1* transcription factors has made them prominent targets for the engineering of oil content in different tissues (Reynolds *et al.*, 2015, Yang *et al.*, 2015). *WRI1* alone is not fully capable of turning on TAG biosynthesis, but when co-produced with a diacylglycerol acyltransferase (DGAT), *Nicotiana benthamiana* leaves were able to achieve higher levels of TAG accumulation than that with *WRI1* production alone (Vanhercke *et al.*, 2013). Increases in oil content of *Arabidopsis* by ectopic production of *WRI1* and suppression of starch synthesis resulted in increases of oils in vegetative tissues (Sanjaya *et al.*, 2011). Combining *WRI1*, DGAT1 and OLE1 ectopic production, while also abolishing sucrose export from leaves and starch synthesis, pushed the flux of carbon to TAG storage even more (Zhai *et al.*, 2017b). In sugarcane, over-expression of *WRI1* resulted in doubling of TAG accumulation, but in this plant TAG biosynthesis did not seem to compete with starch biosynthesis unlike in *Arabidopsis* (Zale *et al.*, 2016).

WRI1 is post-translationally regulated through phosphorylation by KIN10 kinase, which is inhibited by increasing levels of sugar, and the phosphorylated WRI1 is targeted for proteolytic degradation (Zhai *et al.*, 2017a, Zhai *et al.*, 2018). Other aspects of WRI1 protein stability have been described, such as a C-terminal PEST motif that leads to destabilization of the protein, and upon removal of the motif to an increase in oil accumulation (Ma *et al.*, 2015). Because storage TAG biosynthesis involves multiple steps across multiple organelles, the full complexity of this process is not yet fully understood, and much can still be learned to realize the full potential of oil production in plant seeds.

The balance of eukaryotic and prokaryotic lipid species in Arabidopsis seems to be carefully regulated leading to a finely tuned cellular lipid homeostasis. However, many questions remain about the mechanism by which plants maintain their lipid and acyl composition. For example, it seems likely that there are mechanisms that sense membrane fluidity, acyl saturation levels, and membrane curvature. What are these mechanisms? Some enzymes appear to be sensitive to their membrane environment, providing a potential layer of regulation. For example, though DAG is the preferred substrate for MGD1, the presence of PA and PG appears to be required for MGD1 membrane association and activity (Dubots *et al.*, 2010, Sarkis *et al.*, 2014).

Aside from regulation of bulk lipid biosynthesis, some work has been done showing how the degree of plant lipid saturation can be controlled by temperature. The Arabidopsis ω -3 fatty acid desaturase FAD8, one of two isozymes present, was shown to be post-translationally regulated through destabilization of the C-terminus when the *fad7fad8* double mutant producing a Myc-tagged FAD8 fusion protein was subjected to increasing

temperature (Matsuda *et al.*, 2005). More recently, the temperature-dependent stability of ER-localized desaturase FAD3 was shown to be linked to the ubiquitin-proteasome-system, where *B. napus* and *V. fordii* FAD3 genes were expressed in yeast and their respective protein levels were modulated by a PEST-like domain at the N-terminus (O'Quin *et al.*, 2010).

Lipid Signaling and Response to Stress

Lipids are not only integral to the membrane architecture, but they also play an important role in signaling during growth and in times of stress. There is a growing body of work on PA and its role in signaling in response to various cellular conditions. PA and phospholipase D (PLD), which releases PA from other phospholipids, have been implicated in a variety of stress responses by modulating enzyme activity and protein location (Wang, 2005, Ruelland *et al.*, 2015). As in mammalian systems where lipids are found in the bloodstream bound to proteins, PA and other lipid-binding proteins have been identified in the phloem exudates of *Arabidopsis* (Guelette *et al.*, 2012, Barbaglia and Hoffmann-Benning, 2016) suggesting long-distance movement of lipids through the plant vasculature. In mammalian cells, the importance of PA is apparent through its regulation of small GTPase-activating proteins thereby modulating the activation of Ras signaling pathways (Zhang and Du, 2009). MYB transcription factors interact with PA and their location is influenced by lipid binding. For example, phospholipase D has been implicated in ABA-coordinated stomatal closure, where the PLD product, PA, binds and modulates activity of ABI1 and Sphingosine Kinases (Zhang *et al.*, 2009, Guo *et al.*, 2011, Guo *et al.*, 2012). Furthermore, much like negative feedback regulation of other pathways,

PLD α 1 producing PA as a product of its lipid hydrolysis has been shown to be itself inhibited by a PA-bound regulator of G-protein signaling, RGS1, which is a GTPase accelerating protein (Roy Choudhury and Pandey, 2017). The role of G-protein signaling is well known in mammalian systems, and plant G-protein signaling is becoming better understood (Pandey, 2017). As more PA-regulated signaling pathways emerge, it is important to begin investigating the mechanisms by which key regulatory enzymes come directly into contact with PA and are regulated by it. Which pools of PA contribute to signaling? Is there negative feedback regulation of the lipid biosynthetic machinery by PA? Is PA or are other lipids critical for enzymatic function of lipid biosynthetic enzymes?

Another emerging area of lipid-based regulation of cellular processes focuses on the tight interplay between lipid homeostasis in the plastid and oxylipin biosynthesis. Jasmonic acid (JA), a potent oxidized lipid signaling molecule, is derived from α -linolenic acid in the chloroplast and is active in numerous developmental stages of plant growth as well as involved in responses to stress and herbivory (Howe *et al.*, 2018). Since JA is lipid-derived, various hypotheses exist regarding the identity of the acyl-donating lipid as well as the lipases, which release the α -linolenic acid. However, while the exact molecular mechanism has not yet been elucidated, several lipid mutant phenotypes suggest that particular perturbations of plastid lipid metabolism lead to JA biosynthesis. An interesting example is the *dgd1* mutant, which is producing only small amounts of digalactosyldiacylglycerol and as a result, the predominant galactolipid species present in the mutant plant is monogalactosyldiacylglycerol and the mutant is severely stunted in growth (Dörmann *et al.*, 1999). Previously, it was speculated that DGDG was so important that its reduction in content alone would slow down the growth of the plant. However,

when crossed with the JA-insensitive mutant *coi1*, the growth phenotype was rescued (Lin *et al.*, 2016) showing that a disruption in galactolipid biosynthesis also disrupts JA homeostasis leading to the observed growth phenotype. Aside from changes in overall lipid content, JA accumulation has been shown to be triggered by thylakoid-localized lipases (Wang *et al.*, 2018), Plastid LIPases 2 and 3 (PLIP2, PLIP3). The expression of the respective genes is responsive to abscisic acid and the lipases have specificity for PG and MGDG. Thus, the roles that chloroplast membrane lipids and their specific lipases in JA signaling are playing are beginning to come into focus.

A more global plant response to stress is the remodeling of membrane lipid composition. An example is the production of oligogalactolipids during freezing in *Arabidopsis*. During freezing conditions, the activity of SENSITIVE TO FREEZING2 (SFR2) is induced, resulting in the accumulation of oligogalactolipids serving a protective role (Moellering *et al.*, 2010, Moellering and Benning, 2011), since the *sfr2* mutants are more sensitive to freezing (Warren *et al.*, 1997). The activity of SFR2 is induced by divalent cations possibly leaking from the chloroplast as a result of membrane disruption in combination with cytosolic acidification during freezing stress (Barnes *et al.*, 2016).

Spatial Arrangement and Complexes of Lipid Biosynthetic Enzymes

Because changing environmental conditions demand an adjustment of the extent and composition of membranes and the production of lipid-derived signaling compounds, the lipid metabolic machinery must rapidly adjust as well. Much is known about flux through the major lipid biosynthetic pathways, as well as the participating enzymes. However, a knowledge gap remains in understanding the spatial arrangement of lipid enzymes and

their protein interactome. The best described lipid complexes are the ACCase, the fatty acid synthase and the TGD complex. While transport of lipids can refer to their inter-compartment movement, the movement of lipids between enzymes located on opposite sides of the same membrane, as well as the translocation of polar lipids between the two leaflets of adjacent membranes needs to be considered as well. For example, plastid PA is formed on the stromal side of the inner envelope membrane (Xu *et al.*, 2006) and MGDG assembly occurs on the leaflet facing the intermembrane space as MGDG synthase is peripherally associated with the intermembrane leaflet of the inner envelope membrane (Xu *et al.*, 2005, Rocha *et al.*, 2016). Given this topology, one has to predict that there is a mechanism that can move PA from the stromal side of the inner envelope membrane to the leaflet facing the intermembrane space where the PA phosphatase is presumably located. It should be noted, that the PA phosphatase has not been definitively localized to a certain leaflet, but its activity is found in the inner membrane and free magnesium ions in the stroma would inhibit a stromal facing phosphatase (Malherbe *et al.*, 1992), suggesting its location at the intermembrane leaflet of the inner envelope membrane.

While most of the genes encoding lipid biosynthetic enzymes are known, there is little knowledge on the assembly of the respective proteins into higher order complexes. Plant desaturases appear to function as dimers, with a crystallized diiron Δ^9 -desaturase of castor bean providing an example (Schneider *et al.*, 1992, Lindqvist *et al.*, 1996). Recently, the first plant acyl-CoA binding protein structures were solved using rice homologues OsACBP1 and OsACBP2 (Guo *et al.*, 2017). The structure of MGD1 synthase has been described, as well as its PA binding properties (Rocha *et al.*, 2016),

though we do not know of any higher oligomeric states. It has been hypothesized that enzymes such as DGD1 and the TGD complex, which also bind PA, could be aggregating as a result of PA binding (Kelly *et al.*, 2016). Though just a hypothesis, these insights pose interesting questions about the mechanisms of regulated oligomerization and possible substrate channeling by lipid enzymes. Moreover, while more data are being collected on enzymatic activities and physiological roles of lipid biosynthetic proteins, the majority of lipid enzyme structures remain to be solved.

Overall, more biophysical information is needed on lipid biosynthetic enzymes in order to create accurate models of plant lipid metabolism, identify mechanisms of regulation, and ultimately optimize biofuel and food crops for oil accumulation. Numerous efforts have been made to catalogue and characterize the proteome of plant cells, including chloroplasts (Ferro *et al.*, 2003, Froehlich *et al.*, 2003, Breuers *et al.*, 2011, Lundquist *et al.*, 2017). With this basic information available, the plant lipid community is slowly beginning to assemble the 3D landscapes of our current 2D models depicting lipid metabolism.

APPENDIX

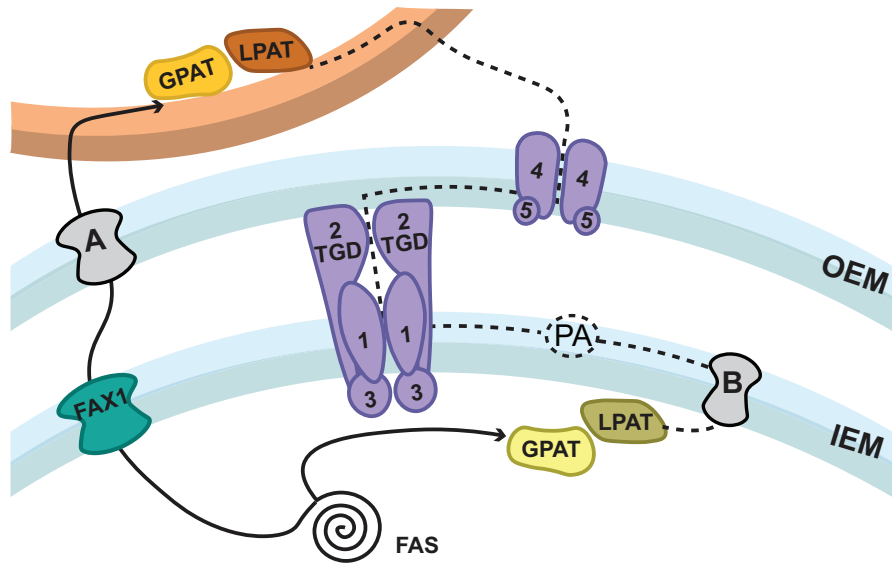


Figure 2.1. Scheme of phosphatidic acid (PA) synthesis in the plastid and the endoplasmic reticulum (ER). Denoted with letters are outstanding transport mechanisms proposed and yet to be characterized: the unknown exporter of acyl groups across the outer envelope membrane (OEM) of the plastid (**A**) and the transport mechanism by which plastid-assembled PA is moved through the inner envelope membrane (IEM) of the plastid (**B**). The abbreviations are as follows: fatty acid synthesis (FAS), fatty acid exporter 1 (FAX1), glycerol-3-P acyltransferase (GPAT), lyso-phosphatidate acyltransferase (LPAT), trigalactosyldiacylglycerol 1, 2, 3, 4, 5 (TGD 1, 2, 3, 4, 5).

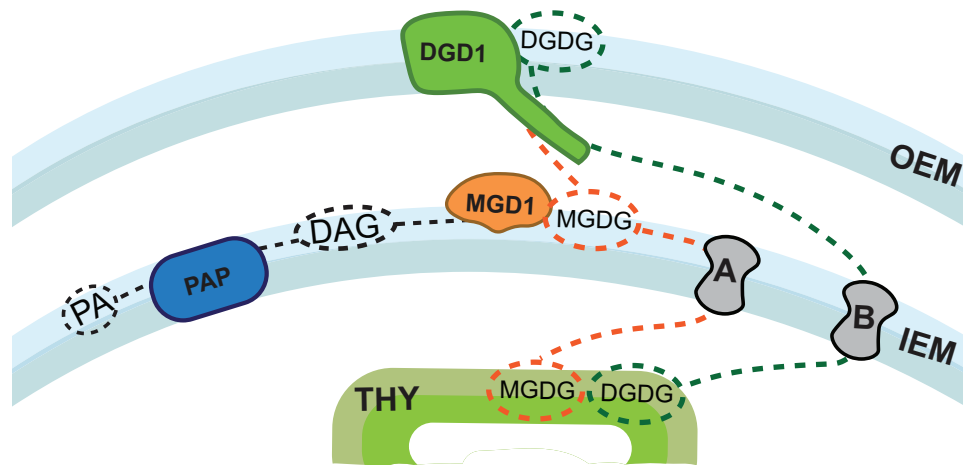


Figure 2.2. Proposed movement of galactolipids after synthesis from diacylglycerol (DAG). Denoted with letters are the unknown mechanisms of transport of mono- and digalactosyldiacylglycerol (MGDG and DGDG) (**A** and **B** respectively) to the thylakoid membranes (THY), after synthesis by MGDG synthase 1 (MGD1) at the inner envelope membrane (IEM) and DGDG synthase 1 (DGD1) at the outer envelope membrane (OEM). PAP denotes the phosphatidic acid phosphatase.

REFERENCES

REFERENCES

- Andersson, M.X., Goksoy, M. and Sandelius, A.S.** (2007) Optical manipulation reveals strong attracting forces at membrane contact sites between endoplasmic reticulum and chloroplasts. *J Biol Chem*, **282**, 1170-1174.
- Andre, C., Haslam, R.P. and Shanklin, J.** (2012) Feedback regulation of plastidic acetyl-CoA carboxylase by 18:1-acyl carrier protein in *Brassica napus*. *Proc Natl Acad Sci U S A*, **109**, 10107-10112.
- Awai, K., Xu, C.C., Tamot, B. and Benning, C.** (2006) A phosphatidic acid-binding protein of the chloroplast inner envelope membrane involved in lipid trafficking. *Proc Natl Acad Sci U S A*, **103**, 10817-10822.
- Barbaglia, A.M. and Hoffmann-Benning, S.** (2016) Long-distance lipid signaling and its role in plant development and stress response. *Subcell Biochem*, **86**, 339-361.
- Barnes, A.C., Benning, C. and Roston, R.L.** (2016) Chloroplast membrane remodeling during freezing stress is accompanied by cytoplasmic acidification activating SENSITIVE TO FREEZING2. *Plant Physiol*, **171**, 2140-2149.
- Bates, P.D., Johnson, S.R., Cao, X., Li, J., Nam, J.W., Jaworski, J.G., Ohlrogge, J.B. and Browse, J.** (2014) Fatty acid synthesis is inhibited by inefficient utilization of unusual fatty acids for glycerolipid assembly. *Proc Natl Acad Sci U S A*, **111**, 1204-1209.
- Bates, P.D., Ohlrogge, J.B. and Pollard, M.** (2007) Incorporation of newly synthesized fatty acids into cytosolic glycerolipids in pea leaves occurs via acyl editing. *J Biol Chem*, **282**, 31206-31216.
- Bin, Y., Wakao, S., Fan, J.L. and Benning, C.** (2004) Loss of plastidic lysophosphatidic acid acyltransferase causes embryo-lethality in *Arabidopsis*. *Plant Cell Physiol*, **45**, 503-510.
- Botella, C., Jouhet, J. and Block, M.A.** (2017) Importance of phosphatidylcholine on the chloroplast surface. *Prog Lipid Res*, **65**, 12-23.
- Botella, C., Sautron, E., Boudiere, L., Michaud, M., Dubots, E., Yamaro-Botte, Y., Albrieux, C., Marechal, E., Block, M.A. and Jouhet, J.** (2016) ALA10, a phospholipid flippase, controls FAD2/FAD3 desaturation of phosphatidylcholine in the ER and affects chloroplast lipid composition in *Arabidopsis thaliana*. *Plant Physiol*, **170**, 1300-1314.
- Botte, C.Y., Deligny, M., Rocchia, A., Bonneau, A.L., Saidani, N., Hardre, H., Aci, S., Yamaro-Botte, Y., Jouhet, J., Dubots, E., Loizeau, K., Bastien, O., Brehelin, L., Joyard, J., Cintrat, J.C., Falconet, D., Block, M.A., Rousseau, B., Lopez, R.**

- and Marechal, E.** (2011) Chemical inhibitors of monogalactosyldiacylglycerol synthases in *Arabidopsis thaliana*. *Nat Chem Biol*, **7**, 834-842.
- Breuers, F.K., Brautigam, A. and Weber, A.P.** (2011) The plastid outer envelope - a highly dynamic interface between plastid and cytoplasm. *Front Plant Sci*, **2**, 97.
- Browse, J., Warwick, N., Somerville, C.R. and Slack, C.R.** (1986) Fluxes through the prokaryotic and eukaryotic pathways of lipid-synthesis in the 16-3 plant *Arabidopsis thaliana*. *Biochem J*, **235**, 25-31.
- Cernac, A. and Benning, C.** (2004) WRINKLED1 encodes an AP2/EREB domain protein involved in the control of storage compound biosynthesis in *Arabidopsis*. *Plant J*, **40**, 575-585.
- Divi, U.K., Zhou, X.R., Wang, P.H., Butlin, J., Zhang, D.M., Liu, Q., Vanhercke, T., Petrie, J.R., Talbot, M., White, R.G., Taylor, J.M., Larkin, P. and Singh, S.P.** (2016) Deep sequencing of the fruit transcriptome and lipid accumulation in a non-seed tissue of chinese tallow, a potential biofuel crop. *Plant Cell Physiol*, **57**.
- Dörmann, P., Balbo, I. and Benning, C.** (1999) *Arabidopsis* galactolipid biosynthesis and lipid trafficking mediated by DGD1. *Science*, **284**, 2181-2184.
- Dubots, E., Audry, M., Yamaro, Y., Bastien, O., Ohta, H., Breton, C., Marechal, E. and Block, M.A.** (2010) Activation of the chloroplast monogalactosyldiacylglycerol synthase MGD1 by phosphatidic acid and phosphatidylglycerol. *J Biol Chem*, **285**, 6003-6011.
- Ekiert, D.C., Bhabha, G., Isom, G.L., Greenan, G., Ovchinnikov, S., Henderson, I.R., Cox, J.S. and Vale, R.D.** (2017) Architectures of lipid transport systems for the bacterial outer membrane. *Cell*, **169**, 273-285 e217.
- Fan, J., Zhai, Z., Yan, C. and Xu, C.** (2015) *Arabidopsis* TRIGALACTOSYLDIACYLGLYCEROL5 Interacts with TGD1, TGD2, and TGD4 to Facilitate Lipid Transfer from the Endoplasmic Reticulum to Plastids. *Plant Cell*, **27**, 2941-2955.
- Ferro, M., Salvi, D., Brugiere, S., Miras, S., Kowalski, S., Louwagie, M., Garin, J., Joyard, J. and Rolland, N.** (2003) Proteomics of the chloroplast envelope membranes from *Arabidopsis thaliana*. *Mol Cell Proteomics*, **2**, 325-345.
- Froehlich, J.E., Wilkerson, C.G., Ray, W.K., McAndrew, R.S., Osteryoung, K.W., Gage, D.A. and Phinney, B.S.** (2003) Proteomic study of the *Arabidopsis thaliana* chloroplastic envelope membrane utilizing alternatives to traditional two-dimensional electrophoresis. *J Proteome Res*, **2**, 413-425.
- Guelette, B.S., Benning, U.F. and Hoffmann-Benning, S.** (2012) Identification of lipids and lipid-binding proteins in phloem exudates from *Arabidopsis thaliana*. *J Exp Bot*, **63**, 3603-3616.

- Guo, L., Mishra, G., Markham, J.E., Li, M., Tawfall, A., Welti, R. and Wang, X.** (2012) Connections between sphingosine kinase and phospholipase D in the abscisic acid signaling pathway in Arabidopsis. *J Biol Chem*, **287**, 8286-8296.
- Guo, L., Mishra, G., Taylor, K. and Wang, X.** (2011) Phosphatidic acid binds and stimulates Arabidopsis sphingosine kinases. *J Biol Chem*, **286**, 13336-13345.
- Guo, Z.H., Chan, W.H.Y., Kong, G.K.W., Hao, Q. and Chye, M.L.** (2017) The first plant acyl-CoA-binding protein structures: the close homologues OsACBP1 and OsACBP2 from rice. *Acta Crystallogr D*, **73**, 438-448.
- Härtel, H., Dormann, P. and Benning, C.** (2000) DGD1-independent biosynthesis of extraplastidic galactolipids after phosphate deprivation in Arabidopsis. *Proc Natl Acad Sci U S A*, **97**, 10649-10654.
- Härtel, H., Dörmann, P. and Benning, C.** (2001) Galactolipids not associated with the photosynthetic apparatus in phosphate-deprived plants. *J Photoch Photobio B*, **61**, 46-51.
- Howe, G.A., Major, I.T. and Koo, A.J.** (2018) Modularity in jasmonate signaling for multistress resilience. *Annu Rev Plant Biol*, **69**, 387-415.
- Hurlock, A.K., Wang, K., Takeuchi, T., Horn, P.J. and Benning, C.** (2018) In vivo lipid 'tag and track' approach shows acyl editing of plastid lipids and chloroplast import of phosphatidylglycerol precursors in Arabidopsis thaliana. *Plant J*, **95**, 1129-1139.
- Jouhet, J., Marechal, E., Bligny, R., Joyard, J. and Block, M.A.** (2003) Transient increase of phosphatidylcholine in plant cells in response to phosphate deprivation. *Febs Lett*, **544**, 63-68.
- Kelly, A.A., Kalisch, B., Holzl, G., Schulze, S., Thiele, J., Melzer, M., Roston, R.L., Benning, C. and Dormann, P.** (2016) Synthesis and transfer of galactolipids in the chloroplast envelope membranes of Arabidopsis thaliana. *Proc Natl Acad Sci U S A*, **113**, 10714-10719.
- Kim, H.U. and Huang, A.H.** (2004) Plastid lysophosphatidyl acyltransferase is essential for embryo development in Arabidopsis. *Plant Physiol*, **134**, 1206-1216.
- Kim, H.U., Li, Y.B. and Huang, A.H.C.** (2005) Ubiquitous and endoplasmic reticulum-located lysophosphatidyl acyltransferase, LPAT2, is essential for female but not male gametophyte development in Arabidopsis. *Plant Cell*, **17**, 1073-1089.
- Kim, Y., Terng, E.L., Riekhof, W.R., Cahoon, E.B. and Cerutti, H.** (2018) Endoplasmic reticulum acyltransferase with prokaryotic substrate preference contributes to triacylglycerol assembly in Chlamydomonas. *P Natl Acad Sci USA*, **115**, 1652-1657.

- Kobayashi, K., Awai, K., Nakamura, M., Nagatani, A., Masuda, T. and Ohta, H.** (2009) Type-B monogalactosyldiacylglycerol synthases are involved in phosphate starvation-induced lipid remodeling, and are crucial for low-phosphate adaptation. *Plant J*, **57**, 322-331.
- Kobayashi, K., Awai, K., Takamiya, K. and Ohta, H.** (2004) Arabidopsis type B monogalactosyldiacylglycerol synthase genes are expressed during pollen tube growth and induced by phosphate starvation. *Plant Physiol*, **134**, 640-648.
- Koo, A.J., Ohlrogge, J.B. and Pollard, M.** (2004) On the export of fatty acids from the chloroplast. *J Biol Chem*, **279**, 16101-16110.
- Kunst, L., Browse, J. and Somerville, C.** (1988) Altered regulation of lipid biosynthesis in a mutant of Arabidopsis deficient in chloroplast glycerol-3-phosphate acyltransferase activity. *Proc Natl Acad Sci U S A*, **85**, 4143-4147.
- Li, N., Gugel, I.L., Giavalisco, P., Zeisler, V., Schreiber, L., Soll, J. and Philippar, K.** (2015) FAX1, a novel membrane protein mediating plastid fatty acid export. *Plos Biol*, **13**, e1002053.
- Li-Beisson, Y., Shorrosh, B., Beisson, F., Andersson, M.X., Arondel, V., Bates, P.D., Baud, S., Bird, D., Debono, A., Durrett, T.P., Franke, R.B., Graham, I.A., Katayama, K., Kelly, A.A., Larson, T., Markham, J.E., Miquel, M., Molina, I., Nishida, I., Rowland, O., Samuels, L., Schmid, K.M., Wada, H., Welti, R., Xu, C., Zallot, R. and Ohlrogge, J.** (2013) Acyl-lipid metabolism. *Arabidopsis Book*, **11**, e0161.
- Lin, Y.T., Chen, L.J., Herrfurth, C., Feussner, I. and Li, H.M.** (2016) Reduced biosynthesis of digalactosyldiacylglycerol, a major chloroplast membrane lipid, leads to oxylipin overproduction and phloem cap lignification in Arabidopsis. *Plant Cell*, **28**, 219-232.
- Lindqvist, Y., Huang, W.J., Schneider, G. and Shanklin, J.** (1996) Crystal structure of Delta(9) stearoyl-acyl carrier protein desaturase from castor seed and its relationship to other di-iron proteins. *Embo J*, **15**, 4081-4092.
- Lu, B. and Benning, C.** (2009) A 25-amino acid sequence of the Arabidopsis TGD2 protein is sufficient for specific binding of phosphatidic acid. *J Biol Chem*, **284**, 17420-17427.
- Lu, B., Xu, C., Awai, K., Jones, A.D. and Benning, C.** (2007) A small ATPase protein of Arabidopsis, TGD3, involved in chloroplast lipid import. *J Biol Chem*, **282**, 35945-35953.
- Lundquist, P.K., Mantegazza, O., Stefanski, A., Stuhler, K. and Weber, A.P.M.** (2017) Surveying the oligomeric state of Arabidopsis thaliana chloroplasts. *Mol Plant*, **10**, 197-211.

- Ma, W., Kong, Q., Arondel, V., Kilaru, A., Bates, P.D., Thrower, N.A., Benning, C. and Ohlrogge, J.B.** (2013) Wrinkled1, a ubiquitous regulator in oil accumulating tissues from Arabidopsis embryos to oil palm mesocarp. *PLoS one*, **8**, e68887.
- Ma, W., Kong, Q., Grix, M., Mantyla, J.J., Yang, Y., Benning, C. and Ohlrogge, J.B.** (2015) Deletion of a C-terminal intrinsically disordered region of WRINKLED1 affects its stability and enhances oil accumulation in Arabidopsis. *Plant J*, **83**, 864-874.
- Malherbe, A., Block, M.A., Joyard, J. and Douce, R.** (1992) Feedback inhibition of phosphatidate phosphatase from spinach chloroplast envelope membranes by diacylglycerol. *J Biol Chem*, **267**, 23546-23553.
- Matsuda, O., Sakamoto, H., Hashimoto, T. and Iba, K.** (2005) A temperature-sensitive mechanism that regulates post-translational stability of a plastidial omega-3 fatty acid desaturase (FAD8) in Arabidopsis leaf tissues. *J Biol Chem*, **280**, 3597-3604.
- Michaud, M., Gros, V., Tardif, M., Brugiere, S., Ferro, M., Prinz, W.A., Toulmay, A., Mathur, J., Wozny, M., Falconet, D., Marechal, E., Block, M.A. and Jouhet, J.** (2016) AtMic60 is involved in plant mitochondria lipid trafficking and is part of a large complex. *Curr Biol*, **26**, 627-639.
- Moellering, E.R. and Benning, C.** (2010) Phosphate regulation of lipid biosynthesis in Arabidopsis is independent of the mitochondrial outer membrane DGS1 complex. *Plant Physiol*, **152**, 1951-1959.
- Moellering, E.R. and Benning, C.** (2011) Galactoglycerolipid metabolism under stress: a time for remodeling. *Trends Plant Sci*, **16**, 98-107.
- Moellering, E.R., Muthan, B. and Benning, C.** (2010) Freezing tolerance in plants requires lipid remodeling at the outer chloroplast membrane. *Science*, **330**, 226-228.
- Mongrand, S., Bessoule, J.-J., Cabantous, F. and Cassagne, C.** (1998) The C16:3/C18:3 fatty acid balance in photosynthetic tissues from 468 plant species. *Phytochemistry*, **49**, 1049-1064.
- O'Quin, J.B., Bourassa, L., Zhang, D., Shockey, J.M., Gidda, S.K., Fosnot, S., Chapman, K.D., Mullen, R.T. and Dyer, J.M.** (2010) Temperature-sensitive post-translational regulation of plant omega-3 fatty-acid desaturases is mediated by the endoplasmic reticulum-associated degradation pathway. *J Biol Chem*, **285**, 21781-21796.
- Pandey, S.** (2017) Heterotrimeric G-protein regulatory circuits in plants: Conserved and novel mechanisms. *Plant Signal Behav*, **12**.
- Petroutsos, D., Amiar, S., Abida, H., Dolch, L.J., Bastien, O., Rebeille, F., Jouhet, J., Falconet, D., Block, M.A., McFadden, G.I., Bowler, C., Botte, C. and Marechal,**

- E. (2014) Evolution of galactoglycerolipid biosynthetic pathways--from cyanobacteria to primary plastids and from primary to secondary plastids. *Prog Lipid Res*, **54**, 68-85.
- Pouvreau, B., Baud, S., Vernoud, V., Morin, V., Py, C., Gendrot, G., Pichon, J.P., Rouster, J., Paul, W. and Rogowsky, P.M.** (2011) Duplicate maize Wrinkled1 transcription factors activate target genes involved in seed oil biosynthesis. *Plant Physiol*, **156**, 674-686.
- Reynolds, K.B., Taylor, M.C., Zhou, X.R., Vanhercke, T., Wood, C.C., Blanchard, C.L., Singh, S.P. and Petrie, J.R.** (2015) Metabolic engineering of medium-chain fatty acid biosynthesis in *Nicotiana benthamiana* plant leaf lipids. *Front Plant Sci*, **6**.
- Rocha, J., Sarkis, J., Thomas, A., Pitou, L., Radzimanowski, J., Audry, M., Chazalet, V., de Sanctis, D., Palcic, M.M., Block, M.A., Girard-Egrot, A., Marechal, E. and Breton, C.** (2016) Structural insights and membrane binding properties of MGD1, the major galactolipid synthase in plants. *Plant J*, **85**, 622-633.
- Roston, R., Gao, J., Xu, C. and Benning, C.** (2011) Arabidopsis chloroplast lipid transport protein TGD2 disrupts membranes and is part of a large complex. *Plant J*, **66**, 759-769.
- Roston, R.L., Gao, J., Murcha, M.W., Whelan, J. and Benning, C.** (2012) TGD1, -2, and -3 proteins involved in lipid trafficking form ATP-binding cassette (ABC) transporter with multiple substrate-binding proteins. *J Biol Chem*, **287**, 21406-21415.
- Roy Choudhury, S. and Pandey, S.** (2017) Phosphatidic acid binding inhibits RGS1 activity to affect specific signaling pathways in Arabidopsis. *Plant J*, **90**, 466-477.
- Ruelland, E., Kravets, V., Derevyanchuk, M., Martinec, J., Zachowski, A. and Pokotylo, I.** (2015) Role of phospholipid signalling in plant environmental responses. *Environ Exp Bot*, **114**, 129-143.
- Ruuska, S.A., Girke, T., Benning, C. and Ohlrogge, J.B.** (2002) Contrapuntal networks of gene expression during Arabidopsis seed filling. *Plant Cell*, **14**, 1191-1206.
- Salie, M.J., Zhang, N., Lancikova, V., Xu, D. and Thelen, J.J.** (2016) A family of negative regulators targets the committed step of de novo fatty acid biosynthesis. *Plant Cell*, **28**, 2312-2325.
- Sanjaya, Durrett, T.P., Weise, S.E. and Benning, C.** (2011) Increasing the energy density of vegetative tissues by diverting carbon from starch to oil biosynthesis in transgenic Arabidopsis. *Plant Biotechnol J*, **9**, 874-883.
- Sarkis, J., Rocha, J., Maniti, O., Jouhet, J., Vie, V., Block, M.A., Breton, C., Marechal, E. and Girard-Egrot, A.** (2014) The influence of lipids on MGD1 membrane

- binding highlights novel mechanisms for galactolipid biosynthesis regulation in chloroplasts. *Faseb J*, **28**, 3114-3123.
- Sasaki, Y., Kozaki, A. and Hatano, M.** (1997) Link between light and fatty acid synthesis: Thioredoxin-linked reductive activation of plastidic acetyl-CoA carboxylase. *P Natl Acad Sci USA*, **94**, 11096-11101.
- Sasaki, Y. and Nagano, Y.** (2004) Plant acetyl-CoA carboxylase: structure, biosynthesis, regulation, and gene manipulation for plant breeding. *Biosci Biotechnol Biochem*, **68**, 1175-1184.
- Schneider, G., Lindqvist, Y., Shanklin, J. and Somerville, C.** (1992) Preliminary crystallographic data for stearoyl-acyl carrier protein desaturase from castor seed. *J Mol Biol*, **225**, 561-564.
- Shintani, D.K. and Ohlrogge, J.B.** (1995) Feedback inhibition of fatty-acid synthesis in tobacco suspension cells. *Plant J*, **7**, 577-587.
- Sperandeo, P., Lau, F.K., Carpentieri, A., De Castro, C., Molinaro, A., Deho, G., Silhavy, T.J. and Polissi, A.** (2008) Functional analysis of the protein machinery required for transport of lipopolysaccharide to the outer membrane of *Escherichia coli*. *J Bacteriol*, **190**, 4460-4469.
- Thelen, J.J., Mekhedov, S. and Ohlrogge, J.B.** (2001) Brassicaceae express multiple isoforms of biotin carboxyl carrier protein in a tissue-specific manner. *Plant Physiol*, **125**, 2016-2028.
- To, A., Joubes, J., Barthole, G., Lecureuil, A., Scagnelli, A., Jasinski, S., Lepiniec, L. and Baud, S.** (2012) WRINKLED transcription factors orchestrate tissue-specific regulation of fatty acid biosynthesis in *Arabidopsis*. *Plant Cell*, **24**, 5007-5023.
- Troncoso-Ponce, M.A., Kilaru, A., Cao, X., Durrett, T.P., Fan, J., Jensen, J.K., Thrower, N.A., Pauly, M., Wilkerson, C. and Ohlrogge, J.B.** (2011) Comparative deep transcriptional profiling of four developing oilseeds. *Plant J*, **68**, 1014-1027.
- Tzafrir, I., Pena-Muralla, R., Dickerman, A., Berg, M., Rogers, R., Hutchens, S., Sweeney, T.C., McElver, J., Aux, G., Patton, D. and Meinke, D.** (2004) Identification of genes required for embryo development in *Arabidopsis*. *Plant Physiol*, **135**, 1206-1220.
- Vanhercke, T., El Tahchy, A., Shrestha, P., Zhou, X.R., Singh, S.P. and Petrie, J.R.** (2013) Synergistic effect of WRI1 and DGAT1 coexpression on triacylglycerol biosynthesis in plants. *Febs Lett*, **587**, 364-369.
- Wada, H., Shintani, D. and Ohlrogge, J.** (1997) Why do mitochondria synthesize fatty acids? Evidence for involvement in lipoic acid production. *Proc Natl Acad Sci U S A*, **94**, 1591-1596.

- Wang, K., Guo, Q., Froehlich, J.E., Hersh, H.L., Zienkiewicz, A., Howe, G.A. and Benning, C.** (2018) Two abscisic acid-responsive plastid lipase genes involved in jasmonic acid biosynthesis in *Arabidopsis thaliana*. *Plant Cell*, **30**, 1006-1022.
- Wang, X.** (2005) Regulatory functions of phospholipase D and phosphatidic acid in plant growth, development, and stress responses. *Plant Physiol*, **139**, 566-573.
- Wang, Z., Anderson, N.S. and Benning, C.** (2013) The phosphatidic acid binding site of the *Arabidopsis* Trigalactosyldiacylglycerol 4 (TGD4) protein required for lipid import into chloroplasts. *J Biol Chem*, **288**, 4763-4771.
- Wang, Z., Xu, C. and Benning, C.** (2012) TGD4 involved in endoplasmic reticulum-to-chloroplast lipid trafficking is a phosphatidic acid binding protein. *Plant J*, **70**, 614-623.
- Warakanont, J., Tsai, C.H., Michel, E.J., Murphy, G.R., 3rd, Hsueh, P.Y., Roston, R.L., Sears, B.B. and Benning, C.** (2015) Chloroplast lipid transfer processes in *Chlamydomonas reinhardtii* involving a TRIGALACTOSYLDIACYLGLYCEROL 2 (TGD2) orthologue. *Plant J*, **84**, 1005-1020.
- Warren, G., McKown, R., Teutonico, R., Kuroki, G., Veale, E. and Sagen, K.** (1997) *Arabidopsis* mutants impaired in freezing tolerance after cold acclimation. *Plant Cold Hardiness*, 45-56.
- Xu, C., Fan, J., Froehlich, J.E., Awai, K. and Benning, C.** (2005) Mutation of the TGD1 chloroplast envelope protein affects phosphatidate metabolism in *Arabidopsis*. *Plant Cell*, **17**, 3094-3110.
- Xu, C., Fan, J., Riekhof, W., Froehlich, J.E. and Benning, C.** (2003) A permease-like protein involved in ER to thylakoid lipid transfer in *Arabidopsis*. *Embo J*, **22**, 2370-2379.
- Xu, C., Moellering, E.R., Fan, J. and Benning, C.** (2008) Mutation of a mitochondrial outer membrane protein affects chloroplast lipid biosynthesis. *Plant J*, **54**, 163-175.
- Xu, C., Moellering, E.R., Muthan, B., Fan, J. and Benning, C.** (2010) Lipid transport mediated by *Arabidopsis* TGD proteins is unidirectional from the endoplasmic reticulum to the plastid. *Plant Cell Physiol*, **51**, 1019-1028.
- Xu, C., Yu, B., Cornish, A.J., Froehlich, J.E. and Benning, C.** (2006) Phosphatidylglycerol biosynthesis in chloroplasts of *Arabidopsis* mutants deficient in acyl-ACP glycerol-3- phosphate acyltransferase. *Plant J*, **47**, 296-309.
- Yang, Y., Munz, J., Cass, C., Zienkiewicz, A., Kong, Q., Ma, W., Sanjaya, Sedbrook, J. and Benning, C.** (2015) Ectopic expression of WRINKLED1 affects fatty acid homeostasis in *Brachypodium distachyon* vegetative tissues. *Plant Physiol*, **169**, 1836-1847.

- Yang, Y., Zienkiewicz, A., Lavell, A. and Benning, C.** (2017) Coevolution of Domain Interactions in the Chloroplast TGD1, 2, 3 Lipid Transfer Complex Specific to Brassicaceae and Poaceae Plants. *Plant Cell*, **29**, 1500-1515.
- Zale, J., Jung, J.H., Kim, J.Y., Pathak, B., Karan, R., Liu, H., Chen, X.H., Wu, H., Candreva, J., Zhai, Z.Y., Shanklin, J. and Altpeter, F.** (2016) Metabolic engineering of sugarcane to accumulate energy-dense triacylglycerols in vegetative biomass. *Plant Biotechnol J*, **14**, 661-669.
- Zhai, Z., Keereetaweep, J., Liu, H., Feil, R., Lunn, J.E. and Shanklin, J.** (2018) Trehalose 6-phosphate positively regulates fatty acid synthesis by stabilizing WRINKLED1. *Plant Cell*, **30**, 2616-2627.
- Zhai, Z., Liu, H. and Shanklin, J.** (2017a) Phosphorylation of WRINKLED1 by KIN10 results in its proteasomal degradation, providing a link between energy homeostasis and lipid biosynthesis. *Plant Cell*, **29**, 871-889.
- Zhai, Z., Liu, H., Xu, C. and Shanklin, J.** (2017b) Sugar potentiation of fatty acid and triacylglycerol accumulation. *Plant Physiol*, **175**, 696-707.
- Zhang, Y. and Du, G.** (2009) Phosphatidic acid signaling regulation of Ras superfamily of small guanosine triphosphatases. *Bba-Mol Cell Biol L*, **1791**, 850-855.
- Zhang, Y., Zhu, H., Zhang, Q., Li, M., Yan, M., Wang, R., Wang, L., Welti, R., Zhang, W. and Wang, X.** (2009) Phospholipase dalpha1 and phosphatidic acid regulate NADPH oxidase activity and production of reactive oxygen species in ABA-mediated stomatal closure in Arabidopsis. *Plant Cell*, **21**, 2357-2377.

CHAPTER 3

A Predicted Plastid Rhomboid Protease Involved in Phosphatidic Acid Metabolism in *Arabidopsis thaliana*

This work has been further edited and is published in The Plant Journal (<https://onlinelibrary.wiley.com/journal/1365313x>).

Lavell, A., Froehlich, J.E., Baylis, O., Rotondo, A.D. and Benning, C. (2019) A predicted plastid rhomboid protease affects phosphatidic acid metabolism in *Arabidopsis thaliana*. *Plant J*, **99**, 978-987.

Abstract

The thylakoid membranes of the chloroplast harbor the photosynthetic machinery that converts light into chemical energy. Chloroplast membranes are unique in their lipid makeup, which is dominated by the galactolipids mono- and digalactosyldiacylglycerol (MGDG and DGDG). The most abundant galactolipid, MGDG, is assembled through both plastid and ER pathways in *Arabidopsis*, resulting in distinguishable molecular lipid species. Phosphatidic acid (PA) is the first glycerolipid formed by the plastid galactolipid biosynthetic pathway. It is converted to substrate diacylglycerol (DAG) for MGDG Synthase (MGD1) which adds to it a galactose from UDP-Gal. The enzymatic reactions yielding these galactolipids have been well established. However, auxiliary or regulatory factors are largely unknown. We identified a predicted rhomboid-like protease 10 (RBL10), located in plastids of *Arabidopsis thaliana*, that affects galactolipid biosynthesis likely through intramembrane proteolysis. Plants with T-DNA disruptions in *RBL10* have greatly decreased 16:3 (acyl carbons : double bonds) and increased 18:3 acyl chain abundance in MGDG of leaves. Additionally, *rb10-1* mutants show reduced [¹⁴C]-acetate incorporation into MGDG during pulse-chase labeling, indicating a reduced flux through the plastid galactolipid biosynthesis pathway. While plastid MGDG biosynthesis is blocked in *rb10-1* mutants, they are capable of synthesizing PA, as well as producing normal amounts of MGDG by compensating with ER-derived lipid precursors. These findings link this predicted protease to the utilization of PA for plastid galactolipid biosynthesis potentially revealing a regulatory mechanism in chloroplasts.

Introduction

Lipid biosynthesis in seed plants is initiated in the chloroplast where de novo fatty acid biosynthesis occurs. Glycerolipids are then assembled at the plastid envelope membranes and the endoplasmic reticulum (ER) (Li-Beisson *et al.*, 2013). Due to the distinct specificity of acyltransferases associated with the different membranes, the lipid species from each compartment have either a 16-carbon acyl chain at the *sn*-2 position (plastid) or an 18-carbon acyl chain (ER) (Browse *et al.*, 1986, Mongrand *et al.*, 1998). Phosphatidic acid (PA) is the initial glycerolipid to be assembled and then converted to other lipids. Through the use of both the chloroplast and ER lipid precursors for galactolipid biosynthesis, *Arabidopsis thaliana* maintains a specific 16:3/18:3 ratio of acyl chains (acyl carbons : double bonds) in its chloroplast MGDG molecules. We know the genes that encode the PA biosynthetic enzymes in the chloroplast that first acylate glycerol-P and then lysophosphatidic acid (Kunst *et al.*, 1988, Nishida *et al.*, 1993, Xu *et al.*, 2006) as well as the genes encoding the galactosyltransferase MGD1, which uses diacylglycerol (DAG) (Jarvis *et al.*, 2000, Awai *et al.*, 2001, Rocha *et al.*, 2016) derived from dephosphorylation of PA by a phosphatase. However, the gene encoding the PA phosphatase responsible for creating the bulk plastid DAG pool in vegetative tissues has only been tentatively identified (Nakamura *et al.*, 2007) and its topology within the inner envelope membrane has yet to be determined, although its activity has been measured in the chloroplast envelopes (Block *et al.*, 1983, Malherbe *et al.*, 1992). The likely location of the plastid PA biosynthetic enzymes on the inside of the inner chloroplast envelope membrane and the presence of the galactolipid biosynthetic enzyme MGD1 on the outer leaflet of the inner chloroplast envelope membrane (Xu *et al.*, 2005) poses the question

for the movement of PA and its conversion product as well as MGD1 substrate, DAG, through the inner envelope membrane. Due to its polarity, PA cannot freely flip between the membrane leaflets and a PA transporter may have to be invoked. In any case, the precise mechanism for providing MGD1 with prokaryotic substrate DAG for the biosynthesis of MGDG is not yet known. On the contrary, a likely mechanism for ER-derived PA insertion into the inner envelope membrane is through the action of the TGD complex, which is a multiprotein ABC transporter, TGD1, 2, 3, proposed to transport ER-assembled PA to the inner envelope membrane of the chloroplast (Xu *et al.*, 2005, Roston *et al.*, 2012, Yang *et al.*, 2017). TGD2, one component of the TGD1, 2, 3 complex contains a PA binding site and is physically located in the inner envelope membrane spanning the intermembrane space between the two envelope membranes (Awai *et al.*, 2006, Lu and Benning, 2009, Roston *et al.*, 2011). TGD4 is a PA-binding protein in the outer envelope membrane also involved in the process (Wang *et al.*, 2013). However, it should be noted that it has not yet been directly shown that PA is actually transported by the TGD proteins.

Thus, while we have a reasonable understanding of how lipid precursors produced at the ER are translocated to the inner envelope membrane and utilized for galactolipid biosynthesis, it is still unclear how chloroplast PA biosynthesis contributes plastid-derived precursors for galactolipid biosynthesis. Identifying genes encoding lipid transporters that could be involved in PA transfer from the stroma side to the intermembrane face of the inner envelope membrane may provide additional targets for the regulation of lipid assembly. One mechanism of regulation yet to be implicated in plant lipid metabolism is intramembrane proteolysis. We identified a candidate gene (At1g25290) encoding a

predicted intramembrane protease, rhomboid-like protein (RBL10) that appears to be involved in the regulation of chloroplast PA metabolism and transport.

Rhomboid-like protein 10 (RBL10) belongs to a superfamily of intramembrane proteases called rhomboids, with the founding member discovered in *Drosophila melanogaster* (Bier *et al.*, 1990). Members of this superfamily are multi-pass integral serine proteases found in nearly all organisms, and they typically serve regulatory roles. Aside from directly initiating a signaling cascade, as in the case of Rhomboid-1 and the epidermal-growth factor pathway (Lee *et al.*, 2001, Urban *et al.*, 2001), rhomboids can also influence assembly of complexes, for example *Providencia stuartii* rhomboid AarA, which processes TatA and directs the oligomerization of the twin arginine translocase complex used in quorum sensing (Stevenson *et al.*, 2007). In humans, rhomboids have been implicated in Parkinson's disease by maintaining mitochondrial integrity through proteolysis of Pink1 by the mitochondrial PARL protein, which affects Pink1 trafficking (Meissner *et al.*, 2011, Meissner *et al.*, 2015). Much like in mice and animals, 13 rhomboids have been predicted to exist in Arabidopsis (Lemberg and Freeman, 2007, Page and Di Cera, 2008), and although they have been compared to characterized animal rhomboids (Kanaoka *et al.*, 2005), a detailed molecular mechanism for any of them has yet to be described. Of the two rhomboid-like proteins predicted to be located in the chloroplast of Arabidopsis, only RBL10 seems to be involved in lipid metabolism based on our own observations. The second plastid rhomboid protease, RBL11, may have other functions that do not relate to lipid homeostasis. Here we describe in detail the analysis of *rb110* mutants and propose how an integral membrane protease may be involved in the metabolism or transport of PA in the Arabidopsis chloroplast.

Results and Discussion

Discovery of a Role for RBL10 in Chloroplast Lipid Metabolism

To investigate possible factors required for metabolism and trafficking of PA assembled in the chloroplast, the Chloroplast Phenomics 2010 database (Ajjawi *et al.*, 2010) was searched for T-DNA mutants showing a shift in the 16/18 carbon ratio in total leaf acyl composition. We predicted that reduced utilization of plastid PA would result in an overall decrease in 16:3 acyl chain abundance. One putative mutant was identified, and the gene disrupted in the T-DNA mutant line encodes a rhomboid-like protein located in the chloroplast (Fig. 3.1a). To corroborate that a mutation in this gene resulted in the observed lipid phenotype, we obtained additional T-DNA insertion mutants for *RBL10* (Fig. 3.1a). They showed decreased *RBL10* transcript abundance when amplifying a cDNA segment by qPCR (Fig. 3.1b). Analyzing the acyl composition of individual lipids using thin-layer chromatography (TLC) in combination with gas-liquid chromatography (GLC) it became apparent that the primary lipid bearing the acyl changes seen in the total lipid FA profile is MGDG (Fig. 3.1c). The ratio of 16:3 to 18:3 acyl chains in *rb10-1*, *rb10-2*, and *rb10-3* was reduced several fold, suggesting a predominance of ER precursors contributing to MGDG biosynthesis. Though each line tested is disrupted in a different location of the *RBL10* gene, all showed similar MGDG acyl compositional changes. Furthermore, the overall amount of MGDG in the mutant lines was slightly reduced compared to wild type but not statistically significant (Fig. 3.S1a). The changes in MGDG acyl composition were restored to wild-type levels by reintroducing an *RBL10* coding sequence into the different mutant alleles under the control of the 35S promoter (Fig.

3.1d). Based on this result we concluded that a disruption in RBL10 is the primary cause for the observed change in acyl composition in MGDG.

Since the chloroplasts of *Arabidopsis* appear to have a second predicted rhomboid-like protease, three independent T-DNA insertion lines disrupting *RBL11* (At5g25752) were analyzed for their total and MGDG acyl compositions. No changes in the acyl composition of *rb11* mutants were observed (Fig. 3.S2) and the analysis of this mutant was not further pursued in the context of this study.

JA and JA-Ile Levels are Affected in *rb10*

The changes seen in MGDG composition did not affect the overall plant appearance or growth under the standard lab conditions tested. Because RBL10 had tentatively been implicated in jasmonic acid (JA) signaling or metabolism, we quantified this hormone (Thompson *et al.*, 2012). Upon leaf wounding, the *rb10-1* and *rb10-2* mutant lines accumulated significantly less JA and the isoleucine derivative of JA, JA-Ile, at 20 minutes compared to wild type (Fig. 3.S3a, b) ($0.006 \geq p$, $0.004 \geq p$ and $0.044 \geq p$, $0.064 \geq p$ respectively). The amount of the JA precursor 12-Oxophytodienoic acid (OPDA) accumulated by the two lines at 20 minutes past wounding was not as reduced when compared to wild type (Fig. 3.S3c) ($0.081 \geq p$, $0.090 \geq p$). These changes are indicative of an attenuation of JA biosynthesis. Aside from generally normal vegetative growth under standard growth chamber conditions, it was previously reported that *rb10* mutants have altered pollen morphology, floral defects along with a reduced number of seeds filled per silique, and longer roots with more side branching (Thompson *et al.*, 2012). An attenuated biosynthesis of JA and JA-Ile could explain some of these reported phenotypes. In our

own work, we were able to corroborate the reduced number of seeds per silique of *rb110-1* as compared to wild type (Fig. 3.S4). At this time, the pollen, seed, and hormone phenotypes cannot be directly linked to altered galactolipid metabolism. However, Thompson et al. (Thompson *et al.*, 2012) suggested that possible disruptions of JA signaling might be the cause of the observed developmental changes in the *rb110* mutants and there is an increasing body of work demonstrating a relationship between chloroplast glycerolipid metabolism and JA biosynthesis (Lin *et al.*, 2016, Wang *et al.*, 2018).

RBL10 is Located in the Inner Envelope Membrane of Chloroplasts

The predicted structure of the *RBL10* transcripts of Arabidopsis suggests two splice forms as shown in Figure 1a. Previously, the subcellular targeting of RBL10 to the chloroplast was demonstrated with fluorescent tagging and chloroplast fractionation (Knopf *et al.*, 2012, Thompson *et al.*, 2012). Here, we further identified into which envelope membrane RBL10 is inserted. In-vitro translated RBL10.1 and RBL10.2 proteins labeled with ³H-Leucine were imported into pea chloroplasts. Fractionation experiments showed that both proteins are present in the chloroplast envelope membranes (Fig. 3.2a). To more precisely evaluate the subcellular localization of RBL10, we performed import and protease protection assays (Fig. 3.2b). We showed that imported RBL10.1 and 10.2 proteins are resistant to trypsin cleavage (Fig. 3.2b) unlike Toc33, a known outer envelope membrane-resident protein. Taken together, we conclude from these results that both versions of RBL10 specifically insert into the inner envelope membrane of the chloroplast. A homology model produced with SWISS protein using the crystal structure of GlpG, which has a 27% amino acid identity with RBL10, (Wang *et al.*, 2006), suggested

how the six transmembrane helices of RBL10 are oriented in the membrane (Fig. 3.2c), with the predicted active site serine and histidine residues close to the leaflet solvent interface. Since rhomboids are membrane-bound proteases, their substrate must be inserted into the same membrane in order for proteolysis to occur (Moin and Urban, 2012, Guo *et al.*, 2016). However, at this time a substrate protein remains to be identified that either directly or indirectly affects lipid metabolism.

ER-Assembled Lipids Serve as Primary Precursors for MGDG Biosynthesis in the *rbl10-1* Mutant

To probe the biochemical basis of the observed changes in MGDG acyl composition, pulse-chase radiolabeling experiments were performed. Detached leaves were floated on [¹⁴C]–acetic acid-containing buffer, which resulted in the incorporation of label into lipid acyl groups by de novo fatty acid synthesis. During the first hour after introducing the radiolabel (pulse), chloroplast lipid assembly was observed by lipid profiling using TLC of lipid extracts from the leaves and determining the incorporation of radiolabel into polar lipids (Fig. 3.3). Comparing the wild type and the *rbl10-1* mutant, less than half of the radiolabel was incorporated into MGDG in *rbl10-1*. The order (from high to low) of levels of incorporation of label into polar lipids during the pulse in wild type was MGDG, phosphatidylcholine (PC), phosphatidylglycerol (PG), PA, phosphatidylinositol (PI)/phosphatidylethanolamine (PE), sulfoquinovosyldiacylglycerol (SQDG), and DGDG respectively. In the *rbl10-1* mutant, this order was changed (from high to low): PC, PG, MGDG, PA, PI/PE, SQDG, and DGDG. In addition to the reduction of label in MGDG in *rbl10-1*, the level of label in PA was equal to that of MGDG at 20 minutes. In comparison,

wild-type leaves accumulated label in MGDG to a level three-fold of that accumulated in PA by 20 minutes. The chase, after the leaves were moved to new buffer containing only unlabeled acetate, showed no major differences in rates of turnover between wild-type and *rb110-1* leaves. Because there was label accumulating in PA and PG, as well as PC, we concluded that the chloroplast pathway is functional up to the step just prior to MGDG biosynthesis.

PA Synthesized in Chloroplasts is Used for PG Biosynthesis but not MGDG

Since MGDG biosynthesis can occur from both plastid and ER lipid precursors, [¹⁴C] – acetate feeding of intact, isolated chloroplasts should allow us to focus on only the plastid pathway reactions. In wild-type intact chloroplasts, radiolabel accumulated to the same levels in both PA and MGDG by 5 minutes, with MGDG accumulating the most label at all time points after 5 minutes (Fig. 3.4a). Intact *rb110-1* chloroplasts accumulated three times as much radiolabel in PA than in MGDG by 5 minutes, and MGDG never accumulated more label than PA or PG (Fig. 3.4a). Based on the TLC plate image (Fig. 3.4b), the differences in label accumulation between wild-type and *rb110-1* chloroplast lipids were striking, corroborating the data observed during the whole leaf pulse-chase experiment.

Figure 3.5a shows the different fates of PA in the chloroplast. Our interpretation of the labeling results was that MGDG biosynthesis from the chloroplast-derived precursor lipid PA is compromised in *rb110-1* mutant plants (Fig. 3.5aii, iii) while the biosynthesis of PG proceeds normally (Fig. 3.5ai).

MGD1 Activity is not Affected by Loss of RBL10

While *rb110-1* chloroplasts were not able to synthesize MGDG from de novo assembled PA, these chloroplasts were not compromised in MGD1 enzymatic activity when supplied with DAG and [¹⁴C] – UDP-galactose (Fig. 3.5B). The ability of *rb110-1* chloroplasts to utilize exogenous MGD1 substrates along with only slightly reduced overall MGDG levels, but altered acyl composition in the *rb110* mutant plants, supports the hypothesis that there is a shift in in the mutants in the utilization of lipid precursors to predominantly ER lipid precursors for MGDG biosynthesis. This shift has also been previously observed for the *ats1* mutant disrupted in the chloroplast glycerol-3-phosphate acyl transferase leading to the formation of lysophosphatidic acid (Kunst *et al.*, 1988). However, in the *ats1* mutant, the effect was less specific to MGDG and chloroplast PG levels are reduced as well. This again speaks for a disruption after the formation of chloroplast PA but prior to MGDG assembly in the *rb110-1* mutant. Therefore, we tested the activity of PA phosphatase activity next.

PA Plastid Phosphatase Activity is Increased in rb110-1 Mutants

To further narrow the possible protein targets affected by the disruption of the *RBL10* gene (Fig. 3.5a), we tested the activity of the PA phosphatase by using [¹⁴C]–PA and mixed inner and outer envelope membranes from wild-type and *rb110-1* chloroplasts. To our surprise, the envelope membranes of *rb110-1* chloroplasts dephosphorylated PA to diacylglycerol at a higher rate than the wild-type membrane preparations, with 11% and 8% conversion at 30 minutes respectively (Fig. 3.5c). Our initial hypothesis was an impaired conversion of PA to MGDG in chloroplasts due to a reduction in PA phosphatase

activity. However, we concluded based on our data that the changes in plastid PA utilization was not due to compromised PA phosphatase activity. Plastid PA is synthesized by two acyltransferases, ATS1 present in the stroma (Xu *et al.*, 2006) and ATS2 likely associated with the stroma side of the inner envelope membrane (Yu *et al.*, 2004). Therefore, we propose that the physical translocation of PA from its place of synthesis by the two acyltransferases ATS1 and ATS2 on the inner leaflet of the inner envelope membrane to its intermembrane-facing leaflet, where presumably the PA phosphatase and, for certain, the MGD1 synthase are located, is disrupted in the *rb110-1* mutant.

A Refined Model of PA Metabolism in Arabidopsis Chloroplasts

To describe this system, it seems instructive to draw parallels with the ER phospholipid transporter ALA10, which is reported to form a complex with the ER desaturases FAD2/FAD3 to modulate the balance between PC and MGDG (Botella *et al.*, 2016). Hence, it seems plausible that a PA transporter could be in complex with the plastid PA biosynthetic enzymes and possibly even the PA phosphatase, resulting in substrate channeling. In our refined model (Fig. 3.6), we accommodate our current knowledge (Hurlock *et al.*, 2014) about the transport of ER-derived PA from the ER through the outer to the inner envelope membrane by the TGD complex (Fig. 3.6a). In addition, we hypothesize that a not yet identified transporter assists in the transfer of chloroplast-assembled PA from the inside of the inner envelope membrane, where it is synthesized, to its intermembrane space-facing leaflet, where it is converted to DAG and ultimately MGDG (Fig. 3.6b). There are currently at least three predictions based on this hypothesis

that need to be satisfied for the model to be correct: 1. The plastid PA phosphatase must be associated with the intermembrane space-facing leaflet of the inner envelope membrane, which would give it access to ER-derived and chloroplast-derived PA precursors for DAG and ultimately MDGD biosynthesis. 2. A transporter must exist that either can flip or channel chloroplast assembled PA through the inner envelope membrane. 3. RBL10 must affect the assembly or insertion of this transporter and associated proteins in the inner envelope membrane.

Aside from testing the hypothesis outlined above, it will be important to actually demonstrate that RBL10 acts as an intramembrane protease. Reconstituting and assaying a six-transmembrane integral protein is challenging. Moreover, even though numerous synthetic rhomboid substrates have been identified and can serve as substrates for diverse rhomboids, finding true *in vivo* substrates for rhomboids has not been trivial in the past. Even for the well-studied rhomboid, GlpG from *E. coli*, the only crystallized rhomboid (Wang *et al.*, 2006), the native substrate remains unknown. Absent of our knowledge of a native RBL10 substrate, it will be difficult to distinguish whether RBL10 directly processes components of a PA-transport/synthesis complex in the inner chloroplast envelope membrane, or whether it releases a signaling peptide that could indirectly affect this process. The list of potential protein interactors/substrates of RBL10 is vast, even though a previous proteomic analysis of an RBL10/RBL11 double mutant (Knopf *et al.*, 2012) may provide a starting point.

An intriguing feature of rhomboids is the nature of their substrate recognition, which is determined by the topology of the substrate in the membrane rather than a specific protein sequence (Urban and Freeman, 2003). Even though rhomboids do not recognize

a consensus sequence, their substrate recognition mechanism offers surprising specificity for their transmembrane helix substrates. Moreover, rhomboids scan for their substrate moving through membranes at biologically relevant rates due to the nature of their interaction with the membrane (Kreutzberger *et al.*, 2019). Unfortunately, the lack of a concrete cleavage consensus site poses a challenge when searching for an endogenous substrate and ultimately a molecular mechanism to explain the observed *rb10* lipid phenotypes. However, our current data point towards a testable working hypothesis that should allow us to narrow down the substrate for RBL10 in the future.

Materials and Methods

T-DNA Lines

Seeds for T-DNA lines used were obtained from the Arabidopsis Biological Resource Center (ABRC). The lines SALK_036100, SALK_037037, and SALK_092293 were denoted as *rb10-1*, *rb10-2*, and *rb10-3* in this study respectively.

Plant Growth Conditions

Seeds were sown directly into soil for lipid analysis and pulse-chase labeling. Plants were grown in a growth chamber at 22°C, a 16-hour light/8-hour dark cycle, and with approximately 120 μmol of light. For isolation of chloroplasts and envelopes, Arabidopsis seeds were sterilized and grown on Murashige and Skoog (MS) agar-solidified medium in Percival growth chambers at 22°C, a 16 hours light/8 hours dark cycle, and 120 μmol of light.

DNA Constructs and Complementation

The RBL10, splice variant AT1G25290.2, coding sequence was amplified from cDNA. Plant RNeasy Mini Kit (Qiagen, www.qiagen.com) was used to extract mRNA of Col-0 plants including the optional on-column DNase digestion, following reverse transcription with SuperScript III Reverse transcriptase (Invitrogen, www.thermofisher.com) and its corresponding first strand synthesis protocol, excluding RNaseOUT (recombinant RNase inhibitor). Full length coding sequence excluding stop codon was amplified using Phusion High-Fidelity DNA polymerase (Thermo Scientific, www.thermofisher.com) and gel-purified. The amplicon was directionally inserted into a Gateway pENTR/D/TOPO entry vector (Invitrogen) and sequence verified vector was linearized using PvuI restriction enzyme (New England Biolabs, www.neb.com) and gel purified. The linear vector was recombined with the pEARLEYGATES101 expression vector using the gateway LR Clonase II kit (Invitrogen). The resulting construct was introduced into *Agrobacterium tumefaciens* GV3101 and used to complement the *rb10-1* mutant plants using the floral dip method and BASTA (glufosinate-ammonium, BASF, www.basf.com) selection (Logemann *et al.*, 2006).

Homology Modeling

Swiss Model software was used to generate a homology model of RBL10 (Biasini *et al.*, 2014) based on the published crystal structure of GlpG (*E. coli*) (Dickey *et al.*, 2013) deposited at the Protein Data Bank (4NJJ). Protein structure further processed in PyMol.

Intact Chloroplast Isolation

Arabidopsis seedlings were plate-grown on agar-solidified MS medium in a dense lawn and harvested at 3-weeks of age and intact chloroplasts were isolated following the protocol in (Cline and Keegstra, 1983) with modifications. Plant tissue was homogenized with a polytron in a grinding buffer at pH7.3 (330mM Sorbitol, 50mM HEPES, 1mM MgCl₂, 1mM MnCl₂, 2mM EDTA, 0.1% BSA), filtered through miracloth, and crude chloroplasts were pelleted at 700xg. The pellet was resuspended and loaded on a continuous Percoll gradient (generated by centrifugation at 39,000 x g, 30 mins, no brake). Intact chloroplasts were collected from the lower phase of the gradient after centrifugation at 2620 x g for 10 mins without braking. Intact chloroplasts were washed twice in an import buffer of pH 8.0 (330mM Sorbitol, 50mM HEPES) and yield approximated by chlorophyll equivalents.

Mixed envelopes were isolated by rupturing purified intact chloroplasts as above using a Dounce homogenizer (Wheaton 15mL) in TE (10mM Tricine pH 7.5, 2mM EDTA) buffer with 0.6M sucrose. Thylakoid membranes were separated by centrifugation of the lysed chloroplast solution at 1,500xg for 5 minutes, repeated 3 times by transferring the supernatant to a new tube each time. The entire volume of supernatant was combined and centrifuged at 100,000xg for 1 hours to collect the remaining inner and outer membranes. The resulting pellet of envelope membranes was then resuspended in approximately 100 μ L of PAP assay buffer and the protein content of each prep was quantified using an RCDC protein quantification kit (Bio-rad).

For in vitro import assays, intact pea chloroplasts were isolated from 8 to 12 day-old pea seedlings (Little Marvel, Dwarf Variety, Livingston Seed Co., Columbus, OH 43216) and purified over a Percoll gradient as previously described (Bruce, 1994). Intact

pea chloroplasts were re-isolated and resuspended in import buffer (330 mM sorbitol, 50 mM Hepes/KOH, pH 8.0) at a concentration of 1 mg chlorophyll per mL.

In Vitro Translation of precursor proteins

Precursor proteins used in import assays were radiolabeled using [³H]-Leucine (approximately 0.05mCi/50µl Translation Reaction is used) and translated using Promega's TNT® Coupled Reticulocyte Lysate System according to the manufacturer's protocol. After translation, labeled precursors were diluted with an equal volume of 'cold' 50mM L-Leucine in 2X Import Buffer (IB).

Import and Protease Protection Assays

Import assays were performed essentially as described in Tripp et al. (Tripp *et al.*, 2007). Essentially: 100 µl chloroplasts (1mg chlorophyll/ml), 4 mM Mg-ATP/IB final concentration, and 100 µl radio-labeled precursor protein to a final volume of 300 µl was incubated for 30 minutes at room temperature, under room light. After import, the reaction was divided into two 150 µl aliquots. One portion was not further treated with protease [(-) control] and intact chloroplasts were directly recovered by centrifugation through a 40% Percoll cushion. The other portion was incubated with Trypsin as previously described (Tripp *et al.*, 2007) for 30 minutes on ice. After quenching Trypsin with Trypsin Inhibitor, chloroplasts were again recovered by centrifugation through a 40% Percoll cushion, lysed and then fractionated into a total soluble (S) and total membrane fraction (P).

Fractionation of Imported RBL10

The membrane association of RBL10.1 and RBL10.2 was determined by performing a large-scale import assays and subsequent fractionation experiments. Briefly, either [³H]-Leucine labeled RBL10.1 or RBL10.2 were incubated with chloroplasts using a large-scale version of our import assay. After import, intact chloroplast were recovered, lysed and applied to a sucrose step-gradient according to the method of Li et al. (Li *et al.*, 2017) and fractionated into envelope membranes (E), stroma (S) and thylakoid membranes (T). All fractions were analyzed by SDS-PAGE and fluorography. Controls: Toc33, outer envelope membrane protein; FtsH8, thylakoid membrane protein and mature small subunit of Rubisco (mSSU), stroma protein. Note: The RBL10.1 and RBL10.2 fluorograms were exposed to film 3X longer than control samples.

Lipid Analysis

Lipids were extracted from detached Arabidopsis rosette leaves as well as isolated chloroplasts and prepared for Gas-Liquid Chromatography (GLC) following Wang et al, 2011 (Wang and Benning, 2011). Polar lipids were separated using a silica TLC plate treated with (NH₄)₂SO₄ and an acetone:toluene:water (91:30:7 v/v) solvent system. Lipid bands were visualized with brief iodine vapor staining. Individual lipids were scraped, and their fatty acid profiles analyzed using GLC. Composition is presented as a mole percentage of total fatty methyl esters detected in each lipid.

Radiolabeling

Pulse-chase labeling was performed with detached four-week old Arabidopsis leaves floated on 25mM 4-Morpholineethanesulfonic acid hemisodium salt (MES-KOH) (pH 5.7), 0.01% TritonX-100 buffer. A table top light (25 Watts at 5.5 cm distance) was used to stimulate lipid biosynthesis. De novo fatty acid synthesis was observed by pulsing with 120 μ Ci of [1,2- 14 C] - acetic acid sodium salt (ARC 0173 - American Radiolabeled Chemical, Inc.) for an hour, washing the leaves with same MES buffer without radiolabel twice, and the chase was performed by continuing to incubate leaves in the MES buffer without radiolabel. At each time point measured, a single leaf was taken, and lipids were extracted for TLC separation. Incorporation of radioactivity was imaged/measured by exposing a Kodak phosphoscreen with the TLC plate and scanning the screen with Quantity One software. Quantification of radioactivity in lipids was also performed by scraping the silica off the TLC plate containing the lipid band and counting using a Liquid Scintillation Counter (LSC) and 4a20 counting cocktail (Research Products International, www.rpicorp.com).

Isolated Arabidopsis chloroplasts were fed with [1,2- 14 C] - acetic acid (ARC 0173, American Radiolabeled Chemical, Inc.) to measure plastid lipid biosynthesis only. Chloroplasts were exposed to table top light to stimulate lipid synthesis, aliquots were taken from each sample at various time points and placed directly into lipid extraction buffer. Lipids were separated with TLC and quantified with a LSC and Quantity One Software.

Intact Arabidopsis chloroplasts were isolated and fed [1- 14 C] – UDP- galactose (ARC 3472, American Radiolabeled Chemical, Inc.) to measure plastid MGD1 activity.

About 0.30 μCi of activity per 220 μg of chlorophyll equivalents was used. Chloroplasts were resuspended in assay buffer pH7.6 (330mM Sorbitol, 50mM Hepes, 1mM MgCl_2 , 1mM MnCl_2 , 5mM EDTA) with 100 μM DAG (1,2-Dioleoyl, Sigma Aldrich D0138), exposed to table top light to stimulate lipid synthesis, and aliquots were taken from each sample at 3,10 and 30 minute time points and placed directly into lipid extraction buffer. Lipids were extracted and separated with polar TLC as described in lipid analysis section above, and then quantified with LSC and Quantity One.

Arabidopsis mixed chloroplast envelopes were used to assay for phosphatidic acid phosphatase activity. Equal amounts of protein were incubated with di[oleoyl-1- ^{14}C] - phosphatidic acid (ARC 1303, American Radiolabeled Chemical, Inc.). Envelope preparation done as described in this study and the PAP assay was performed as in (Xu *et al.*, 2005). Lipids were extracted and separated with TLC and radioactivity in TAG was quantified by LSC.

Acknowledgement

Anna Hurlock, Dr. Patrick Horn, Kun Wang, and Dr. Yang Yang provided advice and useful discussions that aided this work. Dr. John Froehlich performed the chloroplast import assays, contributing to Figure 3.1. Financial support for this work was primarily from the Division of Chemical Sciences, Geosciences and Biosciences, Office of Basic Energy Sciences of the United States Department of Energy (Grant DE-FG02-91ER20021). In addition, Anastasiya Lavell was supported in part by a predoctoral training grant from the National Institute of General Medical Sciences of the National Institutes of Health (Grant Number T32-GM110523).

APPENDICES

APPENDIX 3A

Main Text Figures

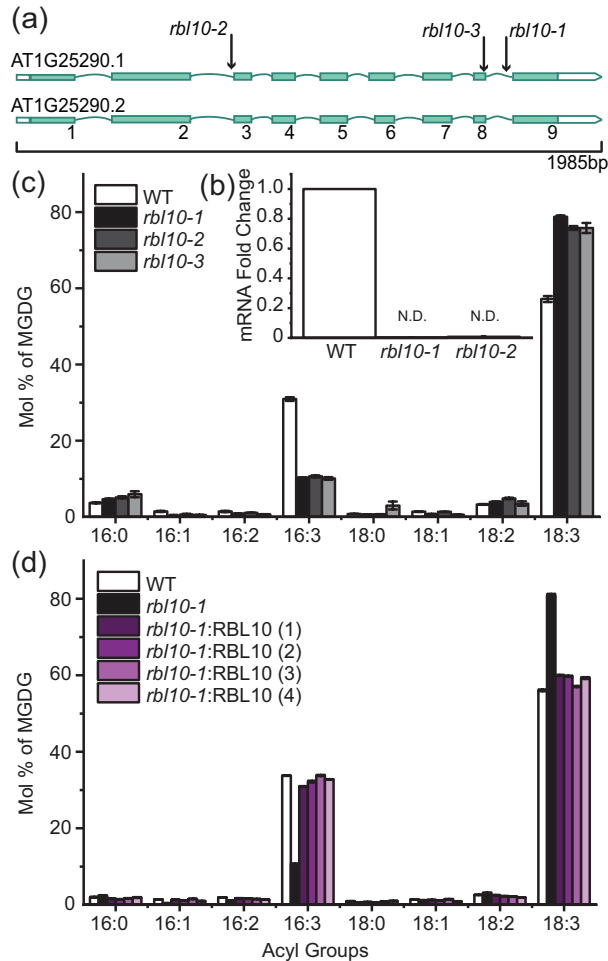


Figure 3.1. Structure and phenotypes of *rbl10* mutant alleles.

(a) Gene model of *RBL10* and the two splice forms (At1g25290.1 and At1g25290.2), where in At1g25290.2 exon 6 has 21 fewer nucleotides at the exon's 5' end. Positions of the T-DNA insertions in the mutant lines used in this study are shown on the gene model. (b) Quantitative PCR showing reduction in *RBL10* gene transcript abundance amplified from cDNA prepared from the *rbl10-1* and *rbl10-2* knock-out mutants (closed bar) or wild type (WT) (open bar) n=4. (c) Acyl composition of MGDG (carbon # : double bond #) measured in the three *rbl10* alleles and WT, showing decreased 16:3 and increased 18:3 relative acyl chain abundance in the mutants n=3. (d) WT acyl chain composition of MGDG restored by expression of the *RBL10* coding sequence driven by a 35S promoter in the *rbl10-1* background n=3. Error bars report SE but are in most cases too small to show.

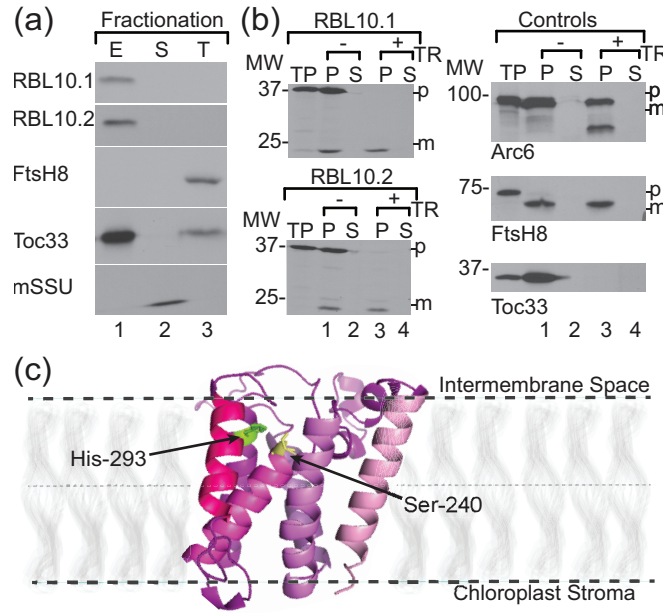


Figure 3.2. Localization of RBL10 to the Inner Envelope Membrane of Chloroplast.

(a) The RBL10 protein was labeled with [³H]-Leucine, imported into chloroplast and subsequently fractionated into various subcellular compartments. The presence of the protein exclusively in the envelope “E”, but not in the stroma “S” or thylakoid “T” fractions confirms its localization. (b) Import and protease protection assays further confirmed that RBL10 was specifically localized to inner envelope membrane. Resistance of imported RBL10 to trypsin (+) digestion is indicated by the presence of a band in the pellet fraction “P”, thus confirming that RBL10 is deeply imbedded into the inner envelope membrane. (c) Homology model of RBL10 made with SwissModel using the GlpG crystal structure as a template (PDB 4njn.1.A). Membrane boundaries are shown for illustration purposes only, predicted catalytic serine and histidine residues are shown in yellow and green respectively.

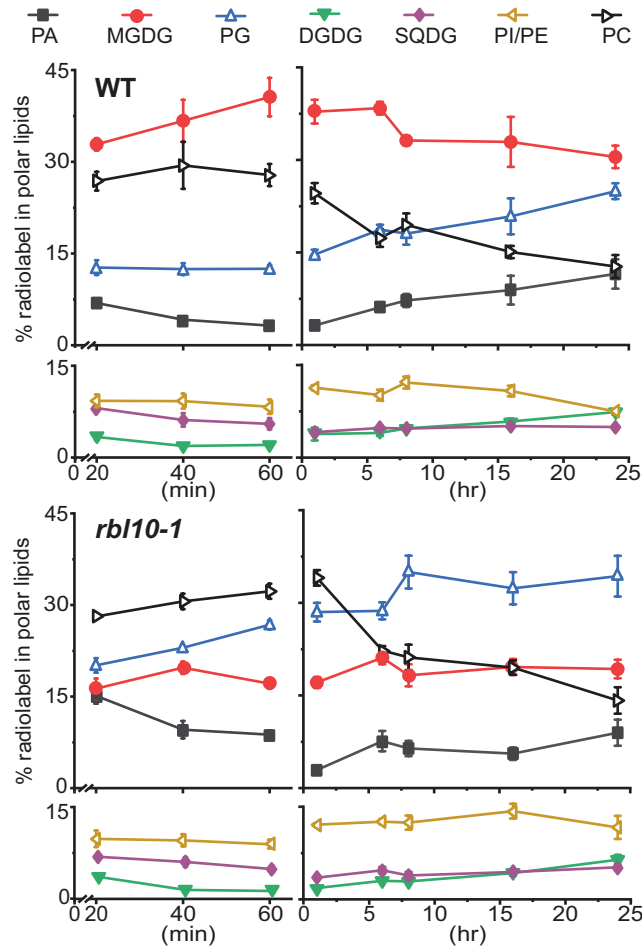


Figure 3.3. Radiolabeled pulse chase of detached leaves using ^{14}C -acetic acid. A decrease in incorporation of radioactivity into MGDG and increased incorporation into PG and PA of the *rbl10-1* mutant (bottom panels) compared to the wild type (WT, top panels) is shown $n=3$. Error bars report SE but are often smaller than the symbol. Abbreviations: DGDG, digalactosyldiacylglycerol; MGDG, monogalactosyldiacylglycerol; PA, phosphatidic acid; PC, phosphatidylcholine; PG., phosphatidylglycerol; PI/PE, phosphatidylinositol/phosphatidylethanolamine; SQDG, sulfoquinovosyldiacylglycerol.

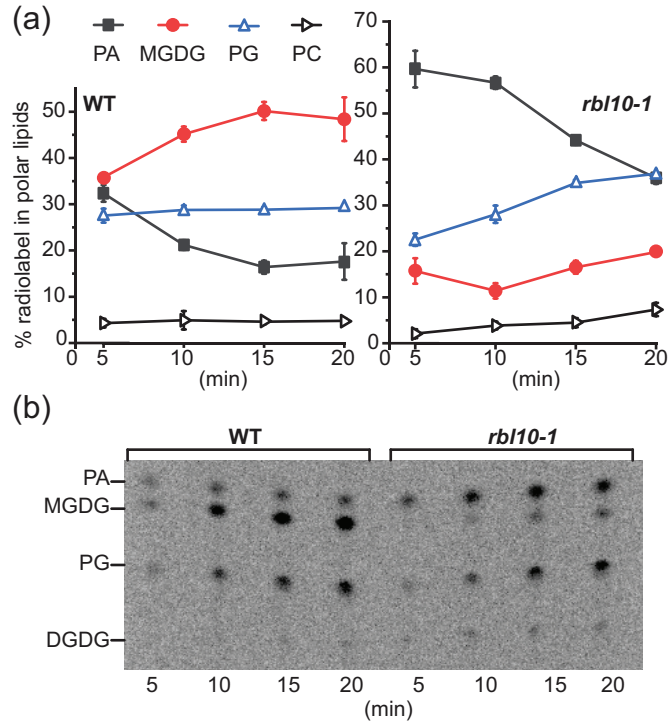


Figure 3.4. Labeling of isolated chloroplasts of *rbl10-1* mutant and WT with ^{14}C -acetate. (a) Labeling time course with isolated chloroplasts of *rbl10-1* (right panel) showing an increased ^{14}C -acetate accumulation into PA with an apparent conversion of PA into PG compared to wild type (WT, a, left) which appears to convert PA to MGDG $n=3$. Error represent SE and are often smaller than the labels. (b) TLC image of the extracted lipids of the chloroplasts labeled with ^{14}C -acetate in (a), one representative of three. The accumulation of radiolabel into MGDG of WT chloroplasts is approximately twice the accumulation of radiolabel into MGDG for *rbl10-1* chloroplasts. The chloroplasts of both mutant and WT appear to be capable of converting PA to PG. Abbreviations of lipids as in the Figure 3 legend.

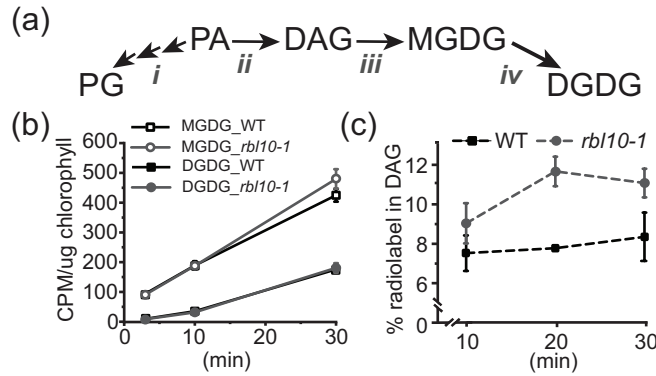


Figure 3.5. Probing PA metabolism in *rbl10-1*. (a) Overview of plastid PA metabolism. PA can be converted to PG (ai) or is dephosphorylated to supply diacylglycerol (DAG) pool (a_{ii}) for galactolipid biosynthesis (a_{iii}, iv). It is important to note that DGDG biosynthesis favors precursors from the ER pathway not shown here (a_{iv}). (b) Activity of the galactolipid enzymes MGD1 and DGD1 in isolated chloroplast using labeled UDP-Gal as precursor. They synthesize MGDG and DGDG respectively and are both functional at wild-type (WT) levels in *rbl10-1* isolated chloroplasts n=3. (c) Phosphatase activity of envelope membranes supplied with ¹⁴C-PA n=3. While *rbl10-1* chloroplasts cannot readily convert *de novo* synthesized PA to MGDG, mixed envelopes of this mutant showed an elevated PA phosphatase activity. Error bars report SE. Error bars are often smaller than the symbols.

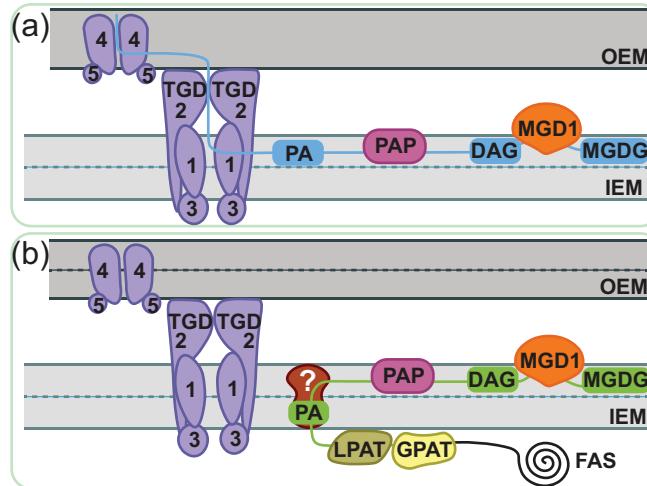


Figure 3.6. Proposed model of PA metabolism in the chloroplast envelope membranes. (a) Fate of PA assembled at the ER and imported back to the plastid. (b) Fate of PA assembled and metabolized in the plastid. Both panels depict ER and plastid PA serving as a substrate for the same PA phosphatase in the intermembrane space leaflet of the inner membrane of the chloroplast. The import of ER sourced PA is hypothesized to be facilitated by the TGD complex in the plastid outer and inner envelope membranes (a). The plastid PA is assembled on the stromal side of the inner envelope membrane. A transport mechanism is proposed, which translocates PA and inserts it into the leaflet of the inner membrane facing the intermembrane space (b). The *rbl10* mutant phenotype can be explained assuming that RBL10 is critical for the function of the inner envelope PA transporter.

APPENDIX 3B

Supplementary Figures

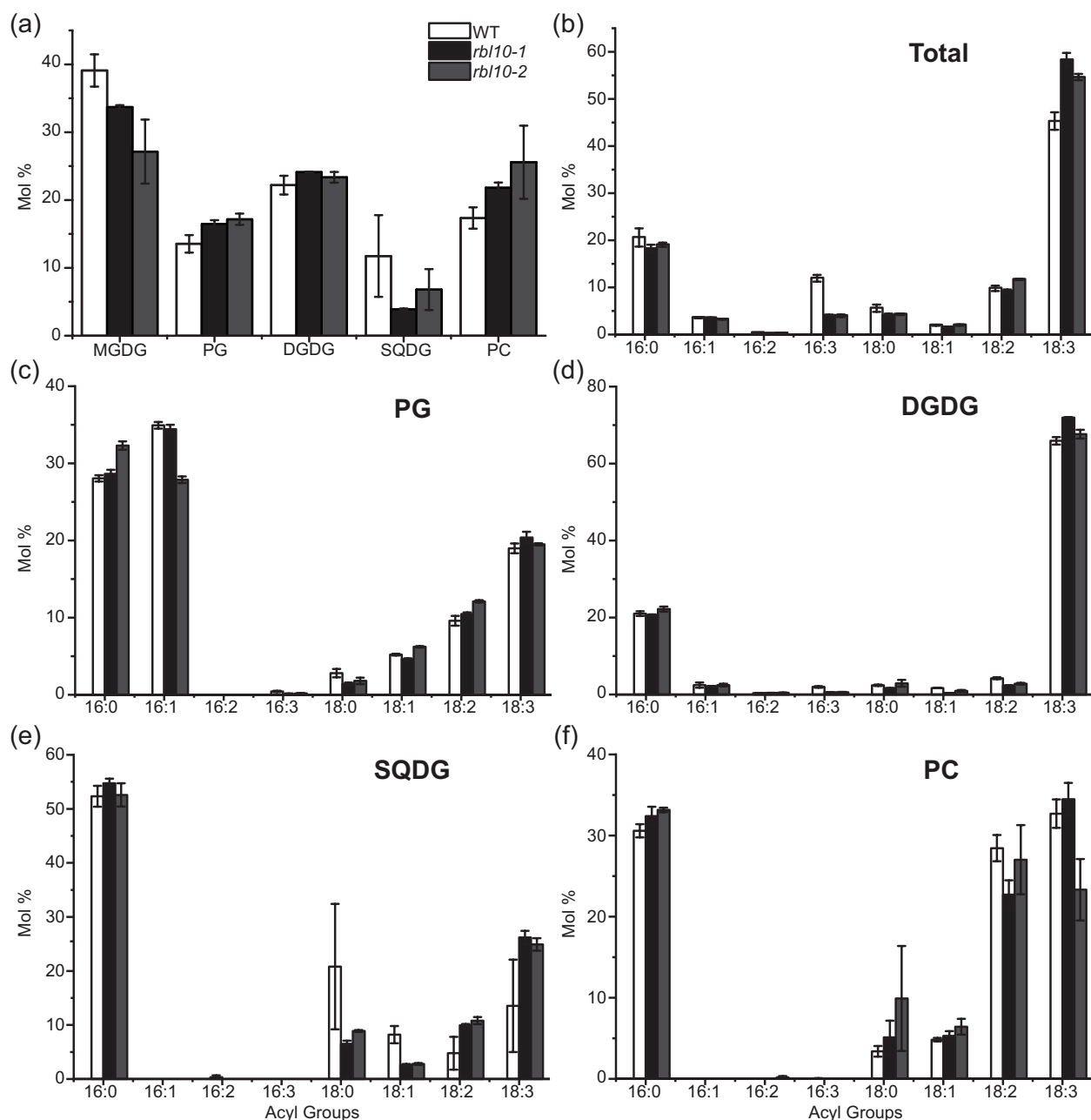


Figure 3.S1. Full lipid analysis of wild-type (WT) and *rbl10* leaves. (a) Polar lipid profile of WT, *rbl10-1* and *rbl10-2* leaves as a mole percentage of the measured polar lipids. Although MGDG appears slightly reduced in the mutant lines, this difference is not significant at the 0.05 level based on a two-tailed t-test (WT compared to *rbl10-1* $0.087 \geq p$ and *rbl10-2* $0.086 \geq p$). Acyl compositions of total lipid extract (b), PG (c), DGDG (d), SQDG (e), and PC (f) are shown for wild type (WT) and the *rbl10-1* and *rbl10-2* mutant lines ($n=3$). Error bars report SE. Abbreviations of lipids are as defined in the legend of Figure 3.

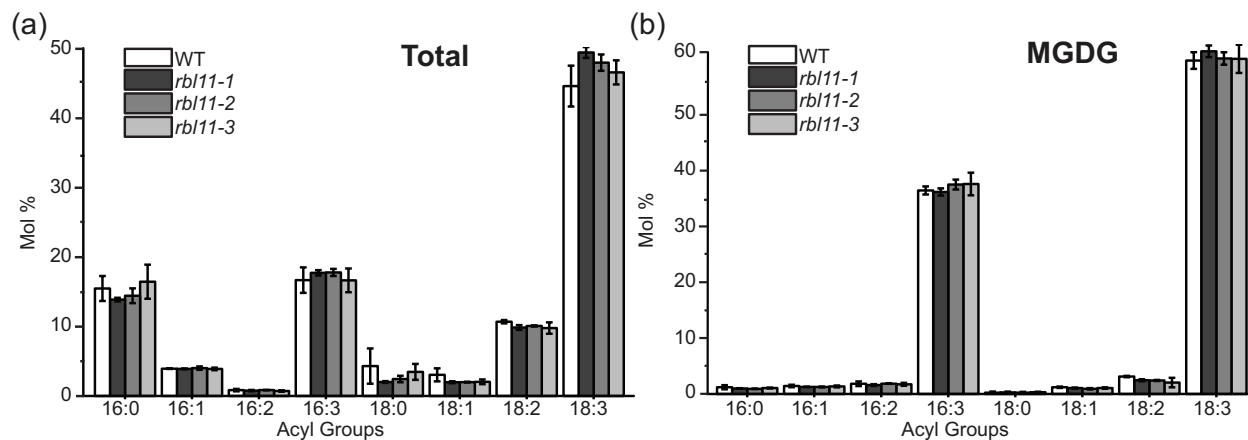


Figure 3.S2. Acyl composition of *rbl11* total leaf lipids and MGDG. (a) Total leaf lipids and (b) MGDG (carbon # : double bond #), measured in three independent *rbl11* alleles and WT, showing no change in 16:3 and 18:3 relative acyl chain abundance in the mutants compared to WT n=3. Error bars report SE.

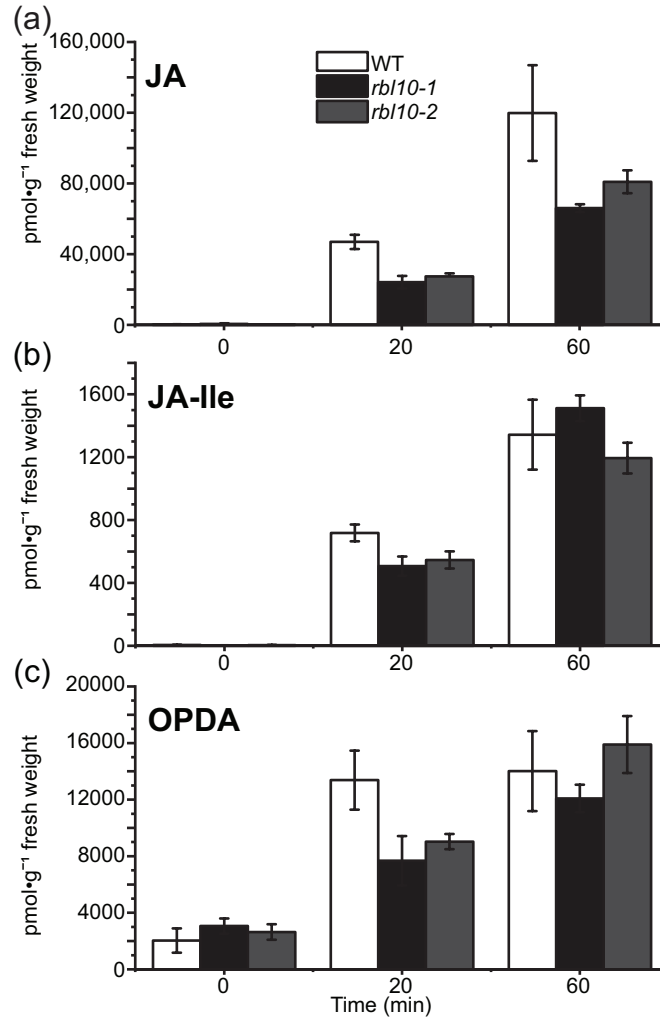


Figure 3.S3. Changes in oxylipin levels in the *rb10* mutants. (a) LC-MS shows that *rb10-1* and *rb10-2* mutant lines accumulate significantly less jasmonic acid (JA) and (b) JA-Ile at 20 minutes after leaf wounding compared to wild type (WT, $0.006 \geq p$, $0.004 \geq p$ and $0.044 \geq p$, $0.064 \geq p$ respectively). (c) Both mutant lines accumulated less 12-Oxophytodienoic acid (OPDA) at 20 minutes after wounding than WT but not to a significant difference at the 0.05 level ($0.081 \geq p$, $0.090 \geq p$ respectively). Error bars represent SE, all panels ($n=4$); a two-tailed t-test was applied.

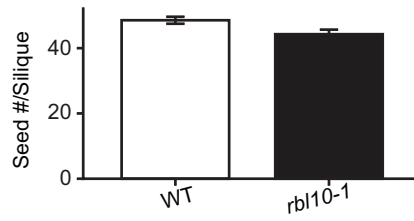


Figure 3.S4. Seed phenotypes of *rbl10* plants. Mature *rbl10* plants had fewer seeds per silique than WT at a significance level of 0.05 ($0.02 \geq p$; $n=20$) based on a two-tailed t-test.

REFERENCES

REFERENCES

- Ajjawi, I., Lu, Y., Savage, L.J., Bell, S.M. and Last, R.L.** (2010) Large-Scale Reverse Genetics in Arabidopsis: Case Studies from the Chloroplast 2010 Project. *Plant Physiology*, **152**, 529-540.
- Awai, K., Marechal, E., Block, M.A., Brun, D., Masuda, T., Shimada, H., Takamiya, K., Ohta, H. and Joyard, J.** (2001) Two types of MGDG synthase genes, found widely in both 16:3 and 18:3 plants, differentially mediate galactolipid syntheses in photosynthetic and nonphotosynthetic tissues in Arabidopsis thaliana. *Proc Natl Acad Sci U S A*, **98**, 10960-10965.
- Awai, K., Xu, C., Tamot, B. and Benning, C.** (2006) A phosphatidic acid-binding protein of the chloroplast inner envelope membrane involved in lipid trafficking. *Proc Natl Acad Sci U S A*, **103**, 10817-10822.
- Biasini, M., Bienert, S., Waterhouse, A., Arnold, K., Studer, G., Schmidt, T., Kiefer, F., Gallo Cassarino, T., Bertoni, M., Bordoli, L. and Schwede, T.** (2014) SWISS-MODEL: modelling protein tertiary and quaternary structure using evolutionary information. *Nucleic Acids Res*, **42**, W252-258.
- Bier, E., Jan, L.Y. and Jan, Y.N.** (1990) rhomboid, a gene required for dorsoventral axis establishment and peripheral nervous system development in Drosophila melanogaster. *Genes Dev*, **4**, 190-203.
- Block, M.A., Dorne, A.J., Joyard, J. and Douce, R.** (1983) The Phosphatidic-Acid Phosphatase of the Chloroplast Envelope Is Located on the Inner Envelope Membrane. *Febs Letters*, **164**, 111-115.
- Botella, C., Sautron, E., Boudiere, L., Michaud, M., Dubots, E., Yamaryo-Botte, Y., Albrieux, C., Marechal, E., Block, M.A. and Jouhet, J.** (2016) ALA10, a Phospholipid Flippase, Controls FAD2/FAD3 Desaturation of Phosphatidylcholine in the ER and Affects Chloroplast Lipid Composition in Arabidopsis thaliana. *Plant Physiology*, **170**, 1300-1314.
- Browse, J., McCourt, P. and Somerville, C.** (1986) A mutant of Arabidopsis deficient in c(18:3) and c(16:3) leaf lipids. *Plant physiology*, **81**, 859-864.
- Bruce, B.P., S; Froehlich, J; Keegstra, K** (1994) *In vitro* import of proteins into chloroplasts. In *Plant Mol Biol Man* (Gelvin, S.S., RA ed: Springer, Dordrecht.
- Cline, K. and Keegstra, K.** (1983) Galactosyltransferases involved in galactolipid biosynthesis are located in the outer membrane of pea chloroplast envelopes. *Plant physiology*, **71**, 366-372.

- Dickey, S., Baker, R., Cho, S. and Urban, S.** (2013) Proteolysis inside the membrane is a rate-governed reaction not driven by substrate affinity. *Cell*, **155**, 1270-1281.
- Guo, R., Gaffney, K., Yang, Z., Kim, M., Sungsuwan, S., Huang, X., Hubbell, W.L. and Hong, H.** (2016) Steric trapping reveals a cooperativity network in the intramembrane protease GlpG. *Nat Chem Biol*, **12**, 353-360.
- Hurlock, A.K., Roston, R.L., Wang, K. and Benning, C.** (2014) Lipid trafficking in plant cells. *Traffic*, **15**, 915-932.
- Jarvis, P., Dormann, P., Peto, C.A., Lutes, J., Benning, C. and Chory, J.** (2000) Galactolipid deficiency and abnormal chloroplast development in the Arabidopsis MGD synthase 1 mutant. *Proc Natl Acad Sci U S A*, **97**, 8175-8179.
- Kanaoka, M.M., Urban, S., Freeman, M. and Okada, K.** (2005) An Arabidopsis Rhomboid homolog is an intramembrane protease in plants. *Febs Lett*, **579**, 5723-5728.
- Knopf, R.R., Feder, A., Mayer, K., Lin, A., Rozenberg, M., Schaller, A. and Adam, Z.** (2012) Rhomboid proteins in the chloroplast envelope affect the level of allene oxide synthase in Arabidopsis thaliana. *Plant J*, **72**, 559-571.
- Kreutzberger, A.J.B., Ji, M., Aaron, J., Mihaljevic, L. and Urban, S.** (2019) Rhomboid distorts lipids to break the viscosity-imposed speed limit of membrane diffusion. *Science*, **363**, 10.1126/science.aao0076.
- Kunst, L., Browse, J. and Somerville, C.** (1988) Altered regulation of lipid biosynthesis in a mutant of Arabidopsis deficient in chloroplast glycerol-3-phosphate acyltransferase activity. *Proc Natl Acad Sci U S A*, **85**, 4143-4147.
- Lee, J.R., Urban, S., Garvey, C.F. and Freeman, M.** (2001) Regulated intracellular ligand transport and proteolysis control EGF signal activation in Drosophila. *Cell*, **107**, 161-171.
- Lemberg, M.K. and Freeman, M.** (2007) Functional and evolutionary implications of enhanced genomic analysis of rhomboid intramembrane proteases. *Genome research*, **17**, 1634-1646.
- Li, Y., Martin, J.R., Aldama, G.A., Fernandez, D.E. and Cline, K.** (2017) Identification of putative substrates of SEC2, a chloroplast inner envelope translocase. *Plant Physiol*, **173**, 2121-2137.
- Li-Beisson, Y., Shorrosh, B., Beisson, F., Andersson, M.X., Arondel, V., Bates, P.D., Baud, S., Bird, D., Debono, A., Durrett, T.P., Franke, R.B., Graham, I.A., Katayama, K., Kelly, A.A., Larson, T., Markham, J.E., Miquel, M., Molina, I., Nishida, I., Rowland, O., Samuels, L., Schmid, K.M., Wada, H., Welti, R., Xu, C., Zallot, R. and Ohlrogge, J.** (2013) Acyl-lipid metabolism. *Arabidopsis Book*, **11**, e0161.

- Lin, Y.T., Chen, L.J., Herrfurth, C., Feussner, I. and Li, H.M.** (2016) Reduced biosynthesis of digalactosyldiacylglycerol, a major chloroplast membrane lipid, leads to oxylipin overproduction and phloem cap lignification in Arabidopsis. *Plant Cell*, **28**, 219-232.
- Logemann, E., Birkenbihl, R.P., Ulker, B. and Somssich, I.E.** (2006) An improved method for preparing Agrobacterium cells that simplifies the Arabidopsis transformation protocol. *Plant Methods*, **2**, 16.
- Lu, B. and Benning, C.** (2009) A 25-amino acid sequence of the Arabidopsis TGD2 protein is sufficient for specific binding of phosphatidic acid. *J Biol Chem*, **284**, 17420-17427.
- Malherbe, A., Block, M.A., Joyard, J. and Douce, R.** (1992) Feedback inhibition of phosphatidate phosphatase from spinach chloroplast envelope membranes by diacylglycerol. *J Biol Chem*, **267**, 23546-23553.
- Meissner, C., Lorenz, H., Hehn, B. and Lemberg, M.K.** (2015) Intramembrane protease PARL defines a negative regulator of PINK1-and PARK2/Parkin-dependent mitophagy. *Autophagy*, **11**, 1484-1498.
- Meissner, C., Lorenz, H., Weihofen, A., Selkoe, D.J. and Lemberg, M.K.** (2011) The mitochondrial intramembrane protease PARL cleaves human Pink1 to regulate Pink1 trafficking. *J Neurochem*, **117**, 856-867.
- Moin, S.M. and Urban, S.** (2012) Membrane immersion allows rhomboid proteases to achieve specificity by reading transmembrane segment dynamics. *Elife*, **1**, e00173.
- Mongrand, S., Bessoule, J.-J., Cabantous, F. and Cassagne, C.** (1998) The C16:3\C18:3 fatty acid balance in photosynthetic tissues from 468 plant species. *Phytochemistry*, **49**, 1049-1064.
- Nakamura, Y., Tsuchiya, M. and Ohta, H.** (2007) Plastidic phosphatidic acid phosphatases identified in a distinct subfamily of lipid phosphate phosphatases with prokaryotic origin. *J Biol Chem*, **282**, 29013-29021.
- Nishida, I., Tasaka, Y., Shiraishi, H. and Murata, N.** (1993) The gene and the RNA for the precursor to the plastid-located glycerol-3-phosphate acyltransferase of Arabidopsis thaliana. *Plant Mol Biol*, **21**, 267-277.
- Page, M.J. and Di Cera, E.** (2008) Serine peptidases: classification, structure and function. *Cell Mol Life Sci*, **65**, 1220-1236.
- Rocha, J., Sarkis, J., Thomas, A., Pitou, L., Radzimanowski, J., Audry, M., Chazalet, V., de Sanctis, D., Palcic, M.M., Block, M.A., Girard-Egrot, A., Maréchal, E. and Breton, C.** (2016) Structural insights and membrane binding

- properties of MGD1, the major galactolipid synthase in plants. *Plant Journal*, 622-633.
- Roston, R., Gao, J., Xu, C. and Benning, C.** (2011) Arabidopsis chloroplast lipid transport protein TGD2 disrupts membranes and is part of a large complex. *Plant J*, **66**, 759-769.
- Roston, R.L., Gao, J., Murcha, M.W., Whelan, J. and Benning, C.** (2012) TGD1, -2, and -3 proteins involved in lipid trafficking form ATP-binding cassette (ABC) transporter with multiple substrate-binding proteins. *Journal of Biological Chemistry*, **287**, 21406-21415.
- Stevenson, L.G., Strisovsky, K., Clemmer, K.M., Bhatt, S., Freeman, M. and Rather, P.N.** (2007) Rhomboid protease AarA mediates quorum-sensing in *Providencia stuartii* by activating TatA of the twin-arginine translocase. *Proceedings of the National Academy of Sciences of the United States of America*, **104**, 1003-1008.
- Thompson, E.P., Smith, S.G. and Glover, B.J.** (2012) An Arabidopsis rhomboid protease has roles in the chloroplast and in flower development. *J Exp Bot*, **63**, 3559-3570.
- Tripp, J., Inoue, K., Keegstra, K. and Froehlich, J.E.** (2007) A novel serine/proline-rich domain in combination with a transmembrane domain is required for the insertion of AtTic40 into the inner envelope membrane of chloroplasts. *Plant J*, **52**, 824-838.
- Urban, S. and Freeman, M.** (2003) Substrate specificity of rhomboid intramembrane proteases is governed by helix-breaking residues in the substrate transmembrane domain. *Mol Cell*, **11**, 1425-1434.
- Urban, S., Lee, J.R. and Freeman, M.** (2001) *Drosophila* Rhomboid-1 defines a family of putative intramembrane serine proteases. *Cell*, **107**, 173-182.
- Wang, K., Guo, Q., Froehlich, J.E., Hersh, H.L., Zienkiewicz, A., Howe, G.A. and Benning, C.** (2018) Two abscisic acid-responsive plastid lipase genes involved in jasmonic acid biosynthesis in *Arabidopsis thaliana*. *Plant Cell*, **30**, 1006-1022.
- Wang, Y., Zhang, Y. and Ha, Y.** (2006) Crystal structure of a rhomboid family intramembrane protease. *Nature*, **444**, 179-180.
- Wang, Z., Anderson, N.S. and Benning, C.** (2013) The phosphatidic acid binding site of the Arabidopsis Trigalactosyldiacylglycerol 4 (TGD4) protein required for lipid import into chloroplasts. *J Biol Chem*, **288**, 4763-4771.
- Wang, Z. and Benning, C.** (2011) Arabidopsis thaliana polar glycerolipid profiling by thin layer chromatography (TLC) coupled with gas-liquid chromatography (GLC). *Journal of visualized experiments*, 1-6.

- Xu, C., Fan, J., Froehlich, J.E., Awai, K. and Benning, C.** (2005) Mutation of the TGD1 chloroplast envelope protein affects phosphatidate metabolism in Arabidopsis. *The Plant cell*, **17**, 3094-3110.
- Xu, C., Yu, B., Cornish, A.J., Froehlich, J.E. and Benning, C.** (2006) Phosphatidylglycerol biosynthesis in chloroplasts of Arabidopsis mutants deficient in acyl-ACP glycerol-3-phosphate acyltransferase. *Plant Journal*, **47**, 296-309.
- Yang, Y., Zienkiewicz, A., Lavell, A. and Benning, C.** (2017) Coevolution of domain interactions in the chloroplast TGD1, 2, 3 lipid transfer complex specific to brassicaceae and poaceae plants. *Plant Cell*, **29**.
- Yu, B., Wakao, S., Fan, J. and Benning, C.** (2004) Loss of plastidic lysophosphatidic acid acyltransferase causes embryo-lethality in Arabidopsis. *Plant Cell Physiol*, **45**, 503-510.

CHAPTER 4

RBL10 Protein Properties and Oligomeric State

Abstract

Intramembrane proteolysis has been implicated in a variety of regulatory mechanisms in cells. A family of rhomboid proteases carry out proteolysis within the membrane and participate in numerous signaling pathways across nearly all organisms. While their roles are proving to be important to human health, characterization of their molecular mechanisms remains challenging. Though many rhomboid-like proteins are predicted in plants, no detailed molecular mechanism is available for any of them yet. Of the 13 predicted rhomboids in *Arabidopsis thaliana*, one rhomboid has been found to influence lipid metabolism in the chloroplast. Rhomboid-like protein 10 (RBL10) seems to alter the trafficking of phosphatidic acid (PA), a key lipid intermediate and signaling molecule, ultimately leading to a change in monogalactosyldiacylglycerol (MGDG) acyl composition in the thylakoid membranes. RBL10 also appears to be part of a large molecular weight complex greater than 660 kDa in size. Furthermore, RBL10, but not active site mutants, undergoes autolytic cleavage in its carboxy-terminal domain. This autocatalytic activity proves that RBL10 has protease activity, although other substrates are not yet known. The identity of the RBL10 complex components as well as the *in vivo* mechanism of autocleavage of RBL10 provide stepping stone towards a deeper understanding of how RBL10 participates in *Arabidopsis* lipid metabolism.

Introduction

Rhomboid family proteins carry out intramembrane proteolysis, utilizing a serine and histidine catalytic dyad to process peptides within the lipid bilayer of the membrane (Cho *et al.*, 2019). Their roles vary depending on the organelle they associate with and the

tissues they are present in. Generally, members of the rhomboid family tend to carry out regulated intramembrane proteolysis, activating ligands (Lee *et al.*, 2001, Urban *et al.*, 2002), initiating peptide trafficking (Meissner *et al.*, 2011), and enabling the oligomerization of complexes (Stevenson *et al.*, 2007). Though they do not require an amino acid target consensus sequence for cleavage, they maintain selectivity while scanning the membrane for their substrates (Moin and Urban, 2012, Kreutzberger *et al.*, 2019). Rhomboid proteases and their regulatory roles in mammals have gained medical relevance since the discovery of the family in *Drosophila melanogaster* (Bergbold and Lemberg, 2013, Freeman, 2016). While an appreciable number of rhomboid roles have been described so far, there are yet to be any rhomboids to be functionally characterized in plants even though many members are predicted in *Arabidopsis thaliana*, *Populus trichocarpa*, and *Oryza sativa* (Garcia-Lorenzo *et al.*, 2006, Tripathi and Sowdhamini, 2006, Lemberg and Freeman, 2007). An active member of the rhomboid family has been confirmed with protease activity assays in *Arabidopsis* (Kanaoka *et al.*, 2005) though the biological role still remains elusive. So far, the best studied plant rhomboid is found in the chloroplasts of *Arabidopsis* and is encoded by At1g25290 or the *Rhomboid-like protein 10 (RBL10)* gene. A number of publications probed the biological relevance of RBL10 as well as its mechanism, showing that knock-outs of RBL10 have altered pollen morphology, floral defects, and might influence jasmonic acid (JA) signaling (Knopf *et al.*, 2012, Thompson *et al.*, 2012). More recently, RBL10 has been implicated in *Arabidopsis* lipid metabolism and the utilization of chloroplast assembled phosphatidic acid (PA) for galactolipid biogenesis (Lavell *et al.*, 2019). Though the involvement of RBL10 in lipid metabolism narrowed its potential biological function, the exact mechanism through which

this rhomboid-like protein affects PA metabolism or trafficking is not clear. This chapter focuses on the oligomeric state and proteolytic properties of RBL10 advancing our understanding of RBL10 function in plants.

Results and Discussion

The Oligomeric State of RBL10 Indicates Stable Protein Interactors

An outstanding question surrounding rhomboid catalysis addresses the oligomeric state of rhomboids and probes the idea that they are obligate monomers. However, there are known rhomboid protein non-substrate interactors (Jeyaraju *et al.*, 2006), but few examples of stable complexes involving rhomboids have been reported. Upon immunoblot analysis of RBL10-YFP-HA analyzed by separating solubilized chloroplast proteins under non-denaturing conditions using Blue-Native Polyacrylamide Gel Electrophoresis (BN-PAGE), it appears that RBL10 may be a part of a large molecular weight complex (Fig. 4.1). The observed band size is much larger than expected for a monomer or even dimer of the protein (~60 and ~120kDa respectively). The anti-HA signal shows three bands, one band nearing 1,000 kDa and the other two are ~400 and 450 kDa respectively. These findings were corroborated by using size exclusion chromatography (SEC), where solubilized chloroplast proteins of *RBL10-YFP-HA*-expressing Arabidopsis were separated on a Superdex 200 column. With larger MW proteins and complexes eluting earlier, we readily observed the elution of the full length RBL10-YFP-HA fusion protein in the earlier fractions corresponding to a MW of >660 kDa (Fig. 4.2).

The RBL10 containing complex could represent a new example of a protein complex involved in lipid metabolism in Arabidopsis. Currently, knowledge about the oligomeric states of lipid biosynthetic enzymes, or multiprotein complexes in which they play a possible role, is generally lacking. One complex involved in PA binding and lipid trafficking from the ER is an ABC transporter consisting of TRIGALACTOSYLDIACYLGLYCEROL 1, 2, and 3, (Xu *et al.*, 2005, Awai *et al.*, 2006, Lu *et al.*, 2007, Lu and Benning, 2009, Roston *et al.*, 2012, Yang *et al.*, 2017) which likely interacts with two additional proteins, TGD4 and 5 (Xu *et al.*, 2008, Wang *et al.*, 2012, Fan *et al.*, 2015). Though the TGD complex is also of a large molecular weight, the RBL10 protein does not seem to overlap with the TGD complex using different sizing approaches. As a next step, we characterized the protein interactome of RBL10 to gain insight into its molecular function. Furthermore, it is not known at this time, what the endogenous protein substrate of RBL10 is, and it seemed possible that it might be part of the complex.

Co-Immunoprecipitation of RBL10 Yields Putative Protein Interactors

To identify possible protein interactors and substrates of RBL10, we used a co-immunoprecipitation approach. The RBL10-YFP-HA fusion protein and with its associated proteins present in chloroplast extracts from transgenic plants expressing the *RBL10-YFP-HA* construct in the *rb10-1* mutant background were bound to magnetic beads with an antibody specific for the HA-tag present on RBL10-YFP-HA. To control for non-specific binding, an isotype control antibody was used, which has no specificity toward HA or other proteins present in the chloroplast lysate. Both samples, were submitted for mass spectrometry to identify any proteins immunoprecipitated with each

set of beads. A few hundred proteins were detected in both sample sets. However, upon comparing the HA-specific and control samples and across three experimental replicates, a small subset of recurring proteins was identified specific to the HA-specific sample (Table 4.1). There was a total of 22 proteins co-immunoprecipitated with RBL10-YFP-HA in at least 2 of the 3 replicates. Of those 22, a single protein (#15) appeared in all three experimental replicates, annotated as ribosomal protein S1 (RPS1) with gene ID At5g30510 (Table 4.1). There is some evidence that RPS1 does indeed function as a ribosomal protein in the chloroplasts of Arabidopsis. It recognizes mRNAs and is important in the translation of RNAs encoding thylakoid membrane proteins (Romani *et al.*, 2012). There is additional evidence that RPS1 might facilitate retrograde signaling from the chloroplast in response to heat stress, and that RPS1 function is important for normal thylakoid ultrastructure (Yu *et al.*, 2012). In light of potential physical interactions between RPS1 and RBL10, the mechanistic relationship between changes in PA metabolism and heat stress response is not immediately clear. However, it is possible that heat-induced stress could require an RBL10-mediated adjustment of the thylakoid membrane lipid composition through varying the accessibility of different PA pools, which affects the acyl chain length of the most abundant thylakoid lipid, MGDG. However, RPS1 does not seem to be associated with any membrane, a prerequisite for a rhomboid substrate. While it is unlikely that RPS1 is the direct protein substrate of RBL10, it is plausible that it could be stably interacting with a soluble region of RBL10, such as its amino terminus, and serve a regulatory role.

The remaining 21 proteins which appear in 2 of 3 experimental replicates have annotations related to processes such as photosynthesis, protein import, chaperonin

function, carbohydrate metabolism, signaling, as well as one protein possibly related to fatty acid metabolism (Table 4.1). Before any more conclusions can be drawn from any of these proteins as well as RPS1, their physical interactions with RBL10 must be tested in different ways. This can be accomplished through a split-ubiquitin yeast two-hybrid approach (Obrdlik *et al.*, 2004). Once there is additional evidence obtained about the direct interaction with RBL10, or interactions between any of these individual components, further conclusions can be drawn about the molecular function of these candidate proteins in the RBL10 complex.

RBL10 is Autolytic Towards its Carboxy-Terminal Domain

Protease activity assays have been challenging to perform with purified RBL10 which was labeled at its carboxy-terminal domain (CTD). Purification of the WT protein appeared unsuccessful, where yields were always quite low, and it seemed implausible that so little protein was being produced in *Nicotiana benthamiana* as well as *Escherichia coli*. Initially this was presumed to be due to the deleterious effects of producing an active protease with many hydrophobic domains. However, there was suspicion that the CTD may be subjected to proteolytic cleavage by the action of RBL10 or another protease. To further investigate, the predicted catalytic residues of RBL10, Serine 240 and Histidine 293, which were previously identified (Chapter 3) were mutagenized using PCR to convert both residues to alanine, resulting in RBL10^{S240A} and RBL10^{S240A;H293A} variants. The expression of these mutant constructs in *E. coli*, yielded a CTD glutathione-s-transferase (GST)-tagged RBL10 protein (Fig. 4.3). The WT RBL10-GST protein cannot be detected with antibody raised against GST, however, the catalytically inactive proteins are detected

with the anti-GST antibody. This finding suggested that the CTD of RBL10 is only cleaved when the catalytic residues are present and that RBL10 cleaves its own CTD. Since there are six main transmembrane segments in the conserved rhomboid fold, the prediction of a seventh transmembrane domain at the CTD may indicate that it is this segment of the protein which gets cleaved by RBL10. While a CTD tag is not detectable on WT RBL10, an amino-terminal domain (NTD) tagged RBL10 yielded detectable protein production in *E. coli* even for WT RBL10 around 70 kDa in size (Fig. 4.4). Autolytic cleavage has previously been reported for the human PARL, where the cleavage product contains a nuclear targeting sequence, which is conserved in mammals, and travels to the nucleus upon release from the mitochondrion (Sik *et al.*, 2004). Though we can observe the cleavage of RBL10 CTD, we do not yet know the fate of the released peptide. Determining the exact site of cleavage as well as any secondary localizations of the released fragment could give us greater insight into the function of this autolysis.

While autolysis appears to happen as protein is produced in a bacterial host, the ability to detect an intact fusion as well as a retained CTD fragment in isolated chloroplasts might give some clues about the coordination of this autocleavage. Interestingly, we were also able to detect a smaller RBL10_{CTD}-YFP-HA in the later fractions of the SEC corresponding to a monomeric form of the fragment (Fig. 4.2). It is unclear whether the remaining amino terminal portion of the protease remains with the complex. Since RBL10 appears to have both a full fusion and the cleaved fragment, while in bacterial cells the autocatalysis occurs as soon as protein is made, it is possible that the interaction with complex members can control autocatalysis of RBL10. The CTD fragment is only found in a monomeric state in the SEC analysis (Fig. 4.2), perhaps indicating that dissociation

from the complex and autocatalysis coincide. It is not currently clear, whether the dissociation from the complex induces autocatalysis or the cleavage of the CTD causes dissociation from the complex. Since we don't yet have an antibody against RBL10 protein, we cannot determine whether the processed RBL10 form remains complex bound or if it dissociates altogether. Understanding the relationship between autocatalysis and complex residency of RBL10 is an important next step towards solving its molecular mechanism.

Catalytic Mutant Constructs of RBL10 Cannot be Stably Transformed into the *rb10-1* Mutant Background

The causal relationship between the observed lipid phenotype in the *rb10* mutants and the *RBL10* gene was shown by rescuing the mutant line with a WT copy of *RBL10* (Lavell *et al.*, 2019) (See Chapter 3). It was then important to establish whether the proteolytic function of RBL10 was important to its role in lipid homeostasis. The point mutants which were generated using PCR mutagenesis, RBL10^{S240A} and RBL10^{S240A;H293A} were cloned into the same pEARLEYGATE101 plant expression vector as used for the WT sequence, possessing a BASTA herbicide marker for screening transformants. However, unlike the WT construct, the floral dipping transformation of constructs bearing the point mutants of RBL10 with *Agrobacterium tumefaciens* did not yield any transformants. With two attempted transformations and thousands of seeds screened for BASTA resistance, no stable transgenic lines were recovered. This indicated that there is possible embryo lethality when introducing non-catalytic RBL10 mutant protein in the *rb10-1* and WT background, with the mutant construct behaving like a dominant negative mutation. A

conclusion that could be drawn from this finding, is that RBL10 is part of an essential complex that is necessary for the function of the plastid galactolipid pathway. We know that this pathway is not essential for embryogenesis and plant growth from the knock out mutants of the *ATS1* gene (Kunst *et al.*, 1988). However, introducing a non-active RBL10 protein seems to imply that the presence of RBL10 protein itself might be influencing the functionality of the complex. In fact, RBL10 is part of a large molecular weight complex as we have shown above, although we do yet not know for certain its components in the wild type or in the *rb110* mutant. With its autolytic activity demonstrated in this study, perhaps RBL10 must process its CTD in order to dissociate from the complex and turn over. Without the ability to process its own CTD, the complex cannot turn over resulting in deleterious effects on developmental processes. It is possible that there is a regulatory step involving this complex which determines the flux through the two lipid biosynthetic pathways. Without any RBL10 protein present, the complex may favor the ER pathway which is essential (Xu *et al.*, 2005), and with a copy of RBL10 protein present, the complex favors the plastid pathway. However, if a null copy is introduced and having proteolytic ability is essential for RBL10 to dissociate from the complex, the null protein would prevent switching between the two biosynthetic pathways. If this is the case, then a null copy of RBL10 would in fact cause embryo lethality due to the plant's inability to utilize the essential ER pathway during embryogenesis.

Due to our lack of understanding of the exact mechanism of RBL10 complex formation and the role of its autocatalytic activity in complex association/dissociation, we cannot fully explain why stable transgenic lines expressing null copies of *RBL10* have not been successfully generated. It would be instructive to test whether the non-functional

versions of RBL10 can be successfully produced with transient expression in *Nicotiana benthamiana* to then test the effects on lipid composition and RBL10 complex formation. It is possible that autocatalysis of RBL10 is important for dissociation from the complex, and without being able to do so, there are deleterious metabolic consequences for the plant.

Materials and Methods

Plant Growing Conditions and Chloroplast Isolation

Arabidopsis seeds were sterilized (1 part bleach and 2 parts water solution with 0.1% Triton X-100) and sown on MS media supplemented with 1% sucrose. Approximately, 30 mg of seeds per plate were evenly distributed. Plates were sealed with 3M micropore tape, stratified for 3 days at 4°C, then placed into a 100 μ mol light growth, 22°C, with a 16 hr day and 8 hr night environment in a Percival chamber. Tissue was harvested for chloroplast isolation between 3 and 4 weeks of age. Plant lines were used as noted in each experiment including Col-0 (WT), *rb10-1*, and the *rb10-1* complemented line expressing *RBL10-YFP-HA* under 35S Cauliflower Mosaic Virus (CaMV) promoter using the pEARLEYGATE101 vector. Chloroplasts were isolated as previously described (Lavell *et al.*, 2019).

SDS-PAGE and Immunoblot Analysis

Sodium dodecyl sulfate polyacrylamide gel electrophoresis (SDS-PAGE) was carried out using Bio-Rad precast 10-12% acrylamide gels (<https://www.bio-rad.com>), or hand-cast 10-12% acrylamide gels. Samples were boiled in Laemmli buffer (50mM Tris-HCL pH6.8,

2% SDS, 0.1% Bromophenolblue, 10% glycerol at 1x) at 95°C for 10 mins, centrifuged for 3 minutes at 13,000 rpm, and loaded onto the gel. A protein standard mixture was used for size reference (Bio-Rad Precision Plus Dual Stained Molecular Weight marker (<https://www.bio-rad.com>)). For running buffer, Tris-Glycine (25 mM Tris, 192 mM Glycine) containing 0.1% sodium dodecyl sulfate SDS was used. Proteins were separated at ~150V until the loading dye front was just running off the bottom of the gel. Resulting gels were either directly stained with a Coomassie staining solution (1.25g Coomassie brilliant blue, 400mL methanol, 100mL acetic acid, 500mL dH₂O) or were used for transferring to a PVDF membrane. Immunoblot transfer was performed using the wet transfer method, using a Tris-Glycine buffer (25 mM Tris, 192mM Glycine, 20% methanol). Protein transfer was achieved with 100 V over 1.5 h chilled on ice with stirring. A 5% milk solution in TBS-T (100 mM Tris, 155 mM NaCl, 0.05% Tween 20) was used to block the resulting blots for an hour at RT or overnight at 4°C. After blocking, blots were incubated with the antibody specified in a 5% milk-TBS-T solution for 1 h at room temperature or overnight at 4°C. Washes in between primary and secondary antibodies were performed with TBS-T buffer, washing the blot three times for 5-15 mins each time. Chemiluminescence was used to detect presence of protein of interest.

Blue Native PAGE

Arabidopsis isolated chloroplasts were freshly prepared on the day of use, using WT, *rb110-1*, and *rb110-1* complemented line expressing *RBL10-YFP-HA* under 35S promoter. Chloroplasts were pelleted at 700 x g, then proteins were solubilized in the BN-PAGE protein solubilization buffer consisting of 333 µL of 3x Gel Buffer (150 mM Bis-tris/HCL,

1.5 M 6-aminocaproic acid, pH 7.0), 125 μ L of 80% glycerol, 100 μ L of 10% n-dodecyl β -D-maltoside (DDM), 10 μ L of 100mM phenylmethylsulfonyl fluoride (PMSF), and water to 1 mL. The final concentration was 1 mg/mL chlorophyll equivalents and the solution was allowed to incubate on ice for 30 mins with occasional tapping to mix. The resulting chloroplast lysate was clarified with a 10 min centrifugation at 100,000 x g. The supernatant was transferred to a clean tube and 5% SERVA Blue G (SERVA No. 35050) dye was added to the solution for a final concentration of 3.0%. An unstained native gel marker was used for size reference (NativeMark; www.thermofisher.com). Chloroplast protein complexes were separated on a 4-16% Bis-Tris polyacrylamide gel overnight at 30V in 4°C. The resulting gel was either stained directly using Coomassie staining solution or transferred to a PVDF membrane for immunoblot analysis. To transfer the proteins to PVDF, the gel was first boiled in a boiling buffer solution (3.3% w/v SDS, 4% 2-mercaptoethanol, and 65mM Tris buffer) for 30 min at 80°C using a glass petri dish on a hot plate in a fume hood with gentle mixing. The gel was then washed in transfer buffer to remove excess SDS and reducing agent. Proteins were transferred as described above. The resulting PVDF membrane was fixed in 8% acetic acid. Any transferred dye was removed with methanol, followed by washing with water. Immunoblot analysis proceeded as described above. RBL10-YFP-HA was detected using an anti-HA antibody from rat directly conjugated to horseradish peroxidase (HRP) enzyme at a 1:1000 dilution (3F10, Roche/Sigma Aldrich, www.sigmaaldrich.com).

Size Exclusion Chromatography

A standard protein mixture was purchased from Sigma-Aldrich (Catalog# 69385), including thyroglobulin (670k Da), bovine γ -globulins (150 kDa), chicken egg albumin (44.3 kDa), bovine ribonuclease A type I-A (13.7 kDa), and p-aminobenzoic acid (137 Da). The standard protein mixture was supplied as a lyophilized powder corresponding to 30 mg of protein. The powder was resuspended with 1 mL of deionized water and any undissolved solids were removed with centrifugation. A GE Superdex 200 (www.gelifesciences.com) column was equilibrated with phosphate buffered saline (PBS) pH 7.4 with 0.01% DDM at 4°C. A 100 μ L injection loop was used to load 100 μ L of the standard mixture onto the equilibrated column. Proteins were separated by size exclusion chromatography using a GE AKTA purifier system (www.gelifesciences.com) at 0.05 mL/min. Fractions of 0.5 mL were collected from the time of injection. A total of 72 fractions were collected, equal to 1.5 times column volume. Protein elution was monitored by absorbance at 280 nm, signals corresponding to individual proteins in the standard mixture were observed for reference. Arabidopsis isolated chloroplasts were freshly prepared the day of use, using the *rb110-1* complemented line expressing *RBL10-YFP-HA*. Chloroplasts were pelleted at 700 x g, then proteins were solubilized in the BN-PAGE protein solubilization buffer as described above to a 1 mg/mL chlorophyll equivalent concentration, allowing the solution to incubate on ice for 30 mins with occasional tapping to mix. The resulting chloroplast lysate was clarified with a 10 min centrifugation at 100,000 x g. The supernatant was removed and a 100 μ L, equal to 100 μ g chlorophyll equivalents, was loaded onto a Superdex 200 SEC column equilibrated with PBS pH 7.4 with 0.01% β -dodecyl-n-maltoside (DDM). The chloroplast lysate was separated at 0.05

mL/min flow rate using the same method as the standard mixture. Again, A280 was used to monitor protein elution off the column. Standard proteins were confirmed with SDS-PAGE of the fractions corresponding to the A280 signals. Elution of RBL10-YFP-HA was observed by immunoblot analysis of the resulting fractions in the same range as the A280 signals for the standards, using an anti-HA antibody from rat directly conjugated to horseradish peroxidase (HRP) enzyme at a 1:1000 dilution (3F10, Roche/Sigma Aldrich, www.sigmaaldrich.com).

Co-Immunoprecipitation

Magnetic Dynabeads with Protein G were prepared prior to the experiment. Mouse IgG specific for hemagglutinin (HA) (Biolegend 16b32) and a mouse K-isotype control IgG were used to couple to the Protein G Dynabeads, using 7.5 μg per 50 μL of beads. Chloroplast protein lysate was prepared as described above for BN-PAGE without the addition of SERVA Blue G dye. Each set of IgG coupled Dynabeads was incubated with the chloroplast protein lysate at room temperature with end over end mixing for 1 hr. Beads were collected with a magnet, supernatant removed, and the beads were washed three times with 1x PBS pH 7.4, DDM 0.02%. The resulting beads were submitted for mass spectrometry identification of peptides present.

Samples were washed with ice-cold 50mM ammonium bicarbonate, 3x and finally resuspended in 10 μL of 5ng/ μL trypsin in the same buffer. Beads were incubated at 37°C for 5hrs to digest proteins. Supernatant was removed following centrifugation, placed into a new tube and the peptide solution acidified to 3% trifluoroacetic acid (TFA). Samples were then purified using c18 stage-tips (Shevchenko *et al.*, 1996) and dried by vacuum

centrifugation. Peptides were then re-suspended in 2% acetonitrile/0.1%TFA to 20 μ L. From this, 10 μ L were automatically injected by EASYnLC 1200 (www.thermo.com) onto a Thermo Acclaim PepMap RSLC 0.1mm x 20mm C18 trapping column and washed with Buffer A for ~5min. Bound peptides were eluted onto a Thermo Acclaim PepMap RSLC 0.075mm x 500mm C18 analytical column over 35min with a gradient of 8%B to 40%B in 24min, ramping to 90%B at 25min and held at 90%B for the duration of the run (Buffer A = 99.9% Water/0.1% Formic Acid, Buffer B = 80% Acetonitrile/0.1% Formic Acid/19.9% Water). Column temperature was maintained at 50C using an integrated column heater (PRSO-V2, www.sonation.com).

Eluted peptides were sprayed into a ThermoFisher Q-Exactive HF-X mass spectrometer (www.thermo.com) using a FlexSpray spray ion source. Survey scans were taken in the Orbi trap (60000 resolution, determined at m/z 200) and the top 10 ions in each survey scan are then subjected to automatic higher energy collision induced dissociation (HCD) with fragment spectra acquired at 15,000 resolution. The resulting MS/MS spectra are converted to peak lists using Mascot Distiller, v2.6.1 (www.matrixscience.com) and searched against all entries in the TAIR, v10, protein sequence database (downloaded from The Arabidopsis Information Network, (www.arabidopsis.org)), appended with common laboratory contaminants (downloaded from www.thegpm.org, cRAP project), using the Mascot searching algorithm, v 2.6. The Mascot output was then analyzed using Scaffold Q+S, v4.9.0 (www.proteomesoftware.com) to probabilistically validate protein identifications. Assignments validated using the Scaffold 1%FDR confidence filter are considered true.

Proteins unique to the RBL10-YFP-HA sample or twice as abundant compared to the control samples in at least 2 of the 3 experimental replicates were considered putative protein interactors. The protein names, gene IDs, molecular weight, net enrichment as well as the occurrence throughout experimental replicates is shown in Table 4.1 .

Protein production in *E. coli*.

Four strains bearing pDEST24 gateway vector (www.thermofisher.com) containing the following were generated: a 50 amino acid peptide of YFP (EV), *RBL10* WT gene, *RBL10*^{S240A} single serine mutant gene, and *RBL10*^{S240A;H293A} serine/histidine double mutant gene. The constructs were generated by recombining the listed genes in pENTR/SD/D/Topo vector (www.thermofischer.com) with the pDEST24 vector using LR Clonase II (www.thermofischer.com). Starter cultures of BL21(DE3) cells transformed with the four pDEST24 constructs were grown overnight from glycerol stock in Luria broth (LB) with ampicillin at 37°C. The following day, 25 mL cultures were inoculated in flasks at a cell density corresponding to an OD₆₀₀ of 0.1, and grown with shaking at 37°C until the cell density was 0.4-0.7. An initial sample was taken, a volume equal to an OD₆₀₀ of 0.5, at timepoint 0, the cells were spun down, supernatant removed, and snap frozen in liquid nitrogen, then kept at -80°C. Expression of plasmids was induced by the addition of 20 µM Isopropyl β-d-1-thiogalactopyranoside (IPTG) to each flask. Samples were taken at later times with the same OD₆₀₀ across all timepoints. Once all the samples were collected, the pellets were resuspended in 40 µL of water and 10 µL of 5 x Laemeli Buffer was added, the samples were boiled at 95°C for 10 mins, then 20 µL were loaded onto a acrylamide gel and separated as described above followed by immunoblot analysis. To

probe for the presence of RBL10 protein fusions with GST, a rabbit anti-GST primary antibody was used at a 1:5000 dilution.

For production of NTD tagged maltose-binding protein (MBP)-RBL10 fusion, the pDEST-His-MBP vector was obtained from Addgene (www.addgene.com). WT and single serine 240 RBL10 constructs in pENTR/SD/D-topo were recombined as described above with the pDEST-His-MBP vector. The generated constructs were transformed into BL21(DE3) cells. Cultures of the resulting strains containing WT *RBL10* and *RBL10*^{S240A} in the pDEST-His-MBP vector were grown up at 37°C overnight in LB with ampicillin. The following day, 25mL cultures of LB with ampicillin were inoculated from the overnight cultures to an OD₆₀₀ of 0.1. The cultures were then grown at 37°C until OD₆₀₀ of 0.6, and were induced with 20 μM IPTG, the temperature was reduced to 16°C. After overnight growth, the cultures were harvested by centrifugation. Pellets were resuspended in 10mL of lysis buffer (PBS pH7.4, 10mM MgCl, 8mg/mL lysozyme, 1 tablet of EDTA-free mini complete protease inhibitor (Roche, www.sigmaaldrich.com)). The cells were disrupted by sonication (1 sec on, 1 sec off, for 3 minutes total) on ice. Cellular debris were spun down at 24,000 x g for 12 minutes. Membranes were pelleted at 100,000 x g for 1 hr. The membrane fraction was resuspended in 2.5mL of lysis buffer amended with 0.2% TritonX-100. The solubilized membranes were passed three times over 2mL of amylose resin prepared by the manufacturer's recommendation (www.NEB.com), Wash and elution steps were performed as per manufacturer's recommendation. The eluted fractions were desalted into PBS pH 7.4, using an amicon centrifugal unit (Millipore) with a molecular weight cutoff of 30kDa. Protein concentration was determined using BCA (Pierce, www.thermofisher.com), and 20ug of protein from both RBL10 WT sample and

RBL10^{S240A} were prepared for SDS-PAGE as described above and loaded onto a 10% polyacrylamide gel twice, half the gel was used for Western blot transfer and the other half was used for direct staining with Coomassie. For Western blot analysis anti-MBP antibody from rabbit was used at a 1:75,000 dilution.

Acknowledgement

This work was possible due to the help and generosity of many individuals. For performing the size exclusion chromatography, Dr. Curtis Wilkerson graciously allowed the use of his instrument and column as well as provided valuable insight. Dr. Mingzhu Fan provided careful training on the use of the Akta instrument and assisted with operation. Cameron De La Mora assisted on generating Figure 4.3. For critical discussions on co-immunoprecipitation experiments and BN-PAGE, Tomomi Takeuchi deserves a big thank you. Identification of potential protein interactors in Table 4.1 would not have been possible without Doug Whitten at the MSU Proteomics Core. Financial support for this work was primarily from the Division of Chemical Sciences, Geosciences and Biosciences, Office of Basic Energy Sciences of the United States Department of Energy (Grant DE-FG02-91ER20021). In addition, Anastasiya Lavell was partially supported by a fellowship from Michigan State University under the Training Program in Plant Biotechnology for Health and Sustainability (T32-GM110523).

APPENDIX

#	Gene Annotation	Accession Number	MW kDa	Net Enrichment	Occurrence
1	PGK1 - phosphoglycerate kinase 1	AT3G12780	50	10.483	2
2	ATPC1 - ATPase, F1 complex, gamma subunit protein	AT4G04640	41	4.765	2
3	Transketolase	AT3G60750	80	4.765	2
4	LHCB3 - light-harvesting chlorophyll B-binding protein 3	AT5G54270	29	4.765	2
5	PSB27 - photosystem II family protein	AT1G03600	19	3.7131	2
6	ATPase, F0 complex, subunit B/B', bacterial/chloroplast	AT4G32260	24	2.6612	2
7	ZKT - protein containing PDZ domain, a K-box domain, and a TPR region	AT1G55480	37	2.859	2
8	APX4 - ascorbate peroxidase 4	AT4G09010	38	1.8071	2
9	TOC159 - translocon at the OEM of chloroplasts 159	AT4G02510	161	1.9833	2
10	CPN60B, LEN1 - chaperonin 60 beta	AT1G55490	64	1.906	2
11	EDA9 - D-3-phosphoglycerate dehydrogenase	AT4G34200	63	1.906	2
12	SBPASE - sedoheptulose-bisphosphatase	AT3G55800	42	1.906	2
13	CLPC1 - CLPC homologue 1	AT5G50920	20	1.906	2
14	ATPB - ATP synthase subunit beta	ATCG00480	54	0.99167	2
15	RPS1 - ribosomal protein S1	AT5G30510	45	0.99167	3
16	RPL2.1 - ribosomal protein L2	ATCG00830	30	0.99167	2
17	Pyridine nucleotide-disulphide oxidoreductase family protein	AT1G74470	52	0.99167	2
18	Thioredoxin superfamily protein	AT3G11630	29	0.95299	2
19	PRK - phosphoribulokinase	AT1G32060	44	0.95299	2
20	FTSH1 - FTSH protease 1	AT1G50250	77	0.95299	2
21	ACP4 - acyl carrier protein 4	AT4G25050	15	0.95299	2
22	CPN20 - chaperonin 20	AT5G20720	27	0.95299	2

Table 4.1. Co-Immunoprecipitation with RBL10-YFP-HA using isolated chloroplast protein lysate, results in recurring appearance of select proteins. Proteins that were identified as at least twice as abundant in the anti-HA sample versus control are described here with their gene annotation, their gene ID, predicted molecular mass, the enrichment in the anti-HA sample compared to the control, and the recurrence out of three experimental replicates.

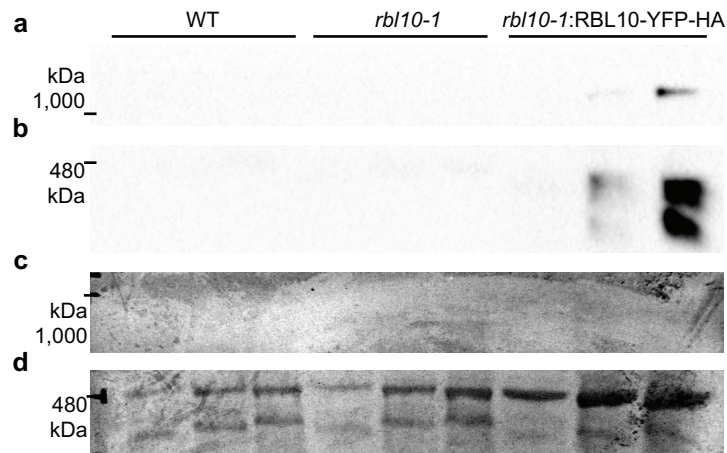


Figure 4.1. Blue Native PAGE of solubilized chloroplasts from WT, *rbl10-1* mutant, and *rbl10-1* complemented lines producing RBL10-YFP-HA protein. (a) Immunoblotting of the resulting BN-PAGE gel, blotted against HA, shows only signal in the complement line with a band above 1,000 kDa and (b) two bands below 480 kDa. (c) The immunoblot stained with Coomassie showing the region corresponding to 1,000 kDa and (d) 480kDa. For each genotype 10, 20, and 30 μ L of chloroplast prep were loaded.

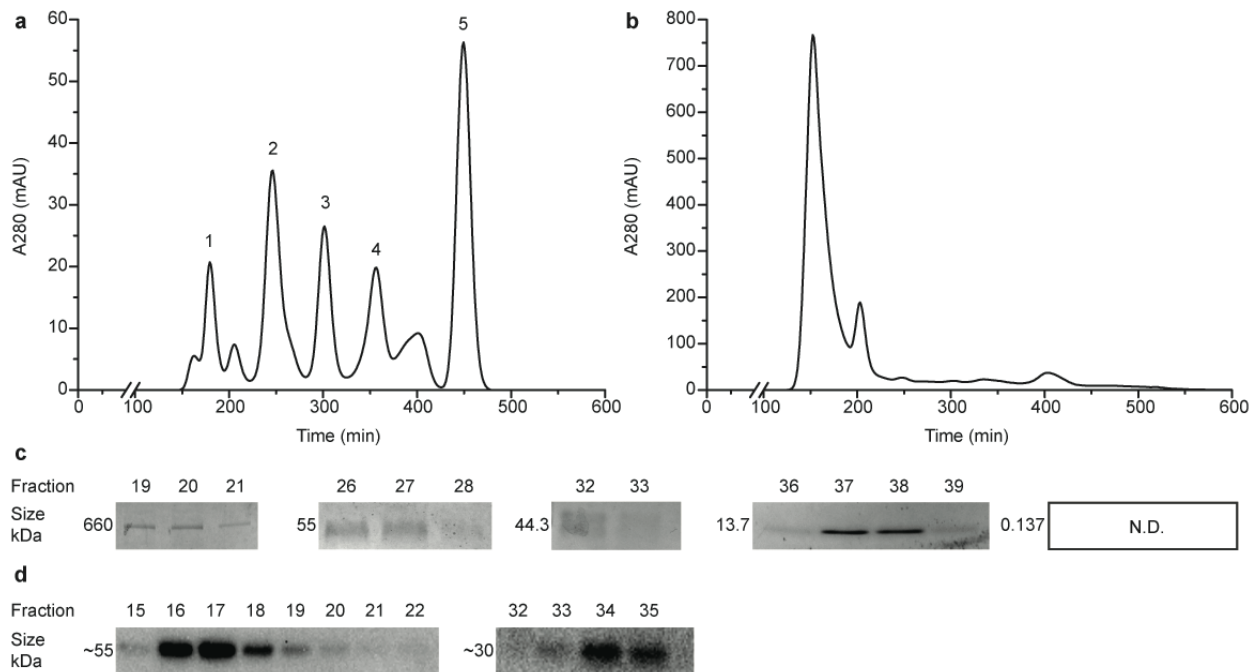


Figure 4.2. Size Exclusion Chromatography of protein standards and solubilized chloroplasts of *rb110-1:RBL10-YFP-HA* line show that RBL10 migrates in a complex at a high MW. (a) The standards used were: 1, Thyroglobulin (660 kDa); 2, Bovine γ -globulins (150 kDa); 3, Chicken albumin (44.3 kDa); 4, Ribonuclease A type I-A (13.7 kDa); 5, P-aminobenzoic acid (pABA)(137Da). They are resolved on a Superdex 200 column with A280 monitoring of protein elution over time. (b) Elution of solubilized chloroplast proteins of the *rb110-1:RBL10-YFP-HA* line from the Superdex 200 column, monitored with A280 over time. (c) SDS-PAGE of the fractions containing separated protein standards from (a), with the exception of pABA, show each standard and the respective fraction number. (d) Immunoblot analysis of fractions containing separated chloroplast proteins from (b), detecting signal with HA antibody.

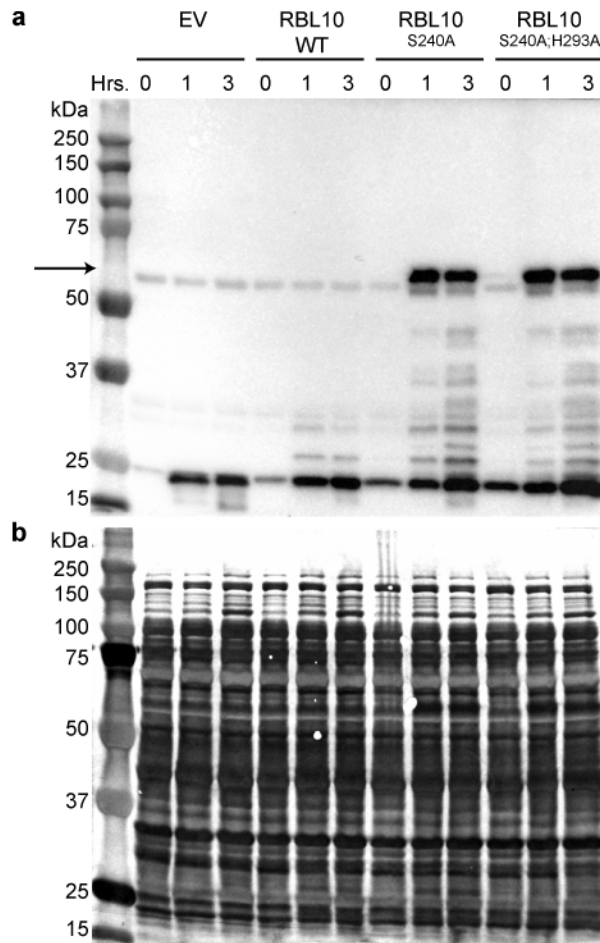


Figure 4.3. Production of C-Terminally tagged RBL10-GST in *E. coli*.

The absence of the fusion protein is observed for WT constructs, and this is rescued by mutagenesis of the active site serine and histidine residues. (a) The fusion protein of RBL10-GST (~64kDa) can be detected after 1 and 3 h post IPTG induction by anti-GST antibody for the single and double catalytic mutant (RBL10^{S240A}-GST and RBL10^{S240A:H293A}-GST) but not WT RBL10-GST, using immunoblot analysis. Equal sample loading was ensured by normalizing to OD₆₀₀ when samples were taken at each time point. (b) Coomassie-Blue stained blot of the PVDF membrane above in (a).

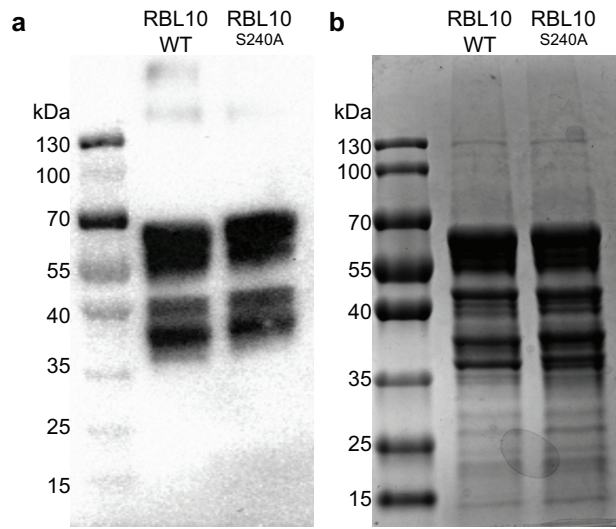


Figure 4.4. The fusion protein of MBP-RBL10 WT and single catalytic mutant can be detected with anti-MBP antibody. (a) The WT fusion protein MBP-RBL10 appears on anti-MBP Immunoblot when the tag is located on the amino-terminal domain of RBL10. (b) Equal protein loading was used in this immunoblot analysis as is shown using SDS-PAGE gel of the same protein samples stained with Coomassie Blue.

REFERENCES

REFERENCES

- Awai, K., Xu, C.C., Tamot, B. and Benning, C.** (2006) A phosphatidic acid-binding protein of the chloroplast inner envelope membrane involved in lipid trafficking. *Proc Natl Acad Sci U S A*, **103**, 10817-10822.
- Bergbold, N. and Lemberg, M.K.** (2013) Emerging role of rhomboid family proteins in mammalian biology and disease. *Biochim Biophys Acta*, **1828**, 2840-2848.
- Cho, S., Baker, R.P., Ji, M. and Urban, S.** (2019) Ten catalytic snapshots of rhomboid intramembrane proteolysis from gate opening to peptide release. *Nat Struct Mol Biol*.
- Fan, J.L., Zhai, Z.Y., Yan, C.S. and Xu, C.C.** (2015) Arabidopsis TRIGALACTOSYLDIACYLGLYCEROL5 interacts with TGD1, TGD2, and TGD4 to facilitate lipid transfer from the endoplasmic reticulum to plastids. *Plant Cell*, **27**, 2941-2955.
- Freeman, M.** (2016) Rhomboids, signalling and cell biology. *Biochem Soc Trans*, **44**, 945-950.
- Garcia-Lorenzo, M., Sjodin, A., Jansson, S. and Funk, C.** (2006) Protease gene families in Populus and Arabidopsis. *Bmc Plant Biol*, **6**, 30.
- Jeyaraju, D.V., Xu, L., Letellier, M.C., Bandaru, S., Zunino, R., Berg, E.A., McBride, H.M. and Pellegrini, L.** (2006) Phosphorylation and cleavage of presenilin-associated rhomboid-like protein (PARL) promotes changes in mitochondrial morphology. *Proc Natl Acad Sci U S A*, **103**, 18562-18567.
- Kanaoka, M.M., Urban, S., Freeman, M. and Okada, K.** (2005) An Arabidopsis Rhomboid homolog is an intramembrane protease in plants. *Febs Lett*, **579**, 5723-5728.
- Knopf, R.R., Feder, A., Mayer, K., Lin, A., Rozenberg, M., Schaller, A. and Adam, Z.** (2012) Rhomboid proteins in the chloroplast envelope affect the level of allene oxide synthase in Arabidopsis thaliana. *Plant J*, **72**, 559-571.
- Kreutzberger, A.J.B., Ji, M., Aaron, J., Mihaljevic, L. and Urban, S.** (2019) Rhomboid distorts lipids to break the viscosity-imposed speed limit of membrane diffusion. *Science*, **363**, 497-+.
- Kunst, L., Browse, J. and Somerville, C.** (1988) Altered regulation of lipid biosynthesis in a mutant of Arabidopsis deficient in chloroplast glycerol-3-phosphate acyltransferase activity. *Proc Natl Acad Sci U S A*, **85**, 4143-4147.

- Lavell, A., Froehlich, J.E., Baylis, O., Rotondo, A.D. and Benning, C.** (2019) A predicted plastid rhomboid protease affects phosphatidic acid metabolism in *Arabidopsis thaliana*. *Plant J*, **99**, 978-987.
- Lee, J.R., Urban, S., Garvey, C.F. and Freeman, M.** (2001) Regulated intracellular ligand transport and proteolysis control EGF signal activation in *Drosophila*. *Cell*, **107**, 161-171.
- Lemberg, M.K. and Freeman, M.** (2007) Functional and evolutionary implications of enhanced genomic analysis of rhomboid intramembrane proteases. *Genome Res*, **17**, 1634-1646.
- Lu, B. and Benning, C.** (2009) A 25-amino acid sequence of the *Arabidopsis* TGD2 protein is sufficient for specific binding of phosphatidic acid. *J Biol Chem*, **284**, 17420-17427.
- Lu, B., Xu, C., Awai, K., Jones, A.D. and Benning, C.** (2007) A small ATPase protein of *Arabidopsis*, TGD3, involved in chloroplast lipid import. *J Biol Chem*, **282**, 35945-35953.
- Meissner, C., Lorenz, H., Weihofen, A., Selkoe, D.J. and Lemberg, M.K.** (2011) The mitochondrial intramembrane protease PARL cleaves human Pink1 to regulate Pink1 trafficking. *J Neurochem*, **117**, 856-867.
- Moin, S.M. and Urban, S.** (2012) Membrane immersion allows rhomboid proteases to achieve specificity by reading transmembrane segment dynamics. *Elife*, **1**, e00173.
- Obrdlik, P., El-Bakkoury, M., Hamacher, T., Cappellaro, C., Vilarino, C., Fleischer, C., Ellerbrok, H., Kamuzinzi, R., Ledent, V., Blaudez, D., Sanders, D., Revuelta, J.L., Boles, E., Andre, B. and Frommer, W.B.** (2004) K⁺ channel interactions detected by a genetic system optimized for systematic studies of membrane protein interactions. *Proc Natl Acad Sci U S A*, **101**, 12242-12247.
- Romani, I., Tadini, L., Rossi, F., Masiero, S., Pribil, M., Jahns, P., Kater, M., Leister, D. and Pesaresi, P.** (2012) Versatile roles of *Arabidopsis* plastid ribosomal proteins in plant growth and development. *Plant J*, **72**, 922-934.
- Roston, R.L., Gao, J., Murcha, M.W., Whelan, J. and Benning, C.** (2012) TGD1, -2, and -3 proteins involved in lipid trafficking form ATP-binding cassette (ABC) transporter with multiple substrate-binding proteins. *J Biol Chem*, **287**, 21406-21415.
- Shevchenko, A., Wilm, M., Vorm, O. and Mann, M.** (1996) Mass spectrometric sequencing of proteins silver-stained polyacrylamide gels. *Anal Chem*, **68**, 850-858.

- Sik, A., Passer, B.J., Koonin, E.V. and Pellegrini, L.** (2004) Self-regulated cleavage of the mitochondrial intramembrane-cleaving protease PARL yields Pbeta, a nuclear-targeted peptide. *J Biol Chem*, **279**, 15323-15329.
- Stevenson, L.G., Strisovsky, K., Clemmer, K.M., Bhatt, S., Freeman, M. and Rather, P.N.** (2007) Rhomboid protease AarA mediates quorum-sensing in *Providencia stuartii* by activating TatA of the twin-arginine translocase. *Proc Natl Acad Sci U S A*, **104**, 1003-1008.
- Thompson, E.P., Smith, S.G. and Glover, B.J.** (2012) An *Arabidopsis* rhomboid protease has roles in the chloroplast and in flower development. *J Exp Bot*, **63**, 3559-3570.
- Tripathi, L.P. and Sowdhamini, R.** (2006) Cross genome comparisons of serine proteases in *Arabidopsis* and rice. *Bmc Genomics*, **7**, 200.
- Urban, S., Lee, J.R. and Freeman, M.** (2002) A family of Rhomboid intramembrane proteases activates all *Drosophila* membrane-tethered EGF ligands. *EMBO J*, **21**, 4277-4286.
- Wang, Z., Xu, C. and Benning, C.** (2012) TGD4 involved in endoplasmic reticulum-to-chloroplast lipid trafficking is a phosphatidic acid binding protein. *Plant J*, **70**, 614-623.
- Xu, C., Fan, J., Froehlich, J.E., Awai, K. and Benning, C.** (2005) Mutation of the TGD1 chloroplast envelope protein affects phosphatidate metabolism in *Arabidopsis*. *Plant Cell*, **17**, 3094-3110.
- Xu, C.C., Fan, J.L., Cornish, A.J. and Benning, C.** (2008) Lipid trafficking between the endoplasmic reticulum and the plastid in *Arabidopsis* requires the extraplastidic TGD4 protein. *Plant Cell*, **20**, 2190-2204.
- Yang, Y., Zienkiewicz, A., Lavell, A. and Benning, C.** (2017) Coevolution of domain interactions in the chloroplast TGD1, 2, 3 lipid transfer complex specific to Brassicaceae and Poaceae plants. *Plant Cell*, **29**, 1500-1515.
- Yu, H.D., Yang, X.F., Chen, S.T., Wang, Y.T., Li, J.K., Shen, Q., Liu, X.L. and Guo, F.Q.** (2012) Downregulation of chloroplast RPS1 negatively modulates nuclear heat-responsive expression of HsfA2 and its target genes in *Arabidopsis*. *PLoS Genet*, **8**, e1002669.

CHAPTER 5

Arabidopsis DGD1 SUPPRESSOR 1 is a Subunit of the Mitochondrial Contact Site and Cristae Organizing System and Affects Mitochondrial Biogenesis

This work has been further edited and is published in *The Plant Cell* (<http://www.plantcell.org/content/31/8/1856>). Anastasiya Lavell contributed to this work by performing polar lipid profiling of total leaf tissues as well as isolated chloroplasts and mitochondria of the lines used in this study. She analyzed and interpreted the data and assisted in the writing of the sections discussing lipids.

Li, L., Lavell, A., Meng, X., Berkowitz, O., Selinski, J., van de Meene, A., Carrie, C., Benning, C., Whelan, J., De Clercq, I. and Wang, Y. (2019) Arabidopsis DGD1 SUPPRESSOR 1 is a subunit of the Mitochondrial Contact Site and Cristae Organizing System and affects mitochondrial biogenesis. *Plant Cell*.

Abstract

Mitochondrial and plastid biogenesis require the biosynthesis and assembly of proteins, nucleic acids and lipids. In *Arabidopsis thaliana* the mitochondrial outer membrane protein DGD1 SUPPRESSOR 1 (DGS1) is part of a large multi-subunit protein complex, which contains the mitochondrial contact site and cristae organizing system (MICOS) 60 kDa subunit (MIC60), the translocase of outer mitochondrial membrane 40 kDa subunit (TOM40), the translocase of outer mitochondrial membrane 20 kDa subunits (TOM20s) and the Rieske FeS protein (RISP). A point mutation in *DGS1* (*dgs1-1*), altered the stability and protease accessibility of this complex. This altered mitochondrial biogenesis, mitochondrial size, lipid content and composition, protein import and respiratory capacity. Whole plant physiology was affected in the *dgs1-1* mutant as evidenced by tolerance to imposed drought stress and altered transcriptional responses of markers of mitochondrial retrograde signaling. Putative orthologs of Arabidopsis DGS1 are conserved in eukaryotes, including the NCA2 (Nuclear Control of ATP Synthase 2) protein in yeast (*Saccharomyces cerevisiae*), but lost in Metazoa. The genes encoding DGS1 and NCA2 are part of a similar co-expression network including genes encoding proteins involved in mitochondrial fission, morphology and lipid homeostasis. Thus, DGS1 links mitochondrial protein and lipid import with cellular lipid homeostasis and whole plant stress responses.

Introduction

Mitochondrial biogenesis requires the import of proteins, RNAs and lipids (Schneider, 2011, Mesmin, 2016, Wiedemann and Pfanner, 2017). The signals and machinery for the import and assembly of proteins are well studied, and one emerging

theme is that many proteins are dually targeted to both mitochondria and chloroplasts, highlighting the coordination of function of these organelles (Murcha *et al.*, 2014). Both mitochondria and plastids contain their own genome, but rely on the import of nuclear-encoded proteins for the replication and expression of their genomes, with many of the involved proteins dually targeted (Elo *et al.*, 2003, Carrie *et al.*, 2009). While some lipids such as cardiolipin are produced in the mitochondria themselves, mitochondrial lipid biogenesis also depends on the import of lipids from other sites of synthesis, i.e., the endoplasmic reticulum and plastids (Michaud *et al.*, 2017). Lipid transfer/import into mitochondria takes place via contact sites and is non-vesicular in nature. However, little is known about the proteins involved in this process in plants. In contrast, in yeast (*Saccharomyces cerevisiae*) many of the proteins involved have been identified and characterized (Michaud *et al.*, 2017).

In yeast and mammals, the mitochondrial contact site and cristae organizing system (MICOS/MINOS/MitOS), which bridges the inner mitochondrial membrane (IMM) and the outer mitochondrial membrane (OMM), has multi-faceted functions in mitochondrial morphology, protein import and abundance, oxidative phosphorylation as well as lipid biogenesis and content (van der Laan *et al.*, 2016, Schorr and van der Laan, 2018). The components of MICOS are conserved in yeast and humans, with at least six subunits in yeast and nine subunits in humans (van der Laan *et al.*, 2012, Kozjak-Pavlovic, 2017). A phylogenetic analysis for eukaryotes proposed that only two core components of MICOS, MIC60 and MIC10, were conserved in plants (Munoz-Gomez *et al.*, 2015a, Munoz-Gomez *et al.*, 2015b). A study in *Arabidopsis* revealed that MIC60, interacting with the translocase of the outer membrane (TOM) via TOM40, forms part of a mitochondrial

transmembrane lipoprotein complex (MTL), and affects mitochondrial lipid trafficking (Michaud *et al.*, 2016).

Mitochondrial membrane lipid homeostasis, including biosynthesis and transfer of phospholipids and cardiolipin, is controlled by MICOS-mediated membrane contact sites with the endoplasmic reticulum (ER) (Aaltonen *et al.*, 2016, Wideman and Munoz-Gomez, 2016). In plants, transfer of lipids from plastids to mitochondria has also been detected and is also dependent on physical contact sites (Jouhet *et al.*, 2004). During phosphate (Pi) limitation, phospholipids are replaced by non-phosphorous galactoglycerolipids synthesized in plastids (Härtel *et al.*, 2000), although some galactoglycerolipids are also found in mitochondria under non-limiting phosphate growth conditions (Jouhet *et al.*, 2004, Michaud *et al.*, 2016). The regulatory mechanism behind determining the amount of mitochondrial galactoglycerolipids are unknown, as are the components responsible for their transfer from plastids to mitochondria.

The bulk of the galactoglycerolipids, i.e., mono- and digalactosyldiacylglycerol (MGDG and DGDG), are synthesized at the inner and outer envelope membranes of the plastid, respectively, and they are highly abundant in the thylakoid membranes of the chloroplast. Galactolipids are unique to photosynthetic membranes under normal conditions. However, in response to Pi deprivation, galactolipids are exported to extra-plastidic membranes (Moellering and Benning, 2011). Galactolipid biosynthesis is carried out in the chloroplast envelope membranes by a set of MGDG synthases (MGDs) that catalyze the formation of MGDG followed by DGD synthases (DGDs) that use MGDG to form DGDG (Benning and Ohta, 2005). *MGD1* and *DGD1* are constitutively expressed while *MGD2/3* and *DGD2* are induced in response to phosphate limitation (Awai *et al.*,

2001, Kelly and Dormann, 2002). To identify regulators of galactoglycerolipid biosynthesis in response to Pi deprivation, a genetic suppressor screen was conducted in the *Arabidopsis thaliana* *dgd1* mutant background. A *dgd1* suppressor mutant allele (*dgd1* suppressor 1, *dgs1-1*) was identified that constitutively activated the DGD1-independent pathway for DGDG biosynthesis (Xu *et al.*, 2003, Xu *et al.*, 2008). The affected protein, DGS1, has two membrane-spanning domains and was localized to the OMM as part of a larger protein complex (Xu *et al.*, 2008, Moellering and Benning, 2010). It contains a conserved domain also found in a yeast protein identified in a genetic screen for assembly of the ATP synthase complex, Nuclear Control of ATP Synthase 2 (NCA2) (Camougrand *et al.*, 1995).

In this study, we demonstrated that the OMM protein DGS1 is a novel subunit of MICOS in plants. We showed that DGS1 constituted part of a multi-subunit protein complex with MIC60. A point mutation of DGS1 affected chloroplast and mitochondrial lipid content and composition as well as mitochondrial biogenesis and function, which were also the effects of MICOS in yeast and mammals (van der Laan *et al.*, 2016, Schorr and van der Laan, 2018). DGS1 was conserved across eukaryotes but absent from Metazoa and Alveolata. NCA2, the yeast putative ortholog of DGS1, and DGS1 had a similar co-expression network including proteins involved in mitochondrial biogenesis.

Results

DGS1 is present in a multi-subunit protein complex with MIC60, TOM40, TOM20s and RISP

Using immunoblotting following blue native PAGE (BN-PAGE), immunoprecipitation and cross-linking with the membrane-permeable chemical crosslinker disuccinimidyl glutarate (DSG), DGS1 was found to be present in a multi-subunit protein complex that contains MIC60, TOM40, TOM20s and the Rieske FeS protein (RISP) of the cytochrome *bc₁* complex (Figure 5.1). Mass spectrometry of excised bands revealed that DGS1 co-migrated with MIC60 in the oxidative phosphorylation complexes (OXPHOS), complex V, complex III and complex F₁ (Figure 5.1A and Supplemental Dataset 1). The immunoblot following BN-PAGE revealed the majority of DGS1 was detected in complex III (Figure 5.11A), while MIC60 co-migrated with a variety of respiratory complexes (Figure 5.1A). Immunoprecipitation using a DGS1 antibody pulled down MIC60, TOM40, TOM20-2 and RISP, while the MIC60 antibody pulled down DGS1, TOM40, TOM20-2 and RISP (Figure 5.1B). RISP was not efficiently pulled down by MIC60. This may be due to the fact that while the majority of the DGS1 protein co-migrates with complex III (Figure 5.1A), MIC60 was found in a number of protein complexes (Figure 5.1A) (Michaud et al., 2016), and thus only a fraction of the MIC60 antibody recognized MIC60 that was in a complex with RISP. The interaction of MIC60 with the TOM complex is in agreement with a previous report that showed interaction between MIC60 and TOM40 (Michaud et al., 2016). COXII (a subunit of complex V) was not pulled down by either DGS1 antibody or MIC60 antibody, presented as a negative control (Figure 1B).

To further confirm the interactions, purified intact mitochondria were treated with membrane-permeable chemical crosslinker disuccinimidyl glutarate to capture transient, semi-stable and stable association of proteins. Disuccinimidyl glutarate is a crosslinker that uses the amine-reactive N-hydroxysuccinimide (NHS) ester group, linking amino to amino groups at $< 8\text{-\AA}$ in proximity. After crosslinking, centrifugation at 500 RCF for 2 min was performed to pellet and remove aggregated proteins. The supernatant (crosslinked sample) was analyzed by SDS-PAGE and immunodetection. The untreated mitochondria (non-crosslinked sample) were loaded beside as size control. Thus, crosslinked and non-crosslinked samples contained different amounts of mitochondrial input protein and cannot be compared for intensity. Therefore, we rather determined if the target proteins could be cross-linked into a complex with DGS1. DGS1, MIC60, TOM40, TOM20-2 and RISP were crosslinked by disuccinimidyl glutarate in a complex with an apparent molecular mass of 250 kDa (Figure 5.1C, indicated with a red line). TOM40 and TOM20-2 were also present in another complex with a molecular mass of around 200 kDa, likely representing the TOM complex (Figure 5.1C, indicated with a blue line). Taken together, DGS1 interacts with MIC60, RISP, TOM40 and TOM20-2 forming a multi-subunit protein complex.

The *dgs1-1* mutation alters the multi-subunit complex

To determine the function of the DGS1 protein in the multi-subunit complex, eight different transgenic and mutant lines of Arabidopsis were functionally characterized (Figure 5.2). The *dgs1-1* point mutation line (*dgs1-1*) was from the original study identifying the DGS1 protein (Moellering and Benning, 2010), which has a change in a

single amino acid from aspartic acid (D) to asparagine (N) at position 457 close to the predicted transmembrane region (Figure 5.2A). The *dgs1* T-DNA insertion line (*dgs1-2*) containing a T-DNA in the 3rd exon of the *dgs1* gene was confirmed by PCR and DNA sequencing (Figure 5.2A) and had a complete loss of DGS1 protein as indicated by immunoblotting (Figure 5.2B). This line was transformed with the sequences encoding the wild type DGS1 and the *dgs1-1* mutant protein, respectively, under the control of a 35S CaMV promoter to generate complemented lines with different levels of the native and mutated DGS1 protein. A summary of the mutants/complemented lines is listed in (Supplemental Dataset 2). The *DGS1* Comp (L) line produced the DGS1 protein at a low level, half of the DGS1 level in wild-type plants; the *DGS1* Comp (H) line produced the DGS1 protein at a high level, more than 10 times of the DGS1 level in wild-type plants (Figure 5.2B); the *dgs1-1* Comp (L) expressed the *dgs1-1* mutant coding sequence producing the *dgs1-1* mutant protein close to the DGS1 level in wild-type plants; *dgs1-1* Comp (M) expressed the *dgs1-1* mutant coding sequence producing 10 times more *dgs1-1* mutant protein than wild type DGS1 levels; and *dgs1-1* Comp (H1) and *dgs1-1* Comp (H2) expressed the *dgs1-1* mutant coding sequence producing 20 times more *dgs1-1* mutant protein than wild type DGS1 levels (Figure 5.2B).

To determine whether the abundance of MIC60, TOM40, TOM20s and RISP was affected in these lines, mitochondria were purified from the eight mutant/complementation lines and wild-type plants (*Arabidopsis* Col-0), and mitochondrial proteins were quantified by immunoblotting. *Arabidopsis* contains four genes that encode TOM20 proteins, but only three are expressed, *TOM20-2*, *TOM20-3* and *TOM20-4* (Lister *et al.*, 2007). The amount of all TOM20 proteins was observed to be reduced by ~ 50% in the *dgs1-1* line

and *dgs1-1* Comp (L) (Figure 5.2B). MIC60 also displayed a 10-15% reduction in abundance in the *dgs1-1* line and *dgs1-1* Comp (L), but this reduction was only statistically significant in the *dgs1-1* Comp (L) line (Figure 5.2B). The other two components of the multi-subunit complex, TOM40 and RISP, remained unchanged in the *dgs1-1* line and the *dgs1-1* Comp (L) line and were also unchanged in the lines over-expressing wild-type DGS1 protein, indicating that the *dgs1-1* mutant protein had a specific effect on MIC60 and TOM20 proteins. Finally, in both the *dgs1-1* Comp (M) and (H) lines with high levels of *dgs1-1* mutant protein, all the components were reduced in abundance (Figure 5.2B). The abundance of COXII that does not interact with the complex components was not changed in any line (Figure 5.2B).

The submitochondrial location of MIC60, TOM40, TOM20-2, RISP and DGS1 was determined by treating intact and outer membrane-ruptured mitochondria with increasing amounts of protease K, with uncoupling protein (UCP) and cytochrome *c* (Cyt *c*) as controls for inner-membrane and intermembrane space location, respectively. As expected, UCP was resistant to protease K with intact mitochondria and outer-membrane-ruptured mitochondria, and no difference was observed in the mutant lines when compared to Col-0 (Figure 5.2C). Cyt *c* was not detected in outer membrane-ruptured mitochondria isolated from Col-0, *dgs1-2* and plants complemented with the native DGS1 protein, showing complete rupture of OMM during swelling, with complete release of Cyt *c* into solution and thus it was absent from the pellet (Figure 5.2C). However, in *dgs1-1*, *dgs1-1* Comp (L), (M) and (H) plants, some Cyt *c* was still detectable in outer membrane-ruptured mitochondria (Figure 5.2C). This indicates that the OMM is not completely ruptured in *dgs1-1*, *dgs1-1* Comp (L), (M) and (H) lines during the swelling-shrinking

procedure. The reason is proposed to be that the structure of MICOS bridging the OMM and IMM has been changed due to the *dgs1-1* mutation. Similarly, MIC60 was accessible to protease K in outer membrane-ruptured mitochondria from Col-0, *dgs1-2* and plants complemented with the native DGS1 protein (Figure 5.2C), as expected for an intermembrane space exposed protein (Michaud *et al.*, 2016). Similar to Cyt *c*, MIC60 was still detectable with *dgs1-1*, *dgs1-1* Comp (L), (M) and (H) plants (Figure 5.2C). The opposite was observed with RISP. While it was totally protected from digestion in mitochondria isolated from Col-0, some digestion was observed in the *dgs1-1*, *dgs1-1* Comp (L), (M) and (H) plants upon rupturing the outer membrane (Figure 5.2C). TOM20-2 and TOM40 are outer-membrane proteins. They were digested by protease K both in intact mitochondria and outer-membrane ruptured mitochondria, and no difference was observed between the lines (Figure 5.S1). DGS1 showed a similar sensitivity as TOM20-2, with no difference among the lines (Figure 5.2C). The ~ 220 amino acid domain (75-297aa) at the N-terminal side of the first transmembrane domain, against which the DGS1 antibody was produced, was digested by protease K. This result suggested an N-out and C-out topology for DGS1 with a loop in the intermembrane space and two transmembrane regions (Figure 5.2A and 5.2C). This result also places the mutation in DGS1-1 on the intermembrane space side of the protein, potentially affecting mitochondrial proteins that may interact with DGS1. Thus, the *dgs1-1* mutant protein decreases the protease accessibility of MIC60 and Cyt *c*, while making RISP more accessible, even though the *dgs1-1* mutant protein is present at wild-type levels.

To determine if the *dgs1-1* mutant protein affected the multi-subunit complex containing DGS1, MIC60, TOM40, TOM20s and RISP (Figure 5.1C), mitochondrial

proteins from *dgs1-1* Comp (L) plants were crosslinked as outlined above. The abundance of DGS1, MIC60, TOM40 and TOM20-2 in the cross-linked 250 kDa complex was significantly reduced in *dgs1-1* Comp (L) plants, compared to Col-0 (Figure 5.2D, indicated with red asterisks). In contrast, the abundance of RISP in the cross-linked 250 kDa complex was increased in *dgs1-1* Comp (L) plants, compared to Col-0 (Figure 5.2D, indicated with blue asterisks). Based on these results, we conclude that the interaction between DGS1, MIC60, TOM40, TOM20 and RISP proteins is disturbed when *dgs1-1* mutant protein is expressed at native levels.

The *dgs1-1* mutation alters mitochondrial size

To determine whether disturbing the multi-subunit complex affects organellar distribution, morphology or size confocal and transmission electron microscopy were carried out. Plant mitochondria exist as a dynamic tubular reticulate network, that is maintained by a balance of fusion and fission (Palmer et al., 2011; Rose and McCurdy 2017). To assess overall morphology in terms of size, constructs for the transient expression of AOX-GFP (targeted to mitochondria) and KDEL-YFP (targeted to the ER) were transiently transformed into protoplasts isolated from Col-0, *DGS1* Comp (L), *DGS1* Comp (H), *dgs1-1* Comp (L), *dgs1-1* Comp (M) and *dgs1-1* Comp (H1) plants. In Col-0 and plants complemented with the native DGS1 protein, mitochondria surrounded chloroplasts, as is typical in protoplasts (Duchene *et al.*, 2005). In contrast, in *dgs1-1* Comp (L) the RFP signal showed that mitochondria were significantly enlarged forming a doughnut shape or oval structures (Figure 5.3A). While these structures varied in size, there were many mitochondria that were much greater in diameter than any mitochondrial

structures observed in Col-0, *DGS1* Comp (L) and *DGS1* Comp (H) lines. With increased levels of the *dgs1-1* mutant protein a further increase of mitochondrial size was observed in *dgs1-1* Comp (M) and *dgs1-1* Comp (H) plants (Figure 5.3A). Enlargement of mitochondria was also observed in yeast *mic60* strains and Arabidopsis *mic60* knockout lines (Rabl *et al.*, 2009, Michaud *et al.*, 2016). A corresponding reduction in chloroplast size was observed with increasing amounts of the *dgs1-1* mutant protein (Figure 5.3A). With *dgs1-1* mutant protein levels similar to native levels of the *DGS1* wild-type protein, the *dgs1-1* Comp (L) line had a significant reduction in chloroplast diameter (Figure 5.3A). By contrast, with higher levels of the *dgs1-1* mutant protein, mitochondrial size and diameter were equal to those of chloroplasts in the *dgs1-1* Comp (M) and *dgs1-1* Comp (H) lines (Figure 5.3A). The YFP signal showed that the ER structure was also affected in *dgs1-1* Comp (L), *dgs1-1* Comp (M), and *dgs1-1* Comp (H) (Figure 5.3A). Together, the shapes of mitochondria, chloroplast and ER were all affected in the lines expressing the *dgs1-1* mutant protein.

Transmission electron microscopy was carried out to investigate if the internal morphology of mitochondria was altered (Figure 5.3B). As transmission electron microscopy allows morphology to be assessed at a nanometer level it will allow assessment of changes in cristae morphology and/or number. Sections obtained from wild-type plants (Col-0) revealed mitochondria with numerous infoldings of the inner membrane that represent cristae. In contrast, in the *dgs1-1* line, *dgs1-1* Comp (L) line and *dgs1-1* Comp (H1) line, consistently fewer cristae could be detected (Figure 5.3B). The alteration of the inner membrane morphology with fewer cristae provides a possible reason why Cyt *c* was not completely released from OMM-ruptured mitochondria in the

dgs1-1, *dgs1-1* Comp (L), (M) and (H) lines observed above (Figure 5.2C). Thus, a change in a MICOS subunit in Arabidopsis results in changes in cristae abundance as described for yeast and mammalian MICOS systems (van der Laan *et al.*, 2016, Schorr and van der Laan, 2018).

The dgs1-1 mutation alters mitochondrial lipid composition

As MIC60 in Arabidopsis has been shown to play a role in lipid trafficking (Michaud *et al.*, 2016) and the *dgs1-1* mutant was identified based on its altered lipid composition (Xu *et al.*, 2008), the lipids of mitochondria and chloroplasts in *dgs1-1*, *dgs1-1* Comp (L), and *dgs1-1* Comp (H1) plants were profiled. The chloroplast lipid analysis showed that the total fatty acid profiles of Arabidopsis lines expressing the *dgs1-1* mutant protein had a dose- dependent decrease in 16:3 and 18:3 acyl chain abundance and a corresponding relative increase in 16:0, 18:1 and 18:2 acyl chain abundance (Figure 5.4A). The decrease in 16:3 methyl esters abundance can be attributed primarily to the change in monogalactosyldiacylglycerol (MGDG) acyl composition. As the predominant chloroplast lipid, it typically carries 16:3 and 18:3 acyl chains in a 1:2 ratio, respectively, at the *sn*-1 and *sn*-2 positions of the glycerol backbone. Additionally, the observed decrease in total abundance of 18:3 acyl chains in the chloroplast lipids was due to a decreased abundance of 18:3 acyl in digalactosyldiacylglycerol (DGDG), phosphatidylglycerol (PG), and sulfoquinovosyldiacylglycerol (SQDG) (Figure 5.4A).

In mitochondria, the most abundant lipids, cardiolipin (CL), phosphatidylcholine (PC), and phosphatidylethanolamine (PE), all showed a significant decrease in 18:2 acyl chain abundance that appeared dependent on the abundance of the *dgs1-1* mutant

protein (Figure 5.4B). Additionally, there was a corresponding increase in the relative amount of 16:0 acyl chains esterified to those lipids (Figure 5.4B). The total lipid profiles showed a significant decrease in the relative amount of CL with increased levels of the *dgs1-1* mutant protein, while the relative amount of PC was increased (Figure 5.4B).

Analysis of total leaf lipids revealed a dose-dependent decrease in 16:3 acyl chain abundance with a relative increase in 18:1 acyl chain abundance (Figure 5.S2A). The total leaf DGDG and MGDG showed the same trend as in chloroplasts as would be expected. A decrease in the 18:2 acyl chains in PC and 18:3 acyl chains in PG was accompanied by a relative increase in 18:1 acyl chains. For PE a decrease in 18:2 chains was also observed in total leaf lipid profiles like in mitochondria, but an increase in 18:3 acyl chains was observed in total lipids that was not observed for mitochondrial lipids. For PC the same pattern was observed in lipids from mitochondria and total leaf lipids; a decrease in 18:2 acyl chains with a corresponding increase in the 18:1 acyl chains. Thus, the total leaf lipid composition was changed, but the largest effect was observed with mitochondria and chloroplast lipids. It should be noted that in the line with the highest amount of *dgs1* mutant protein galactolipids MGDG and DGDG and oligogalactolipids were observed to be associated with the mitochondrial fraction above wild-type background levels (Figure 5.S2B). Typically, MGDG and oligogalactolipids are restricted to chloroplasts. The latter are formed under stress conditions by the action of SFR2 (Moellering et al., 2010).

To interpret why the mitochondrial DGS1 protein could affect chloroplast lipid composition, the locations of the DGS1 wild-type protein and the *dgs1-1* mutant protein were investigated. The constructs expressing the DGS1 wild-type protein and the *dgs1-*

1 mutant protein tagged with C-terminal GFP or N-terminal GFP were transiently transformed into wild-type protoplasts, with SSU-RFP as chloroplast control, AOX-RFP as mitochondrial control and KDEL-RFP as ER control. The fluorescence imaging revealed that the DGS1 protein was located in mitochondria, while the *dgs1-1* mutant protein was associated with both mitochondria and the ER (Figure 5.4C). To confirm these results, chloroplast, mitochondria and ER fractions were isolated from Col-0, *dgs1-1*, *dgs1-2* mutant and complemented lines, followed by immunoblotting with the DGS1 antibody. In Col-0, the DGS1 wild-type protein was only detectable in mitochondria (Figure 5.4D). In contrast, in the mutant lines that expressed the *dgs1-1* mutant protein, it was detectable in both mitochondria and the ER (Figure 5.4D), even when expressed at native levels. No DGS1 protein or *dgs1-1* mutant protein was detected in chloroplasts (Figure 5.4C and 5.4D).

The *dgs1-1* mutation affects mitochondrial protein abundance, protein import and alternative respiratory capacity

MICOS was reported to affect mitochondrial protein import and respiration in yeast and mammals (Schorr and van der Laan, 2018). To determine whether disturbing the multi-subunit complex by the presence of *dgs1-1* mutant protein had the same effects in plants, the abundance of various proteins involved in protein import and respiration was determined. Notably the *dgs1-2* null mutant did not affect the abundance of any protein or the activity of the respiratory chain (Figure 5.5A and 5.5B). However, both the *dgs1-1* mutant and the *dgs1-1* Comp (L) line with protein levels comparable to wild type showed decreased abundance of an outer membrane α -barrel protein in plant mitochondria

(OM47) (Li *et al.*, 2016), TIM44, and alternative oxidase (AOX) (Figure 5.5A). The consistent decrease in abundance of TOM20s (Figure 5.2B), OM47, TIM44 and AOX (Figure 5.5A) in all lines expressing the *dgs1-1* mutant protein indicates that the mutated *dgs1-1* protein has an effect on specific proteins or pathways. However, it is worth noting that abundance of almost all mitochondrial proteins tested showed a decrease of various degrees in lines expressing medium and high levels of the *dgs1-1* mutant protein (Figure 5.5A). We consider that this is an unspecific effect that may result from the altered mitochondrial lipid content and high level of *dgs1-1* mutant protein (Figure 5.4A), and such decreases were not observed in the lines expressing high levels of the DGS1 wild type protein (Figure 5.5A). Along with the alterations in abundance of mitochondrial proteins, a similar trend was observed in respiratory capacity (Figure 5.5B). The activity of the alternative oxidase pathway as assessed by the reduction in n-propyl gallate sensitive oxygen uptake was specifically inhibited by the expression of the *dgs1-1* mutant protein (Siedow and Girvin 1980). This reduction in activity of the alternative pathway was observed even when the *dgs1-1* mutant protein was expressed at physiological levels. A general reduction in total respiration and respiration through the cytochrome *c* oxidase pathway, and oxygen consumption driven by oxidation of substrates by complex I and complex II was observed only with high levels of *dgs1-1* mutant protein, but not DGS1 wild-type protein (Figure 5.5B).

To examine if mitochondrial protein import ability was affected by the presence of the *dgs1-1* mutant protein, *in vitro* import of radiolabeled plant mitochondrial precursor proteins into mitochondria isolated from Col-0, *dgs1-1* Comp (L) and *dgs1-1* (H1) plants was carried out (Figure 5.5C). For the precursor protein of AOX, representing the general

import pathway, and the adenine nucleotide carrier ANT, representing the carrier import pathway, strongly reduced import rates were observed with both *dgs1-1* Comp (L) and *dgs1-1* Comp (H) plants, compared to Col-0 (Figure 5.5C), indicating an impairment of mitochondrial protein import by the presence of the *dgs1-1* mutant protein.

Higher drought stress tolerance in dgs1-1 mutant plant lines

Quantitative phenotypic analysis revealed that the plants expressing the *dgs1-1* mutant protein were smaller than Col-0 and the severity of the retarded growth phenotype was associated with the levels of the *dgs1-1* mutant protein (Figure 5.S3). The *dgs1-1* Comp (H1) and *dgs1-1* Comp (H2) plants, which express high levels of *dgs1-1* mutant protein, displayed an early senescence phenotype as evidenced by leaves losing chlorophyll after 3 weeks, a lower number of rosette leaves, and smaller inflorescence (Figure 5.S3). No growth defect was observed for the *dgs1-2* null allele, *DGS1* Comp (L) and *DGS1* Comp (H) plants (Figure 5.S3). Exposing mutant lines to drought stress revealed that *dgs1-1*, and *dgs1-1* Comp (L) were more tolerant than Col-0, *dgs1-2*, *DGS1* Comp (L) and *DGS1* Comp (H) plants (Figure 5.6A). The *dgs1-1* Comp (H1) plants also displayed higher drought tolerance. To determine the underlying biochemical changes, the rosette leaves #5-7 were subjected to 3,3'-diaminobenzidine tetrahydrochloride (DAB) and nitroblue tetrazolium (NBT) staining to visualize the accumulation of hydrogen peroxide and superoxide radicals, respectively. The *dgs1-1*, *dgs1-1* Comp (L) and *dgs1-1* Comp (H1) lines displayed less ROS accumulation after 8 and 10 days of drought treatment as evidenced by the lower intensity of stains (Figure 5.6A). After 14 days of water deprivation followed by 3 days of recovery after resupply of water, more than 80%

of plants survived with *dgs1-1*, *dgs1-1* Comp (L) and *dgs1-1* Comp (H) lines, while less than 10% of the Col-0, *dgs1-2*, *DGS1* Comp (L) and *DGS1* Comp (H) plants survived (Figure 5.6A). Quantification of relative water content, quantum efficiency of photosystem II (F_v/F_m), total chlorophyll concentration and CO₂ fixation (Figure 5.6B) suggested that the plants expressing the *dgs1-1* mutant protein were more effective at maintaining water content and photosynthetic efficiency during drought stress.

DAB staining of the *dgs1-1* lines revealed that the *dgs1-1* Comp (H1) plants, which displayed an early senescence phenotype (Figure 5.S3), contained higher levels of H₂O₂ than Col-0 plants even when not subjected to adverse (drought) conditions (Figure 5.6A, bottom panel), yet these plants displayed survival under drought compared to lines expressing the DGS1 native protein. Quantification of H₂O₂ in leaves revealed that plants with high levels of the *dgs1-1* mutant protein contained higher levels of endogenous H₂O₂ (Figure 5.S4). This is consistent with the original identification of *dgs1-1* where over-expression resulted in growth defects and an increase of two to three-fold in H₂O₂ (Xu et al., 2008). The *dgs1-1* and *dgs1-1* Comp (L) plants, expressing lower level of *dgs1-1* mutant protein, contained a similar level of H₂O₂ as Col-0 plants and did not show acceleration of dark-induced leaf senescence (Figure 5.S4). Thus, the amount of the *dgs1-1* mutant protein present is important in determining the phenotypes observed.

To determine the underlying molecular alterations in *dgs1-1* and *dgs1-1* Comp lines, transcriptomes of mutant and wild-type plants were analyzed by RNA-Sequencing. The transcriptome of plants grown under non-limiting growth conditions was not severely altered in the mutant lines, except for the complemented lines with high levels of DGS1 wild-type protein or *dgs1-1* mutant protein (Figure 5.7A, 5.7B). *DGS1* Comp (H) and *dgs1-*

1 Comp (H1) had 52 and 162 genes with altered basal expression, respectively, while all other lines had less than 10 differentially expressed genes (DEGs) (fold change > 2 and FDR < 0.05) compared to the wild type (Supplemental Dataset 3). Under water limited conditions, the transcriptome of plants containing the *dgs1-1* mutant protein different to wild type and *dgs1-2* lines complemented with the wild type coding sequence for DGS1. Compared to the wild-type that had 2230 and 2848 genes up- and down-regulated by drought, plants showed a reduced number of DEGs, with 1884, 1740 and 1640 genes up-regulated and 2450, 2333 and 2222 genes down-regulated in *dgs1-1*, *dgs1-1* Comp (L) and *dgs1-1* Comp (H1), respectively (Figure 5.7A). From the total number of drought-responsive genes in the wild type, only 65%, 66% and 55% were similarly (> 2-fold change in the same direction and FDR < 0.05) responsive in *dgs1-1*, *dgs1-1* Comp (L) and *dgs1-1* Comp (H1), respectively.

To further reveal the effect of the *dgs1-1* allele on the drought-responsive processes, genes that were commonly altered in *dgs1-1* and *dgs1-1* Comp (L) were analyzed as both these lines provide a read-out of the effects of the *dgs1-1* allele expressed at native levels (Figure 5.7B, Supplemental Dataset 3). From the 720 DEGs in *dgs1-1* and *dgs1-1* Comp (L) compared to Col-0 under drought stress, three clusters could be identified that are indicated in blue, red and green (Figure 5.7B). Genes in each cluster were functionally classified by GO term enrichment analysis as indicated with the same colors (Figure 5.7C). Two hundred and sixty-five genes (blue cluster) were drought induced in Col-0, *dgs1-2*, *DGS1* Comp (L) and *DGS1* Comp (H), but their induction was partially or completely abolished in *dgs1-1* mutant lines (Figure 5.7B). These genes are associated with GO terms related to abiotic stresses such as drought, salt, hydrogen

peroxide, cold and stress-induced senescence, indicating that all the DGS1-1 expressing plants have largely not activated abiotic stress responses (Figure 5.7C). Among them are genes encoding transcription factors for drought-induced gene expression (ANAC019, ANAC072 and ANAC032), proteins involved in osmoprotection (EARLY RESPONSE TO DEHYDRATION SIX-LIKE 1, ARABIDOPSIS MITOCHONDRIAL BASIC AMINO ACID CARRIER 2, and LATE EMBRYOGENESIS ABUNDANT and DEHYDRIN family proteins) and proteins involved in cell wall remodeling (GLYCOLIPID TRANSFER PROTEIN, XYLOGLUCAN ENDOTRANSGLUCOSYLASE/HYDROLASE, and CELLULOSE SYNTHASE family proteins). A second cluster (red) consists of 367 genes involved in photosynthesis, primary metabolism and auxin signaling. These are down-regulated in Col-0, *dgs1-2*, *DGS1* Comp (L) and *DGS1* Comp (H) plants during drought stress conditions. This re-direction of energy/growth metabolism during drought stress was severely diminished in all lines expressing the mutated *dgs1-1* protein, again consistent with a lack of stress response. A third cluster (green) contains genes that are up-regulated in the three *dgs1-1*-expressing genotypes only. These are involved in sulfur metabolism and glucosinolate biosynthesis pathways (METHYLTHIOALKYLMALATE SYNTHASE1, METHIONINE AMINOTRANSFERASE4, CYTOCHROME P450 79F1, 3-ISOPROPYLMALATE DEHYDRATASE SMALL SUBUNIT 1 and the MYB28, MYB29 and MYB76 transcription factors). Together, these data indicate that the dampened transcriptomic responses to drought stress in all genotypes expressing *dgs1-1* are attributed to the increased drought tolerance, which are probably caused by the altered physiological characteristics (e.g. lipid composition) or the ectopically expressed genes, e.g. involved in glucosinolate biosynthesis.

Phylogenetic and co-expression networks of DGS1 putative orthologs

As DGS1 was putatively orthologous to NCA2 of yeast, a comparative analysis of their phylogeny was performed. DGS1/NCA2 orthologues were detected in plants and fungi and in a limited number of animal groups, in Amoebozoa, Chromists and Excavates, but not the Metazoa. It was also absent from the Alveaeolata (Figure 5.8A, Supplemental Dataset 4). However, the widespread presence in plants, fungi and the Choanoflagellata (*Salpingoeca rosetta*), Filasterea (*Capsaspora owcazarzaki*) and Ichthyosporea (*Sphaeroforma arctica*) suggests that it was lost in multi-cellular animals.

To further explore their relationship, *DGS1* and *NCA2* were analyzed for co-expressed genes (Figure 5.8B, Supplemental Dataset 5). *DGS1* was strongly co-expressed with *MIC60* (15th most co-expressed genome wide), but not with *MIC10*, whereas *NCA2* was co-expressed with *MIC27*, *MIC26*, *MIC60*, and *MIC12*. Both *DGS1* and *NCA2* were co-expressed with genes related to mitochondrial fission and morphology. These included the Arabidopsis gene encoding dynamin-related GTPase DRP3B and its yeast ortholog Dnm1. Those together with yeast mitochondrial fission 1 (Fis1) are required for mitochondrial and peroxisome fission (Otsuga et al., 1998; Mozdy et al., 2000; Bleazard et al., 1999; Fujimoto et al., 2009). Arabidopsis *drp3b* mutants and yeast *dnm1* and *fis1* mutants are defective in mitochondrial fission and display altered mitochondrial morphology, similar to the *dgs1-1* mutant. Interestingly, cardiolipins are required for mitochondrial fission by stabilizing the Arabidopsis DRP3 oligomer complexes (Pan et al., 2014). Similarly, a functional MICOS and cardiolipins are required for Drp1 complex stability and mitochondrial morphology in mammalian cells (Bustillo-

Zabalbeitia *et al.*, 2014, Pan *et al.*, 2014). In addition, *DGS1* was co-expressed with *MIRO-RELATED GTP-ASE 1* that is involved in mitochondrial motility and morphology, in a pathway independent of the DRP3 fission machinery (Yamaoka and Leaver, 2008). *NCA2* was co-expressed with various genes involved in lipid metabolism and transport. For instance, the OMM protein Mitochondrial distribution and morphology 34 (Mdm34) is a core component of the ER-mitochondrial tethering (ERMES) complex and functions in mediating lipid import from the ER into the mitochondria (Kornmann *et al.*, 2009, Klecker *et al.*, 2015). Translocator, assembly and maintenance 41 (TAM41), a mitochondrial phosphatidate cytidyltransferase is required for cardiolipin biosynthesis (Kutik *et al.*, 2008), and Cardiolipin-specific deacylase 1 (CLD1) is a mitochondrial cardiolipin-specific phospholipase (Beranek *et al.*, 2009). *DGS1* was co-expressed with *PHOSPHOLIPASE D P1* that is required for extraplastidial galactolipid biosynthesis during phosphate starvation (Cruz-Ramirez *et al.*, 2006). In addition, *NCA2* (but not *DGS1*) was co-expressed with genes encoding several components of the mitochondrial complex III, complex IV, and the F₁F₀-ATP synthase complex. These results showed that *DGS1* and *NCA2* were co-expressed with conserved cellular processes, indicating a similar function across phyla.

Discussion

A number of lines of evidence indicate that the outer mitochondrial membrane protein *DGS1* from *Arabidopsis* forms a multi-subunit complex that contains MIC60, a conserved core subunit of MICOS and previously identified in *Arabidopsis* as an important component involved in lipid trafficking in a complex called MTL (Michaud *et al.*, 2016)

(Figure 5.8C). Consistent with our results, TOM40 and TOM20 proteins and RISP were also identified as components of MTL previously (Michaud *et al.*, 2016), and our work establishes a link between DGS1 and this complex. We found that DGS1 represented an outer membrane component of MICOS that played a role in lipid homeostasis in plant organelles, possibly by forming contact sites with the ER and/or chloroplast/plastids to facilitate lipid import into plant mitochondria. A complete loss of the DGS1 protein in *dgs1-2* had no apparent effect on mitochondrial activity, mitochondrial protein composition and size. By contrast, the presence of the *dgs1-1* mutant protein resulted in a number of alterations. At a comparable molecular level, the introduction of the *dgs1-1* mutant protein resulted in decreased amounts of TOM40, TOM20 and MIC60 in this MICOS complex (Figure 5.2D) and weakened protease K sensitivity of MIC60 in our experiments (Figure 5.2C), while the increased amounts of the RISP (Figure 5.2D) and its increased sensitivity to protease K (Figure 5.2C), indicate an altered structure of the MICOS complex (Figure 5.8C). This is likely the consequence of the point mutation present at the intermembrane space side of the *dgs1-1* protein, altering its binding affinity with these proteins (Figure 5.8C). Notably, a decrease in the amount of TIM44 in mitochondria was evident (Figure 5.5A), likely being responsible for the reduced rates of protein import observed (Figure 5.5C). In plants, the general mitochondrial processing peptidase (MPP) is integrated into the cytochrome *bc₁* complex (Braun *et al.*, 1992, Glaser *et al.*, 1994), and therefore an increased association of the *dgs1-1* mutant protein with the RISP may destabilize TIM44.

Alternatively, altered mitochondrial membrane protein abundances could be due to the altered lipid composition of mitochondria, with fewer cristae present in mitochondria that contain the *dgs1-1* mutant protein (Figure 5.3B). The non-bilayer-forming

phospholipids CL and PE are required for cristae structures and stabilization of respiratory complexes, whereas bilayer-forming phospholipid PC stabilizes TIM complexes (Schuler *et al.*, 2016). Together, alterations in lipid composition, protein abundance and potentially also altered mitochondria-ER contacts (that are hotspots for mitochondrial fission) by dysfunctional MICOS may be part of the reasons for the altered organelle size of mitochondria, chloroplasts and the ER as evidenced by visualization with fluorescence tagging of proteins (Figure 5.3A). The significantly altered size of mitochondria that express the *dgs1-1* mutant protein at physiological levels suggests that the balance between fusion and fission is altered in the *dgs1-1* mutant lines. This may result from an interaction of DGS1 with proteins involved in mitochondrial fusion and fission and mitochondrial dynamics (Figure 5.8B). Alternatively, cardiolipins which were altered in *dgs1-1* mutant lines stabilize Arabidopsis DRP3 that is required for fission (Pan *et al.*, 2014).

While the majority of DGS1 co-migrated with MIC60 in complex III on BN-PAGE, it was clear that MIC60 was present in a number of other complexes including supercomplexes I+III, complex I, III and V (Figure 5.1A). Previously, it was reported that the MTL complex in Arabidopsis is comprised of 200 proteins, including DGS1 (Michaud *et al.*, 2016). Thus, it is likely that the interaction of DGS1 with MIC60 is a dynamic interaction, positioning MIC60 at the interface with protein and lipid import into plant mitochondria. Notably the impact of the *dgs1-1* mutant protein on protein and lipid import into mitochondria, directly or indirectly decreasing the abundance of both TOM20s and TIM44, indicates that mitochondrial biogenesis is affected by disordering the stability or dynamics of this complex. While MIC60 and MIC10 seem to be the only subunits

conserved between yeast, plants and animals, alteration of the MICOS complex appears to have very similar impacts in all three phyla. MICOS in yeast and mammals has multifaceted effects on mitochondrial morphology, protein import and abundance, oxidative phosphorylation and lipid synthesis (van der Laan *et al.*, 2016, Schorr and van der Laan, 2018), which are similar to the alterations observed in this study with the expression of the *dgs1-1* mutant protein.

DGS1 in plants displays sequence similarity with a yeast protein that has been called Nuclear Control of ATP Synthase 2 (NCA2), identified in a genetic screen for genes required for the assembly/accumulation of the ATP synthase complex in yeast by yet unknown mechanisms (Pelissier *et al.*, 1995). A comprehensive analysis of the yeast mitochondrial proteome identified it as an outer membrane protein (Zahedi *et al.*, 2006). DGS1/NCA2 proteins are present in a wide range of eukaryotes, but appear to have been lost in Metazoa (Figure 5.8A). The DGS1/NCA2-encoding genes also displayed similarities in their co-expressed genes that encode MICOS proteins, but also proteins involved in mitochondrial fission, morphology and lipid homeostasis (Figure 5.8B). These proteins are conserved across kingdoms and act at mitochondria-ER contact sites where mitochondrial fission is initiated (Friedman *et al.*, 2011). We propose that the DGS1 and NCA2 proteins play similar, but not identical, roles in yeast and plants for lipid import. This hypothesis is based on the fact that the decrease in ATP synthase in yeast is likely a secondary effect of an altered lipid composition, and cardiolipin may be a specific target that is required for the stability of the ATP synthase complex (Mehdipour and Hummer, 2016). To be noted, DGS1 and NCA2 also have specific functions. Plants carrying a homozygous null allele *dgs1-2* had no detectable alterations in plant growth or

mitochondrial function. Thus, while a specific point mutation of DGS1 in *dgs1-1* resulted in an altered phenotype, a complete knockout can be compensated by other routes. This suggests that while DGS1 is part of the plant MICOS complex, import of lipids into mitochondria can still take place in the absence of the DGS1 protein. It should also be noted that it is possible that DGS1 in plants has developed additional functions needed for the complex interaction of plants with the changing environment.

AOX is a well-established marker of mitochondrial retrograde signaling (Ng *et al.*, 2014) as it is induced upon perturbation of mitochondrial functions. An original observation for the *dgs1-1* line was that the amount of AOX in mitochondria was reduced (Moellering and Benning, 2010). Altered AOX levels are likely attributed to altered lipid membrane homeostasis and/or membrane morphology affecting protein stability. However, as AOX is typically induced by a variety of abiotic stresses (Ng *et al.*, 2014), and the drought stress responsive transcriptome was affected by the *dgs1-1* allele, altered signaling in *dgs1-1* mutant cannot be excluded. Although most of the altered responses represent a dampened stress response due to the increased drought tolerance of *dgs1-1* plants, a small set of genes involved in sulfur metabolism and glucosinolate biosynthesis was mis-expressed in these lines (Figure 5.7B). Up-regulation of glucosinolate biosynthesis and metabolism has been linked to responses to drought stress (Eom *et al.*, 2018). A positive regulator of glucosinolate metabolism in Arabidopsis, MYB29, has been previously shown to be a negative regulator of AOX expression (Zhang *et al.*, 2017), and this may account for the reduction of AOX observed in the *dgs1-1* lines (Figure 5.5A). This supports the suggestion that there is an antagonistic relationship in the induction of glucosinolate metabolism and AOX (Zhang *et al.*, 2017), with the former

favored in the *dgs1-1* lines. Glucosinolate biosynthesis is also regulated by jasmonic acid and there is an antagonistic interaction between the jasmonic and salicylic acid hormone signaling pathways in *Arabidopsis* (Thaler *et al.*, 2012). Salicylic acid is involved in the induction of AOX, and research has indicated that this acts at the post-transcriptional level (Rhoads and McIntosh, 1992, Ho *et al.*, 2008). Thus, the reduction in AOX may be due to altered plant hormone signaling. Additionally, the *GENOMES UNCOUPLED 4* (*GUN4*) gene was greatly up-regulated upon drought in the *dgs1-1* background (Figure 5.7B). *GUN4* plays a regulatory role in promoting chlorophyll accumulation in response to changing environmental conditions (Larkin *et al.*, 2003). This is consistent with the observed drought-resistant phenotype, with chlorophyll concentrations and photosynthetic capacity maintained longer in *dgs1-1* mutant lines than in the wild type.

Materials and Methods

Plant Materials

The *Arabidopsis* *DGS1* (AT5G12290) mutant *dgs1-2* (SAIL_391_F04) and *dgs1-1* alleles were described previously (Xu *et al.*, 2008, Moellering and Benning, 2010). All complementation lines, *DGS1* Comp (Low/High) with low (L) or high (H) expression of native *DGS1* protein and *dgs1-1* Comp (Low/ Middle /High) with low (L), moderate (M) or high (H) expression of the *dgs1-1* mutant protein were generated in the null allele *dgs1-2* background by gateway cloning of the *DGS1* or *dgs1-1* coding sequence into the binary destination vector pK7WG2 and *Agrobacterium*-mediated transformation via floral dipping. The cloning primers are listed in (Supplemental Dataset 6). *dgs1-1* Comp (H1)

and *dgs1-1* Comp (H2) are two individual complementation lines with high but nearly equal levels of *dgs1-1* mutant protein. The mutants and complementation lines were confirmed by quantification of the DGS1 or *dgs1-1* mutant protein.

Plant Growth and Treatments

For normal conditions, Arabidopsis plants were grown in growth chambers at 22°C, 100 $\mu\text{mol m}^{-2} \text{s}^{-1}$ light (color code 840, light color 4000K – cool white, 5240 Lumen and 150 cm long, Philips Master TL-D 56 W / 840 RefleX) in a 16-h light/8-h dark photoperiod. Seeds were sterilized and sown on Gamborg's B5 medium (PhytoTechnology, Austratec) supplemented with 3% (m/v) sucrose, 0.43 g/L Gamborg's B5 salts (Austratec), 2 mM MES hydrate (Sigma-Aldrich), and 0.90% (w/v) Difco™ agar (BD Biosciences). The pH was adjusted to 5.7. Seeds were stratified for 48 h before being transferred to growth chambers in all experiments. For soil-based phenotyping or drought treatment, all lines were grown in a randomized design on soil mix. Watering was withheld when plants were 24 days old and plants were resupplied with water after 14 days.

Isolation of mitochondria, chloroplast and ER

Mitochondria, chloroplasts and ER were isolated as described (Cline *et al.*, 1981, Bessoule *et al.*, 1995, Lister *et al.*, 2007), respectively, from seedlings grown on Gamborg's B5 medium for 2 weeks. Fractions were stored at -80°C and maintained on ice when in use.

Blue-native PAGE

Twenty micrograms of mitochondria was solubilized in 2 μ l 5% (w/v) digitonin and separated on a NativePAGE™ Novex® 4-16% Bis-Tris Gel (Life Technology, Melbourne, Australia). One-dimensional BN-PAGE was carried out as described previously (Eubel *et al.*, 2005). Following separation, gels were fixed and stained with Coomassie colloidal dye (Bio-Rad) or transferred to a PVP membrane followed by immunodetection with the antibodies of DGS1, MIC60, TOM40, RISP and COXII detailed in Supplemental Dataset 7.

Immunoprecipitation (IP)

Two hundred micrograms of mitochondrial proteins was solubilized and immunoprecipitated using the Immunoprecipitation Kit (Protein A) (Roche, Germany). Sample buffer was added after wash and denaturing of proteins was achieved by heating to 100°C for 3 min that was followed by 30 seconds centrifugation at 12,000 RCF at 25°C to release proteins from beads. Samples were resolved by SDS-PAGE, transferred to a nitrocellulose membrane, and immunodetected with the antibodies of DGS1 and MIC60 detailed in Supplemental Dataset 7.

Cross-Link Assay

Protein cross-linking using disuccinimidyl glutarate was performed according to manufacturer's instruction (Thermo Scientific, Melbourne, Australia). One milligram of freshly isolated mitochondria from 2-week-old water cultured Arabidopsis wild-type and mutant plants were precipitated by centrifugation at 17,500 RCF at 4°C for 2 min and

resuspended with PBS buffer (100 mM sodium phosphate, 0.15 M NaCl, pH 7.2) to a final concentration of 2 µg/ µl. The samples were subsequently incubated with 5 mM disuccinimidyl glutarate (DSG)-PBS buffer. Samples were placed on ice for 2 h and quenched with 1 M Tris-HCl (pH 7.5) for 15 min at room temperature. Centrifugation at 500 RCF at 4°C for 2 min was performed to pellet and remove aggregated proteins. The supernatant was kept for further analysis by SDS-PAGE and immunodetection.

Generation of the DGS1 antibody

The fragment of the DGS1 protein (amino acids 75–297) before the first predicted transmembrane-spanning domain (TM) was cloned by PCR reactions using primers listed in Supplemental Dataset 6, cloned into the Gateway pDEST17 vector (Invitrogen, Sydney, Australia), and transformed into the *E.coli* BL21-AI™ (DE3) expression strain according to the manufacturer's instructions (Invitrogen, Sydney, Australia). A single colony was cultured in 50 ml of LB medium containing 50 µg ml⁻¹ carbenicillin, 0.1% (m/v) glucose and 0.05% (m/v) L-arabinose with shaking overnight at 37°C until the OD₆₀₀ reached 0.6–1.0. Afterwards, 950 ml of fresh LB medium was inoculated and cells were grown with shaking until the OD₆₀₀ reached 0.4. Protein expression was induced with 1.0 mM isopropyl-β-D-thiogalactopyranoside (IPTG) and the cell culture was harvested after 3 h incubation by centrifugation at 8,000 RCF at 4°C for 20 min. Cells were resuspended in 50 ml wash buffer (50 mM KH₂PO₄, 300 mM KCl, 5 mM imidazole, pH 8.0) and lysed by sonication. The protein was purified by denaturing immobilized metal affinity chromatography (IMAC) using the Profinia protein purification system (Bio-Rad, Sydney,

Australia). Three aliquots of 200 µg purified protein were used for injection into rabbits (WEHI, Australia) and the serum was tested by immunoblot.

Immunoblot Analysis

Proteins of different cell fractions were resolved by SDS-PAGE and transferred to a Hybond-C extra nitrocellulose membrane. Immunodetections were performed as described previously (Wang *et al.*, 2012). The antibodies used in this study were listed in Supplemental Dataset 7. The intensities of bands of interest were quantified using Image Lab™ software (Bio-Rad) and calculated relative to the wild type. Three biological replicates were performed. Significant difference was determined using a Student's *t*-test and $P \leq 0.05$ is indicated by asterisks or numbers in red. Antibodies used in this study are listed in Dataset S7.

Outer membrane ruptured mitochondria preparation and protease treatment

Two hundred micrograms of freshly isolated mitochondria were precipitated, and the pellet was gently resuspended in 20 µl SHE buffer (250 mM sucrose, 1 mM EDTA and 10 mM HEPES-KOH, pH 7.4) and incubated on ice for 15 min after mixing with 310 µl 20 mM HEPES-KOH (pH 7.4). Following incubation, 50 µl 2 M sucrose and 20 µl 3 M KCl were added to rupture the outer membrane. Equal amounts of outer membrane ruptured mitochondria and intact mitochondria were incubated for 30 min on ice with 0 to 2 mg/ml protease K, and 4 µl of 100 mM phenylmethane sulfonyl fluoride (PMSF) was added to terminate the reaction. Samples were precipitated by centrifugation at 13,000 RCF at 4°C for 3 min and, resuspended in 100 µl of SDS-PAGE sample buffer (10% (m/v) SDS, 1%

(v/v) β -mercaptoethanol, 18.75% (v/v) glycerol, 0.1% (m/v) bromophenol blue and 150 mM Tris-HCl, pH 6.8). Ten microliters of each sample was used for SDS-PAGE and immunodetection.

Protoplast Preparation and Fluorescence Microscopy

Protoplasts were isolated from the true leaves of 4-week-old *Arabidopsis* plants using Tape-*Arabidopsis* Sandwich methods as described (Wu *et al.*, 2009). A mixture of protoplasts ($2-5 \times 10^5$ cells/ml) and 20 μ g of plasmid DNA was incubated with 0.2 ml 40% (m/v) PEG 4000 at room temperature for 20 min, precipitated at 100 RCF for 1 min and resuspended with 1 ml W5 solution. Washes were repeated twice and protoplasts incubated in the dark at 19-20°C overnight. Fluorescence imaging was carried out using a Zeiss LSM780 laser scanning confocal microscope with an LD C-Apochromat 40x/1.1 water or 100x/1.4 Oil-immersion objective in multi-track channel mode. Image processing was performed using ZEN 2.3 (blue edition, Carl Zeiss Microscopy GmbH, 2011).

Electron Microscopy

Leaf tissue samples were cryofixed using a Leica EM ICE high pressure freezer (Leica Microsystems) followed by freeze substitution in 1% osmium tetroxide in acetone for 72 h at -85°C. The samples were then slowly warmed to room temperature over the course of 24 h. The fixative was removed and samples were washed three times with acetone before infiltration and embedding with Spurr's epoxy resin. Thin (70 nm) sections were cut using a Leica UC7 microtome and the samples were imaged using a Biotwin CM120 or FEI Spirit transmission electron microscope (Thermo Fisher Scientific).

Lipid Extractions and Analysis

Lipids were extracted from isolated Arabidopsis mitochondria and chloroplasts, and prepared for gas-liquid chromatography (GLC) following (Wang and Benning, 2011). Mitochondrial phospholipids were separated using a silica TLC plate treated with 2.3% boric acid and a chloroform:ethanol:water:triethylamine solvent system (30:35:7:35, v/v). Lipid bands were visualized with a non-destructive primuline stain. Chloroplast polar lipids were separated using a silica TLC plate (Si250 with pre-adsorbent layer, Mallinckrodt Baker, NJ) treated with $(\text{NH}_4)_2\text{SO}_4$ and an acetone: toluene: water (91:30:7, v/v) solvent system. Lipid bands were visualized with brief iodine vapor staining. Individual lipids were scraped, and their fatty methyl ester profiles analyzed using GLC (Xu *et al.*, 2003).

Measurements of Respiratory Parameters on Plant Mitochondria

Oxygen uptake by isolated mitochondria was measured as described previously (Jacoby *et al.*, 2015), using a Clark-type O_2 electrode (Hansatech, United Kingdom). Oxygen consumption driven by NADH oxidation was measured by adding malate (5 mM) and NADH (1 mM). Malate generates NADH in the mitochondrial matrix via oxidation of malate in the tricarboxylic acid cycle and added NADH can be oxidized by the alternative external NADH dehydrogenases (Palmer and Passam1971; Coleman and Palmer 1972; Palmer and Ward 1985). Rotenone (5 μM) was added to specifically inhibit complex I to determine complex I NADH driven oxygen consumption, and the activity remaining after rotenone addition represents oxygen consumption driven by the internal and external NADH dehydrogenases. Complex II-driven oxygen consumption was assessed by adding succinate (5 mM) and assessing the malonate (5 mM) sensitive oxygen consumption rate,

with malonate acting as a complex II inhibitor. Activity of the cytochrome c oxidase pathway was measured in a 1 ml reaction volume of aerated respiration medium containing 0.3 M sucrose, 5 mM KH_2PO_4 , 10 mM TES, 10 mM NaCl, 2 mM MgSO_4 and 0.1% (w/v) BSA (pH 7.2), in the presence of saturating concentrations of succinate (5 mM) and NADH (1 mM), ATP (0.5 mM), ADP (0.3 mM), malate (10 mM), pyruvate (10 mM), coenzyme A (12 μM), thiamine pyrophosphate (0.2 mM) and NAD^+ (2 mM). Potassium cyanide (KCN, 1 mM) and n-propylgallate (nPG, 0.5 mM) were used to inhibit complex IV and AOX, respectively.

Data were analyzed based on three biological replicates. Statistical evaluations were conducted by means of the two-way ANOVA with post-hoc Tukey HSD test integrated in GraphPad Prism 7 (GraphPad Software Inc.). Differences with P-value < 0.05, P-value < 0.01 and P-value < 0.001 were considered as significant and indicated as *, **, and ***, respectively.

In Vitro Mitochondrial Protein Import

[^{35}S]-Met-labelled precursor proteins were synthesized and imported into freshly isolated mitochondria as described previously (Lister *et al.*, 2007). Equal quantities of mitochondria from different genotypes were used for import reactions. Following import, mitochondria were precipitated at 20,000 RCF for 5 min and subjected to SDS-PAGE. Gels were stained in Coomassie Brilliant Blue, dried, and exposed to a BAS TR2040 phosphor-imaging plate (Fuji) for 24 h. The exposed plate was visualized using the BAS 2500 Bio-Imaging Analyzer (Fuji).

In Situ Detection of Reactive Oxidative Species (ROS)

Detection of H₂O₂ by 3,3-diaminobenzidine staining was carried out as previously described (Förster *et al.*, 2005) and reactive oxygen species in the form of O₂^{•-} were determined by staining with nitroblue tetrazolium as described (Sedigheh *et al.*, 2011). Detached leaves were incubated in freshly prepared 1 mg/ml DAB solution (pH 7.0) or 600 µM NBT solution (pH 7.0) at room temperature in the dark (DAB stain 8 h, NBT stain 4 h), and then transferred to destaining solution (ethanol: acetic acid = 3:1, v/v) to remove the chlorophyll. The bleaching solution was changed every 12 h until all chlorophyll was removed. Leaves were fixed in 50% (v/v) glycerol and scanned. Three leaves (true leaves 5, 6, and 7) per plant and three plants per genotype were assayed for both H₂O₂ and O₂^{•-} detection.

Dark-induced Senescence

Arabidopsis plants were grown on soil in growth chambers at 22°C, 100 µmol m⁻² s⁻¹ light intensity in a 16-h light/8-h dark photoperiod. For dark-induced senescence, the true leaves 6 and 7 from 3-week-old Arabidopsis plants were covered with foil for 5 days. The control plants were not covered with foil, and were kept growing in a 16-h light/8-h dark photoperiod.

Quantification of H₂O₂

H₂O₂ was quantified as described previously (Liu *et al.*, 2010), using leaf extracts from 3-week-old plants. The extract was diluted accordingly and then used for H₂O₂ determination with an Amplex Red Hydrogen Peroxide/Peroxidase Assay Kit

(ThermoFisher, Melbourne, Australia). The values were obtained from three biological replicates, and each replicate was a pooled sample of the sixth and seventh leaves from one plant. The data were analyzed by analysis of variance (ANOVA), and means were compared using a Student's *t*-test.

Relative Water Content Analysis

The relative water content of each genotype was measured as described previously (Giraud *et al.*, 2008). Five biological replicates were measured for each genotype and each replicate contained the whole rosette leaves from one plant. Student's *t*-test was performed to determine significant differences ($P \leq 0.05$).

Chlorophyll analysis and fluorescence

The total chlorophyll content was measured as described previously (Li *et al.*, 2016). The chlorophyll fluorescence F_v/F_m (maximum quantum yield of PSII) was pulsed with $120 \mu\text{mol m}^{-2} \text{s}^{-1}$ of actinic light using the IMAGING-PAM M-series Chlorophyll Fluorescence System (Walz) after a 20 min dark acclimation as previously described (Rossel *et al.*, 2006). At least three biological replicates were measured for each genotype and each replicate was a pooled sample of true leaves 5, 6 and 7 from one plant. Student's *t*-test was performed to determine significant differences ($P \leq 0.05$).

Gas Exchange

Individual leaves were enclosed in a 1 cm reach chamber (Li-COR, 6400-15) that was attached to a Li-COR portable photosynthesis system (BioScientific Ltd) according to (Li *et al.*, 2014) with some modifications. Net photosynthetic CO₂ fixation rate was measured at 22°C, 400 μmol m⁻² s⁻¹ PPFD RGB light source (Li-COR, 6400-18A), 400 μmol mol⁻¹ CO₂ concentration, and 65–75% relative humidity. The rate of respiration was determined by measuring the net photosynthetic CO₂ fixation rate in darkness. The true leaves 5, 6, and 7 from each plant, and 5 plants from each genotype were measured. Student's *t*-test was performed to determine significant differences ($P \leq 0.05$).

Total RNA Preparation and cDNA Synthesis

Total RNA was isolated in biological triplicates from pooled #5, 6 and 7 true leaves from 3-week-old plants using the Sigma Spectrum™ plant total RNA isolation kit (Sigma-Aldrich) according to manufacturer's instructions. On column DNase treatment was carried out to remove genomic DNA (Thermo Scientific™). The cDNA was synthesized using the iScript™ cDNA Synthesis Kit (Bio-Rad, Hercules, CA, USA) according to the manufacturer's instructions.

Global Transcript Analysis

Total RNA was isolated in biological triplicates from pooled #5, 6 and 7 true leaves of well-watered and 8-day-drought-treated wild-type (Col-0) and mutant plants after growth under normal conditions for 3 weeks. RNA isolation was performed using the RNeasy Plant mini kit and DNA was removed via on-column DNase digestion using the RNase-

Free DNase kit according to the manufacturer's instructions (Qiagen, Sydney, Australia). The RNA was eluted in molecular grade DNase- and RNase-free water and the integrity was validated using a TapeStation 2200 system (Agilent, Mulgrave, Australia). RNA-seq libraries were prepared using the TruSeq Stranded mRNA Library Prep Kit according to the manufacturer's instructions (Illumina) and sequenced on a HiSeq1500 system (Illumina) as 60 bp reads or a NextSeq550 system as 75 bp reads with an average quality score (Q30) of above 95%.

The raw reads (on average 19.7M per sample) were quality controlled by FASTQC (v 0.11.5, <https://www.bioinformatics.babraham.ac.uk/projects/fastqc/>) and trimmed by trimgalore (v 0.4.5, <https://github.com/FelixKrueger/TrimGalore>). Clean reads were pseudo-aligned to the representative transcript models of the Arabidopsis Araport 11 annotation (Cheng *et al.*, 2017) using Kallisto (v 0.43.1) to generate TPM/counts tables (Bray *et al.*, 2016). Next, glmFit function in edgeR (Robinson *et al.*, 2010) was used to fit the negative binomial generalized linear model (GLM) and glmLRT was used to carry out the likelihood ratio test. Differentially expressed genes were identified with a threshold of fold change > 2 and FDR < 0.05.

For the Gene Ontology enrichment analyses, the Cytoscape (v3.5.1) (Shannon *et al.*, 2003) plug-in ClueGO (Bindea *et al.*, 2009) was used. ClueGO was run with default settings, except for setting the *P* value cutoff < 0.1, GO tree interval level to 4–9, and ≥ 3 or more genes from either cluster associated to a GO term, representing $\geq 4\%$ (for clusters Blue and Red) or $\geq 2\%$ (for cluster Green) of the associated GO term genes. All sequencing data have been submitted to the NCBI SRA archive under Project ID PRJNA475427.

Mass Spectrometry

Preparation of samples from BN gel bands

Individual samples were excised from BN gels and destained (50 mM ammonium bicarbonate/acetonitrile) overnight. Proteins were reduced in 1 μ l of 200 mM tris(2-carboxyethyl)phosphine (TCEP) in 100 μ l of water for 1 h. After washing the gel bands (50 mM ammonium bicarbonate/acetonitrile), samples were alkylated with 4 μ l of 1 M iodoacetamide (IAA) in 100 μ l of water for 30 min in the dark. Proteins were then digested with trypsin (0.2 μ g trypsin (Promega Sequencing Grade) for 16 h at 37°C) and peptides collected after extraction (70% acetonitrile/water).

LC-MS/MS analysis

Peptides were reconstituted in 0.1% TFA and 2% acetonitrile (ACN) and loaded onto a C18 PepMap 100 μ m ID \times 2 cm trapping column (Thermo-Fisher Scientific) at 5 μ l/min for 6 min, and washed for 6 min before switching the pre-column in line with the analytical column (PepMap RSLC C18, 2 μ m, 75 μ m i.d. \times 25 cm, Thermo Fisher Scientific). Peptides were loaded and separated for 60 min. The separation was performed at 250 nl/min using a non-linear ACN gradient of buffer A (0.1% formic acid, 2% ACN) and buffer B (0.1% formic acid, 80% ACN), starting at 5% buffer B to 55% over 55 min, then 100% buffer B for 5 min followed by an equilibration step of 15 min (0.1% formic acid, 2% ACN). Data were acquired using the Xcalibur software v4.1 (Thermo Fisher Scientific). The mass spectrometer was programmed to acquire in a data-dependent mode using a maximum ion injection time of 50 ms. Full scans were acquired in the Orbitrap mass analyzer with a resolution of 120,000 at 200 m/z (3E6 ions were accumulated) from 350 to 1500 m/z. The top 10 intense ions with charge states ≥ 2 were sequentially isolated to

a target value of 1E5 (maximum injection time of 110 ms), fragmented by HCD (NCE 28%) and detected in the Orbitrap at R = 15,000, m/z 200.

Data analysis

Identification and isotopic quantification of proteins were performed on raw output files from LC-ESI-MS/MS using MaxQuant (Version 1.5.8.3) (Cox *et al.*, 2011) together with its built-in search engine Andromeda. Carbamidomethylation of cysteines was set as a fixed modification, acetylation of protein N-termini, methionine oxidation was included as variable modifications. For quantitative analysis, dimethyl labeled DimethylLys0, DimethylNter0, DimethylLys4, DimethylNter4, DimethylLys8 and DimethylNter8 were used as labels together with the optional iBAQ (Intensity Based Absolute Quantification) calculation. Parent mass tolerance was set to 4.5 ppm (after refinement by MaxQuant) and fragment mass tolerance to 20 ppm. Trypsin was set as the digestion enzyme with up to two missed cleavages allowed. The match between runs feature of MaxQuant was used to transfer peptide identifications from one run to another based on retention time and mass to charge ratio. Both peptide and protein identifications were reported at a false discovery rate (FDR) of 1%. Maxquant was used for quantitation of labelled peptides and the calculation of normalized protein ratio.

Phylogenetic analysis

Amino acid sequences for DGS1 or NCA2 related proteins were obtained by blast searches using either the yeast NCA2 or Arabidopsis DGS1 against the species listed in Supplemental Dataset 4A (Altschul *et al.*, 1990). Full-length amino acid sequences were aligned using Clustal Omega (Li *et al.*, 2015) and gaps were removed using TrimAl with

the gappyout algorithm (Capella-Gutierrez *et al.*, 2009) (Supplemental Dataset 4B). The resulting sequence alignment was used to create a maximum-likelihood phylogeny using the program IQTREE (Nguyen *et al.*, 2015). Branch support values were gained by bootstrapping with 1000 replicates.

Co-expression analysis

The 200 top co-expressed genes were obtained from the Genevestigator Co-expression tool using the perturbation transcriptomic dataset (10615 samples for Arabidopsis and 1771 samples for *S. cerevisiae*). All pairwise Pearson's correlations coefficients were calculated in R and the network was visualized in Cytoscape v3.5.1. Edges were displayed if the Pearson correlation coefficient (PCC) was higher than 0.65 (*DGS1* network) or 0.75 (*NCA2* network).

Accession Numbers

DGS1 (At5g12290), MIC60 (At4g39690), TOM40 (At3g20000), Tom20-2 (At1g27390), Tom20-3 (At3g27080), Tom20-4 (At5g40930), RISP (At5g13430)

Supplemental Data Sets

The additional data sets may be found at: <https://doi.org/10.1105/tpc.18.00885>.

Supplemental Dataset 1. Mass Spectrometry of Supercomplex I+III, complex I, complex V, complex III and the F₁ sub-complex of complex V excised from BN-PAGE.

Supplemental Dataset 2. Mutant and complementation lines used in the study.

Supplemental Dataset 3. Hierarchical clustering of 720 genes differentially expressed ($|\log_2 \text{FC}| > 1$ and $\text{FDR} < 0.05$) in *dgs1-1* and *dgs1-1* Comp (L) compared to wild type under drought stress conditions.

Supplemental Dataset 4. A) List of organisms and protein accession numbers where a DGS1/NCA2 type ortholog could be detected. B) Aligned amino acid sequences for DGS1 or NCA2 related proteins with gaps removed as outlined in Methods.

Supplemental Dataset 5. List of the top co-expressed genes for A) *DGS1* and B) *NCA2*.

Supplemental Dataset 6. Primers used in this study.

Supplemental Dataset 7. List of antibodies used in this study.

Acknowledgment

We would like to thank Asha Haslem for technical assistance and the La Trobe University Genomics Platform for access to next generation sequencing equipment. Mass spectrometry was undertaken at the Proteomic Platform, La Trobe University. Electron microscopy was undertaken at the Biosciences Microscopy Unit, School of Biosciences, the University of Melbourne and the RMIT Microscopy & Microanalysis Facility, RMIT University. Confocal microscopy was undertaken at LIMS Bioimaging facility, La Trobe University. We thank Juliette Jouhet for providing the MIC60 antibody.

This work was supported by the Australian Research Council Centre of Excellence in Plant Energy Biology (CE140100008) to JW. IDC is supported by the Fonds Wetenschappelijk Onderzoek (Postdoctoral Fellowship no. 12N2415N and Travel Grant for a long stay abroad no. 450215N). JS is supported by a Feodor Lynen Research Fellowship (Alexander von Humboldt Foundation, Germany). The contribution by AL and

CB was supported by the Division of Chemical Sciences, Geosciences and Biosciences, Office of Basic Energy Sciences of the United States Department of Energy (DE-FG02-91ER20021), MSU AgBioResearch, and partially supported by a fellowship from Michigan State University under the Training Program in Plant Biotechnology for Health and Sustainability (T32-GM110523).

Author Contribution

YW, IDC and JW conceived the project. LL performed the experiments with XM contributing with physiological analyses. OB carried out the RNA-Seq and IDC analyzed the RNA-Seq data and performed the co-expression analyses. AvdM carried out the electron microscopy. JS measured the activities of respiratory chain complexes and quantified the H₂O₂ content together with YW. AL and CB carried out and interpreted the lipid analysis. CC carried out the phylogenetic analysis. LL drafted the manuscript that was edited by JW, IDC and YW. The final version was produced with contributions from all authors.

APPENDICES

APPENDIX 5A

Main Text Figures

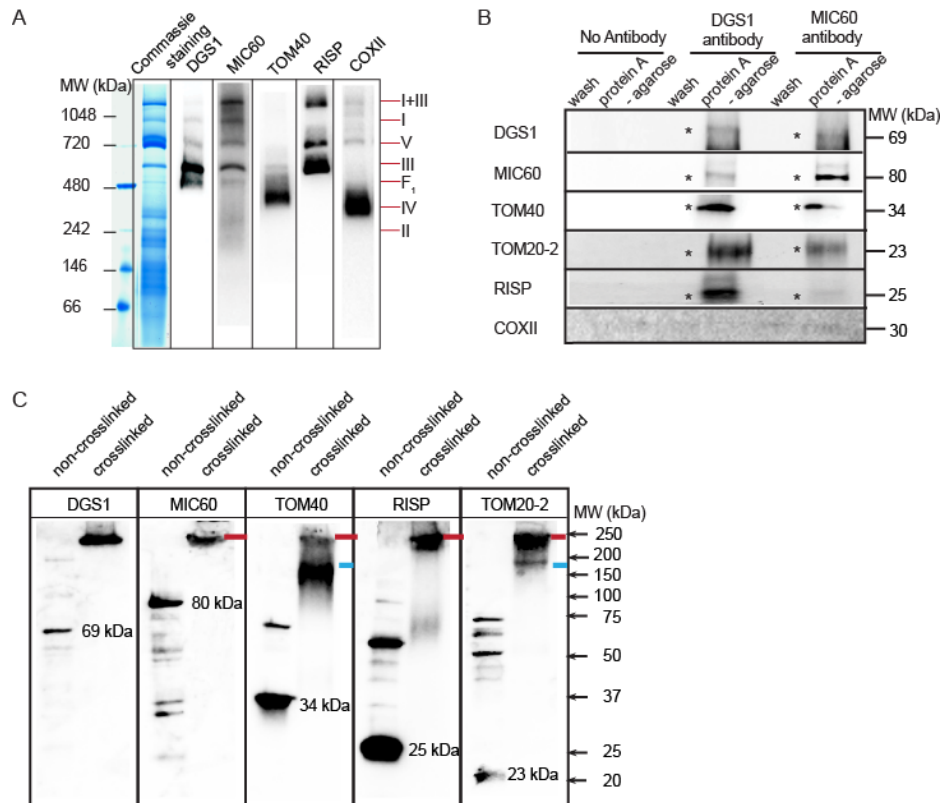


Figure 5.1. DGS1 is present in a large multi-subunit protein complex with MIC60, TOM40, TOM20s and RISP. A) Immunodetection of DGS1, MIC60, TOM40, complex III subunit RISP, and complex IV subunit cytochrome oxidase II (COXII) in total mitochondrial proteins separated by BN-PAGE. Coomassie blue staining was performed showing the distribution of supercomplex and complex I to V. MW, molecular weight. B) Mitochondrial proteins from wild-type (Col-0) plants were incubated without or with antibodies raised against DGS1 and MIC60. The wash and protein A-agarose pellet fractions were resolved by SDS-PAGE and immunodetected with antibodies as shown. The interaction between proteins is indicated by asterisks and the corresponding molecular weight for each protein is indicated in kDa. C) Mitochondrial proteins incubated with or without cross-linker were resolved by SDS-PAGE and followed by immunodetection. Red lines indicate proteins that exist in the same complex with DGS1 while blue lines indicate association with another complex. The size of non-crosslinked protein is indicated in each panel.

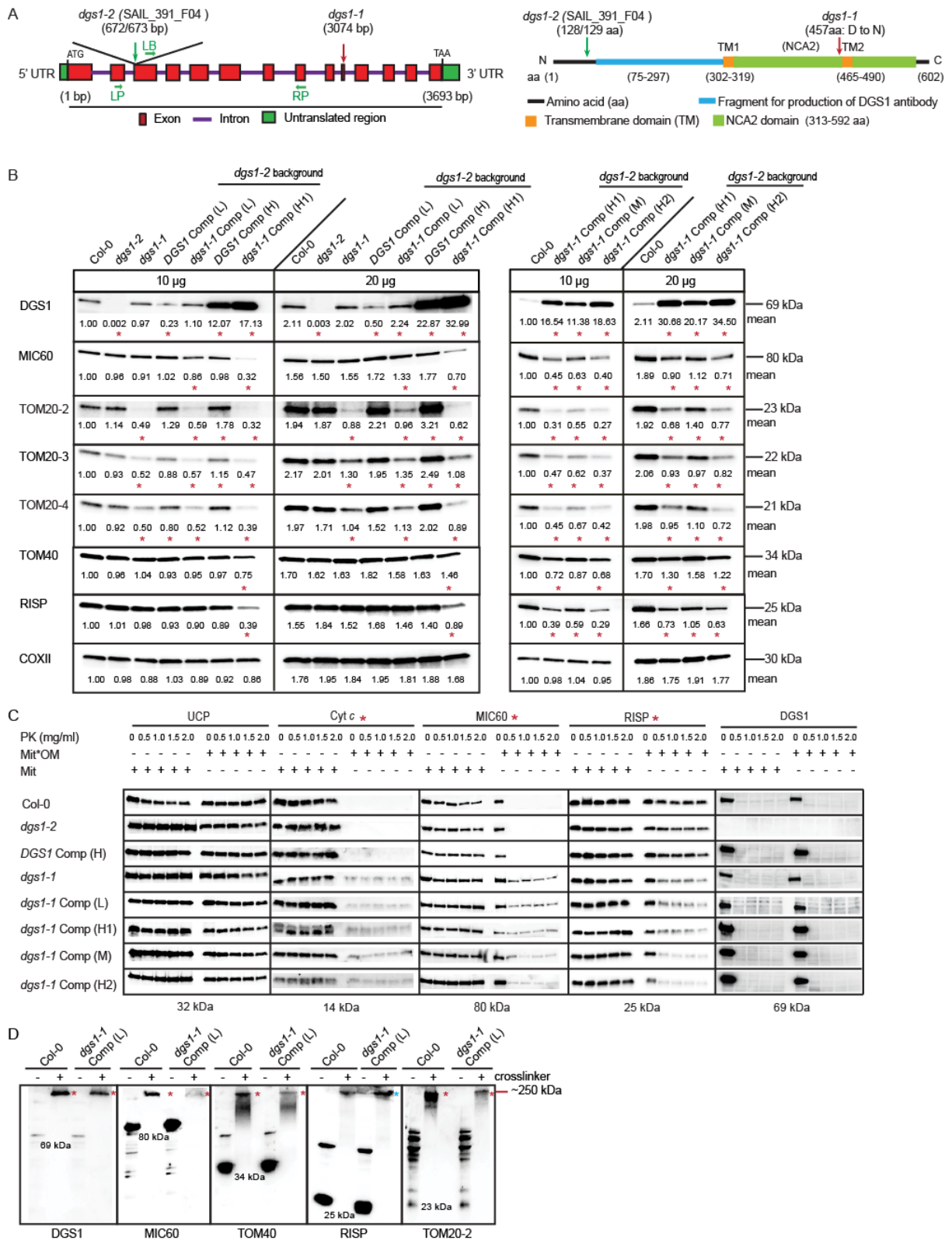


Figure 5.2. A single point mutation in DGS1 alters the multi-subunit complex. A) A schematic gene (left panel) and protein (right panel) model of DGS1. The position of the

Figure 5.2 (cont'd) EMS point mutation and T-DNA insertion is indicated. Primers used for screening of homozygous plants are indicated as LP, RP and LB (Supplemental Dataset 6). Two transmembrane domains, the Nuclear Control of ATPase 2 (NCA2) domain and the fragment used for the generation of the DGS1 antibody are indicated in different colors. B) The protein abundance of DGS1, MIC60, TOM20s, TOM40, RISP and COXII was determined by immunoblot analysis of mitochondrial proteins isolated from wild-type (Col-0), *dgs1-1* and *dgs1-2* mutant lines as well as several lines expressing the *dgs1-1* mutant protein. Ten micrograms and twenty micrograms of mitochondrial proteins were loaded to ensure linearity of detection. Mean values are shown for three biological replicates. P-value ≤ 0.05 from a Student's *t*-test is indicated with red asterisks. C) Freshly isolated mitochondria (Mit) and outer membrane ruptured mitochondria (Mit*OM) from wild-type (Col-0), *dgs1-1* and *dgs1-2* mutant lines as well as several lines expressing the *dgs1-1* mutant protein were treated with protease K at different concentrations, followed by immunodetection. Proteins displaying altered protease K sensitivity are indicated with red asterisks. D) Crosslinked and non-crosslinked mitochondrial proteins from wild-type (Col-0) plants and *dgs1-1* Comp (L) plants were resolved by SDS-PAGE followed by immunodetection. Red asterisks indicate the protein abundance in the crosslinked complex was reduced in the *dgs1-1* Comp (L) line, while the blue asterisk indicates the protein abundance was increased. The size of non-crosslinked protein is indicated in each panel.

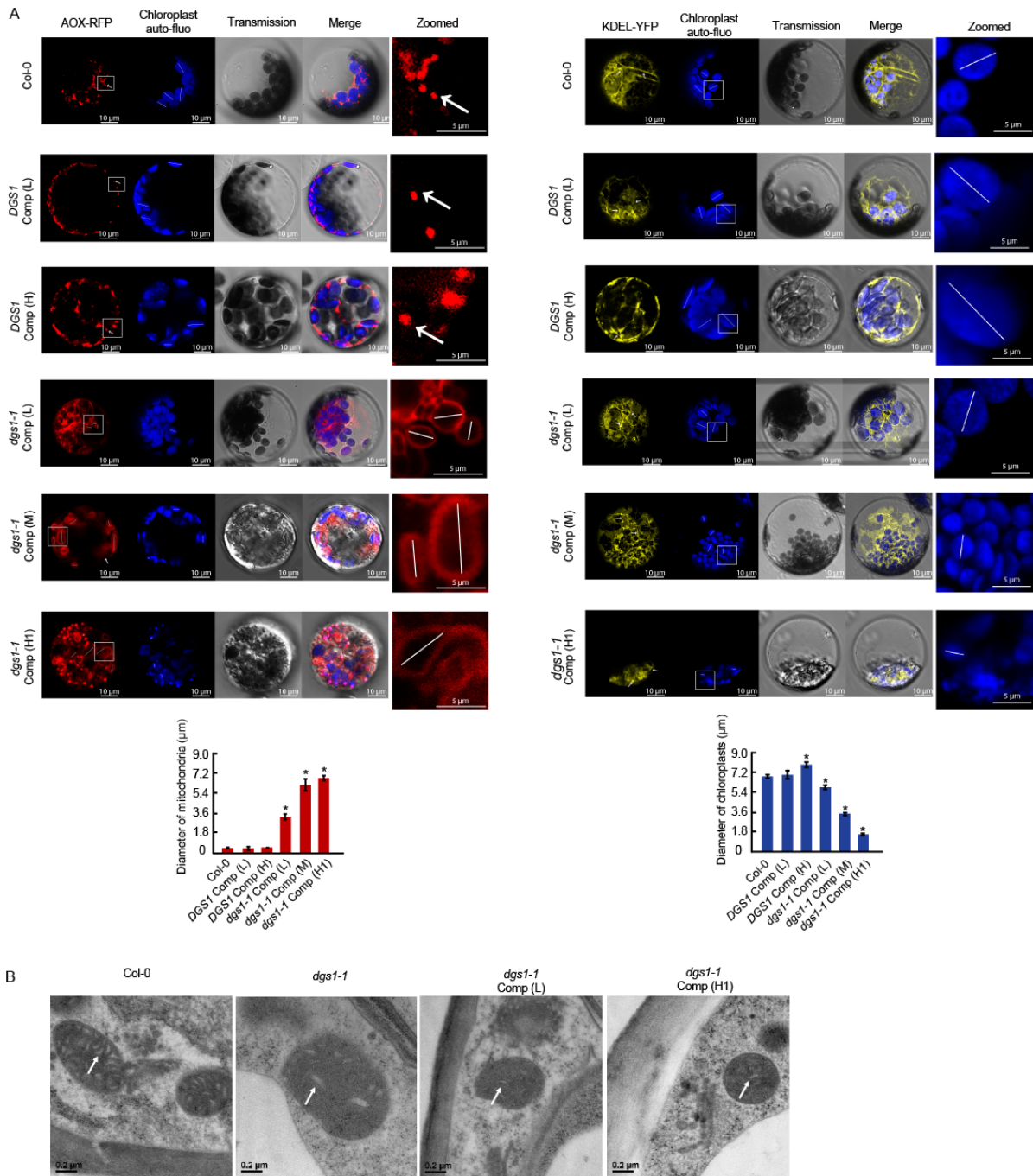


Figure 5.3. The *dgs1-1* mutation alters mitochondrial size. A) Protoplasts isolated from the indicated genotypes were transiently transformed with AOX-RFP (mitochondria targeting construct) and KDEL-YFP (ER targeting construct), respectively. Chloroplasts were observed using chlorophyll auto-fluorescence. Scale bars = 10 μm . The rectangle areas were zoomed in to show the altered mitochondrial and chloroplast size; scale bars = 5 μm . The diameter of chloroplasts and mitochondria were averaged from 30 protoplast

Figure 5.3 (cont'd) cells and the significant differences were assessed using Students' t-test with $P \leq 0.05$ indicated by asterisks. The white line(s) indicate the diameter measurement used. B) Electron microscopy images of mitochondria cross sections from leaf tissue of the Col-0, *dgs1-1* line, *dgs1-1* Comp (L) line and *dgs1-1* Comp (H1) line. The internal cristae membranes are indicated with white arrows. Scale bars = 0.2 μm .

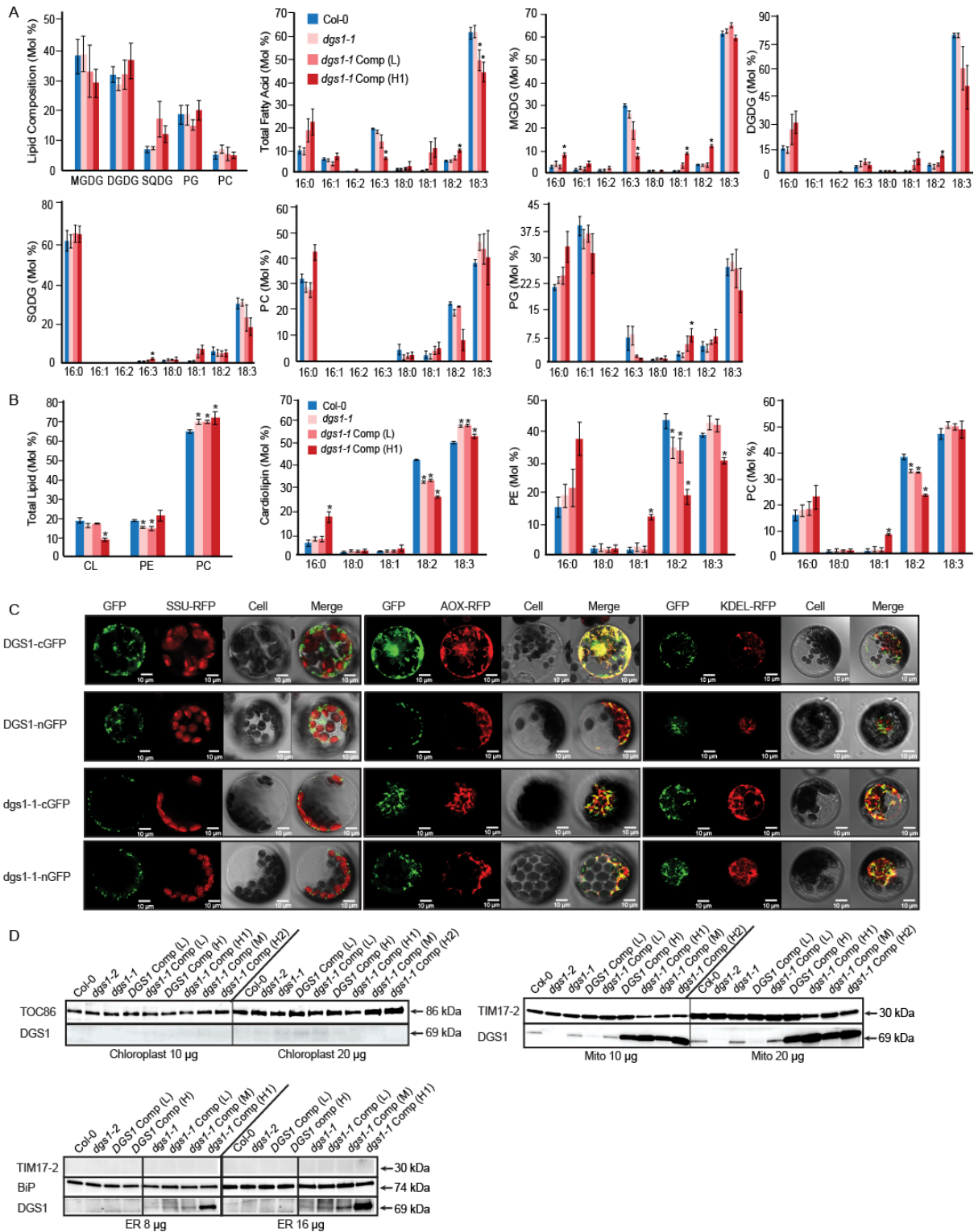


Figure 5.4. The *dgs1-1* mutation alters mitochondrial lipid composition. Lipid analysis by Gas-Liquid Chromatography (GLC) of chloroplasts (A) and mitochondria (B) extracted from wild-type (Col-0) and *dgs1* mutant lines. MGDG,

Figure 5.4 (cont'd) monogalactosyldiacylglycerol; DGDG, digalactosyldiacylglycerol; SQDG, sulfoquinovosyldiacylglycerol; PC, phosphatidylcholine; PG, phosphatidylglycerol; PE, phosphatidylethanolamine; CL, cardiolipin. Significant differences in relative composition of each acyl chain and total lipids were determined by Students' t-test with P-value ≤ 0.05 (n = 3) indicated by asterisks, with error bars = SE.

C) The construct expressing full-length DGS1 protein or *dgs1-1* mutant protein with C- or N- terminal GFP was transiently transformed into protoplasts isolated from Arabidopsis Col-0 plants. SSU-RFP (targeting to chloroplasts), AOX-RFP (targeting to mitochondria) or KDEL-RFP (targeting to ER) were co-transformed as controls. Scale bars = 10 μm .

D) Proteins of chloroplasts, mitochondria and ER isolated from Col-0 and *dgs1* mutant plants were separated by SDS-PAGE and followed by immunoblotting using the DGS1 antibody, the TOC86 antibody as a chloroplast marker, the TIM17-2 antibody as a mitochondria marker, and BiP as an ER marker.

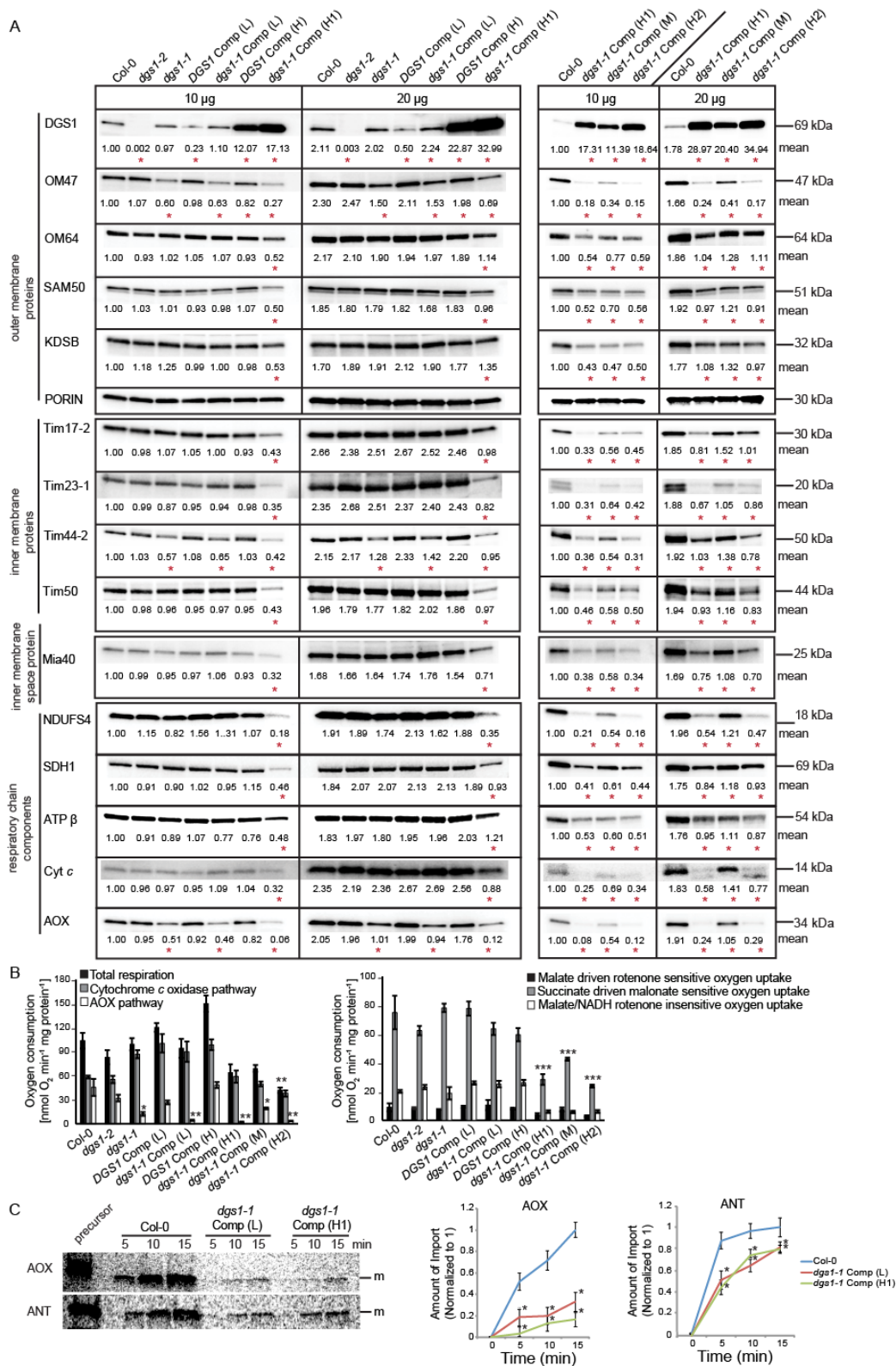


Figure 5.5. The *dgs1-1* mutation affects mitochondrial protein abundance, protein import and alternative respiratory capacity. A) The protein abundance of various

Figure 5.5 (cont'd) mitochondrial protein import components and respiratory chain components was determined by immunoblot analysis of mitochondria isolated from Col-0 and *dgs1* mutant plants. 10 µg and 20 µg of mitochondrial proteins were loaded for linearity of detection. Mean values are shown for three biological replicates. P-value ≤ 0.05 from a Student's t-test is indicated with red asterisks. B) The activity of mitochondrial respiratory chain complexes from wild-type (Col-0), mutant and complementation lines was measured using a Clark-type oxygen electrode and are shown as means ± SE of three biological replicates. Asterisks indicate the significant differences with * P < 0.05; ** P < 0.01 and *** P < 0.001 between oxygen consumption of wild-type mitochondria (Col-0) and mitochondria from different *dgs1* mutants as determined by two-way analysis of variance (ANOVA) with a post-hoc Tukey HSD test. C) *In vitro* protein import of [³⁵S]-Met-radiolabeled AOX and ANT into mitochondria isolated from Col-0 and *dgs1-1* Comp (L) plants. Aliquots were removed at 5, 10 and 15 min and then treated with protease K. The left panel shows a typical image of an *in vitro* import assay, the precursor and mature (m) forms of the protein are indicated. The right panel shows the rate of import was determined at all time points and normalized to Col-0 at the last time point for each replicate (n ≥ 3). Standard errors for average ratios are indicated on graphs. Asterisks indicate the significant differences compared to Col-0 (P < 0.05, Student's t-test).

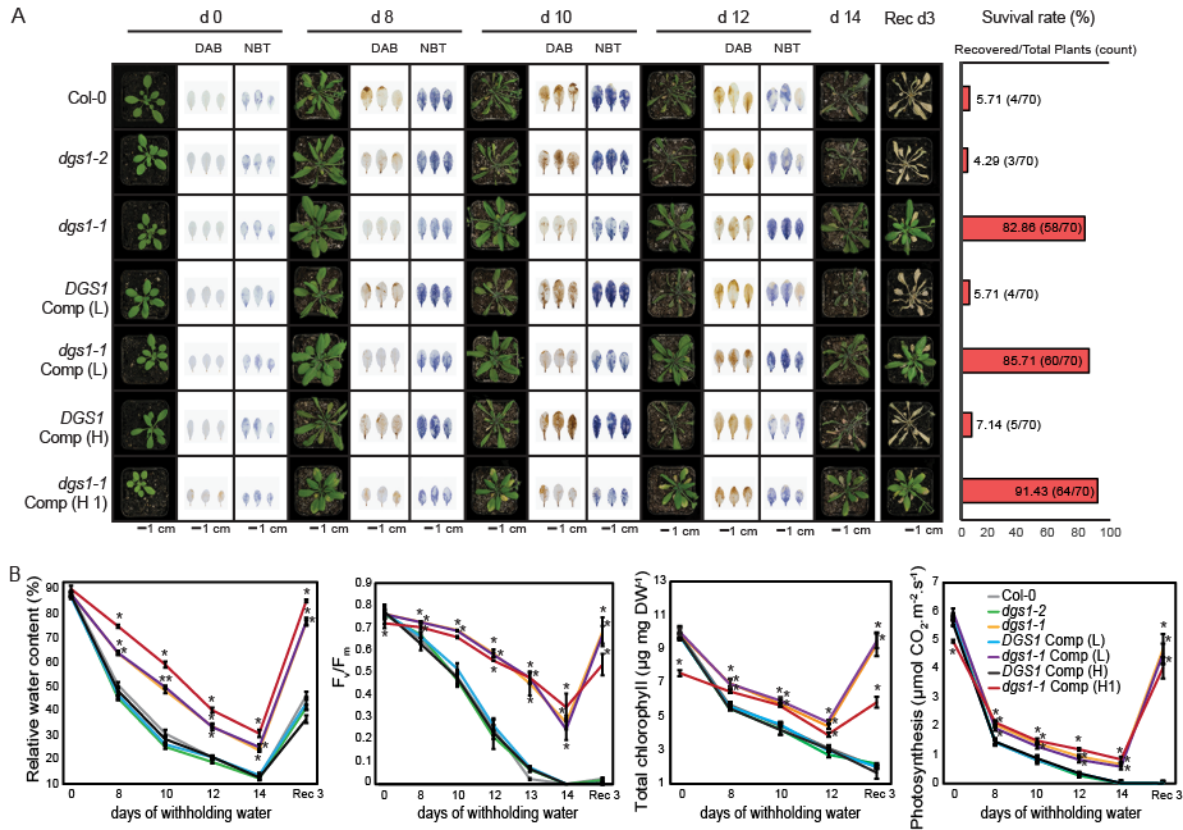


Figure 5.6. The *dgs1-1* mutation imparts higher drought stress tolerance. A) Wild-type (Col-0) and *dgs1* mutant lines were grown under normal conditions for 24 days, then water was withheld for 14 days followed by rewatering for 3 days to recover. Representative plants were imaged at the indicated time points. True leaves 5, 6 and 7 were harvested at the indicated time points and stained for H_2O_2 (3,3'-diaminobenzidine [DAB]) and $O_2^{\cdot-}$ (nitroblue tetrazolium [NBT]). The bar chart shows the survival ratio after 3 days of rewatering. B) The relative water content, maximum quantum yield (F_v/F_m), total chlorophyll content and photosynthesis rate were measured during the drought treatment at the days as indicated. Shown are means \pm SE of five biological replicates. Asterisks indicate a significant difference compared to wild-type (Col-0) at each time point ($P \leq 0.05$, Student's t-test).

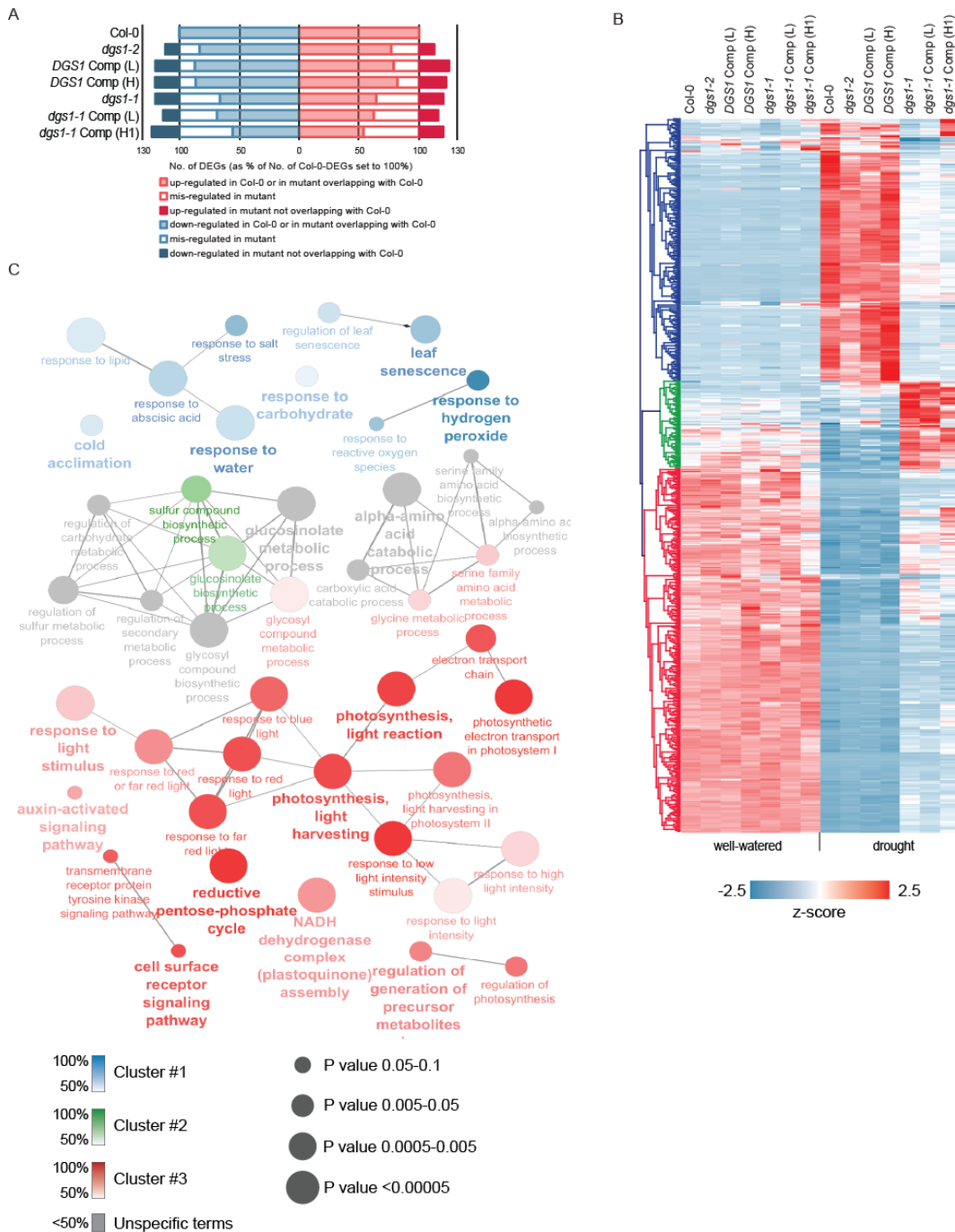


Figure 5.7. Transcriptome analysis of *dgs1* mutants. A) The number of up-regulated genes and down-regulated genes ($|\log_2(\text{fold change})| > 1$, $\text{FDR} < 0.05$) of each genotype leaves from plants of 24 days old plus 8-day drought treatment, compared to plants grown under normal conditions. B) Heatmap visualization of genes differentially expressed ($|\log_2(\text{fold change})| > 1$, $\text{FDR} < 0.05$) in *dgs1-1* and *dgs1-1* Comp (L) compared to wild type during drought stress conditions. Hierarchical clustering of the z-scores of \log_2 -

Figure 5.7 (cont'd) transformed transcripts per million values based on Euclidian distance with Genesis 1.6.0 identified three clusters (Blue, Green and Red). C) GO enrichment analysis of genes differentially expressed in *dgs1-1* and *dgs1-1* Comp (L) during drought stress conditions using ClueGO v2.5.1. The size of the nodes is proportional to the Bonferroni-corrected *P* value. GO terms were grouped based on their similarity (edge thickness represents the kappa score of similarity between two GO terms) and the most significant term in each group is shown in bold. GO terms were defined as specific for one of the clusters (Blue, Green or Red) if the proportion of associated genes from this cluster is higher than 50%. Common GO terms are indicated in grey.

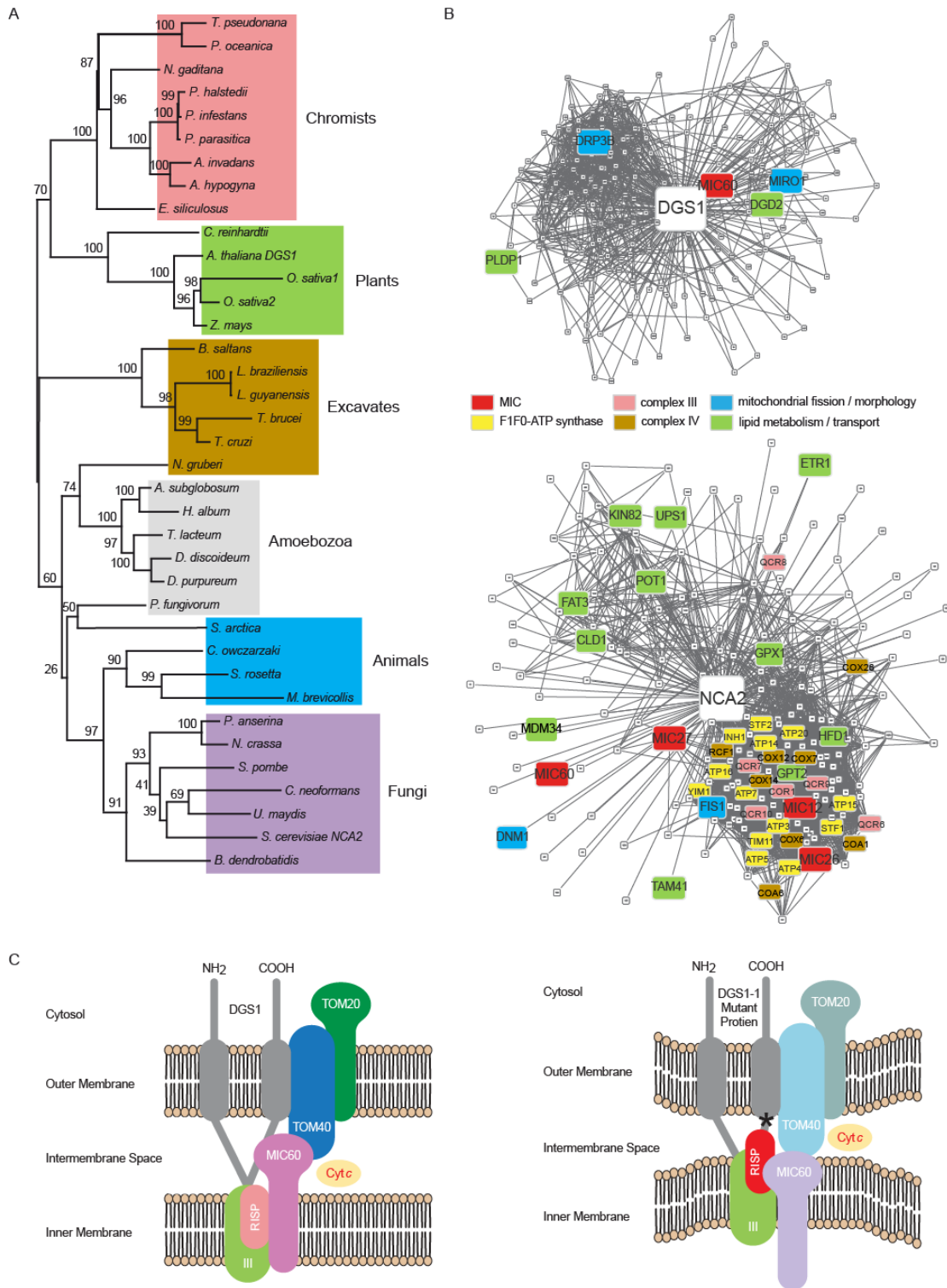


Figure 5.8. Phylogenetic analysis of DGS1- and NCA2-related proteins. A) A maximum-likelihood phylogenetic tree of DGS1- and NCA2-related proteins. Numbers represent ultrafast bootstrap values after 1000 replicates from IQTREE. Some numbers have been manually moved for better visibility. B) *DGS1* and *NCA2* co-expression

Figure 5.8 (cont'd) networks displaying the 200 top co-expressed genes. C) A model of the DGS1 and *dgs1-1* mutant protein in plant mitochondria. For the native DGS1 protein, an ability to pull down TOM40, MIC60 and RISP along with cross-linking results suggests a direct interaction. The association with TOM20 is not defined and may be via TOM40. When *dgs1-1* mutant protein was expressed, MIC60 was more protected by the inner membrane while RISP was more exposed to the intermembrane space. The abundance of TOM40 and MIC60 was reduced in the MICOS, and the abundance of RISP was increased. The alterations of MICOS due to the presence of the *dgs1-1* mutant protein may change the contact between the outer and inner membrane. The asterisk indicates the mutation site of the *dgs1-1* protein. RISP, the Rieske FeS protein; MICOS, the mitochondrial contact site and cristae organizing system; Cyt *c*, cytochrome *c*; MIC60, 60 kDa subunit of MICOS; TOM40, the translocase of outer mitochondrial membrane 40 kDa subunit; TOM20, the translocase of outer mitochondrial membrane 40 kDa subunit.

APPENDIX 5B

Supplementary Figures

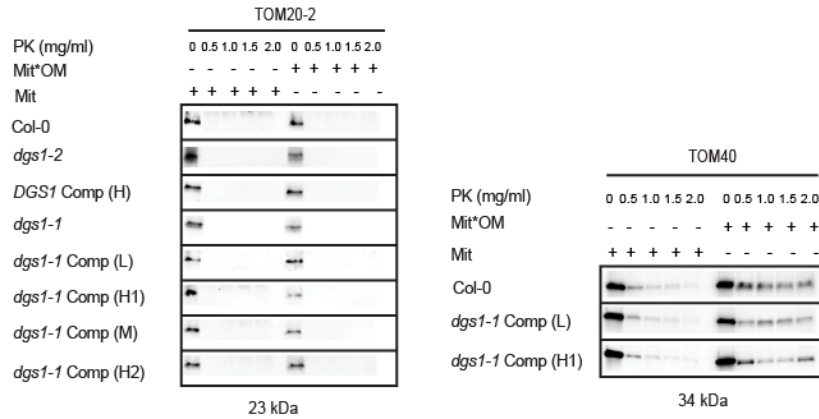


Figure 5.S1. The intramitochondrial localization of TOM20-2 and TOM40 in Col-0 and *dgs1* mutant lines. Supports Figure 5.2C. Freshly isolated mitochondria (Mit) and outer membrane ruptured mitochondria (Mit*OM) from wild-type (Col-0) and *dgs1* mutant lines were treated with Proteinase K of different concentrations, followed by immunoblotting of TOM20-2 and TOM40.

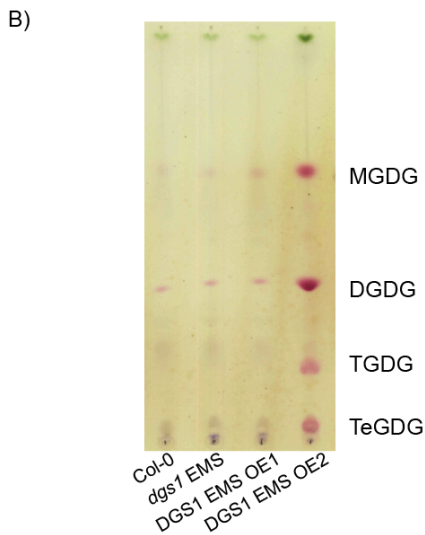
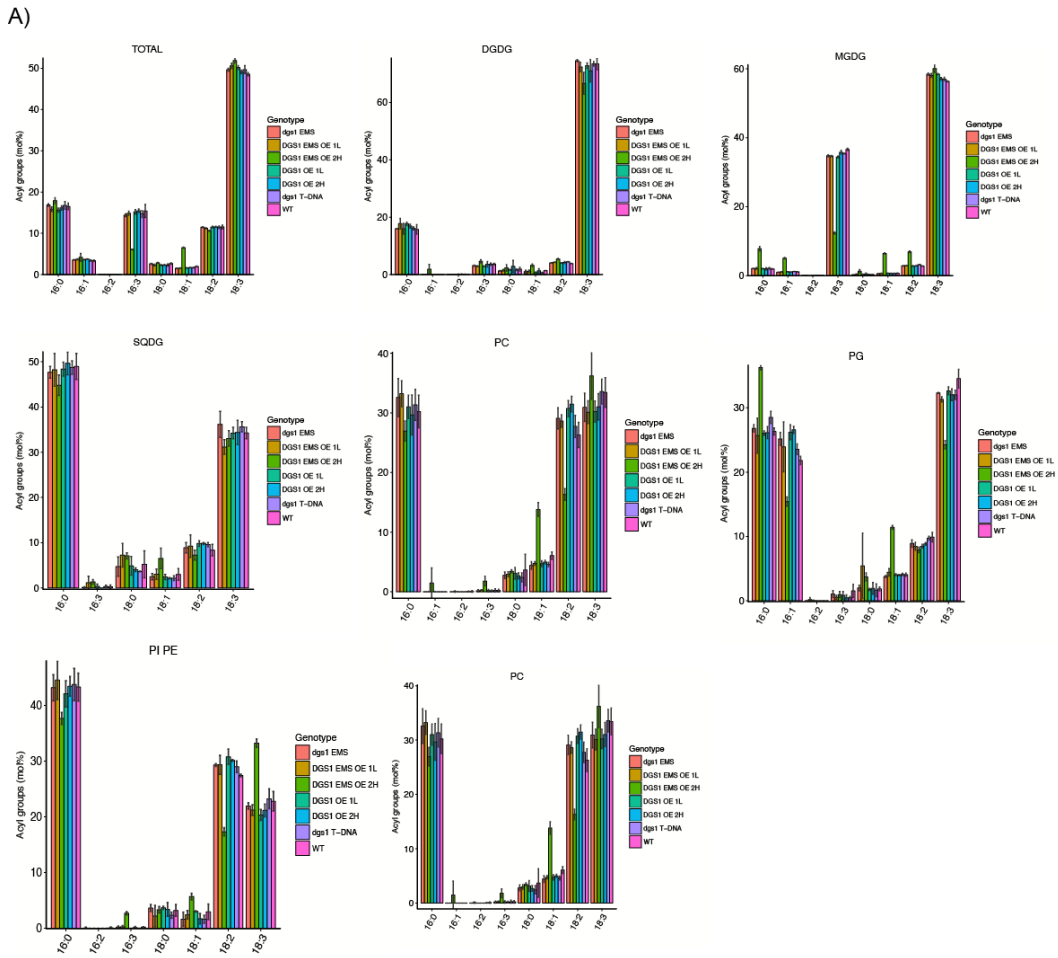


Figure 5.S2. Related to Figure 4A and 4B. Leaf lipid analysis of wild type and mutant lines. A) Total Leaf lipids analyzed by Gas-Liquid Chromatography (GLC) total leaf Lipids extracted from wild-type (Col-0) and *dgs1* mutant lines, n = 2 with error bars = SE. MGDG,

Figure 5.S2 (cont'd) monogalactosyldiacylglycerol; DGDG, digalactosyldiacylglycerol; SQDG, sulfoquinovosyldiacylglycerol; PC, phosphatidylcholine; PG, phosphatidylglycerol; PE, phosphatidylethanolamine. B) TLC image of mitochondrial lipids is attached with labels, the line with the highest amount of DGS1 point mutant protein has the oligogalactolipids.

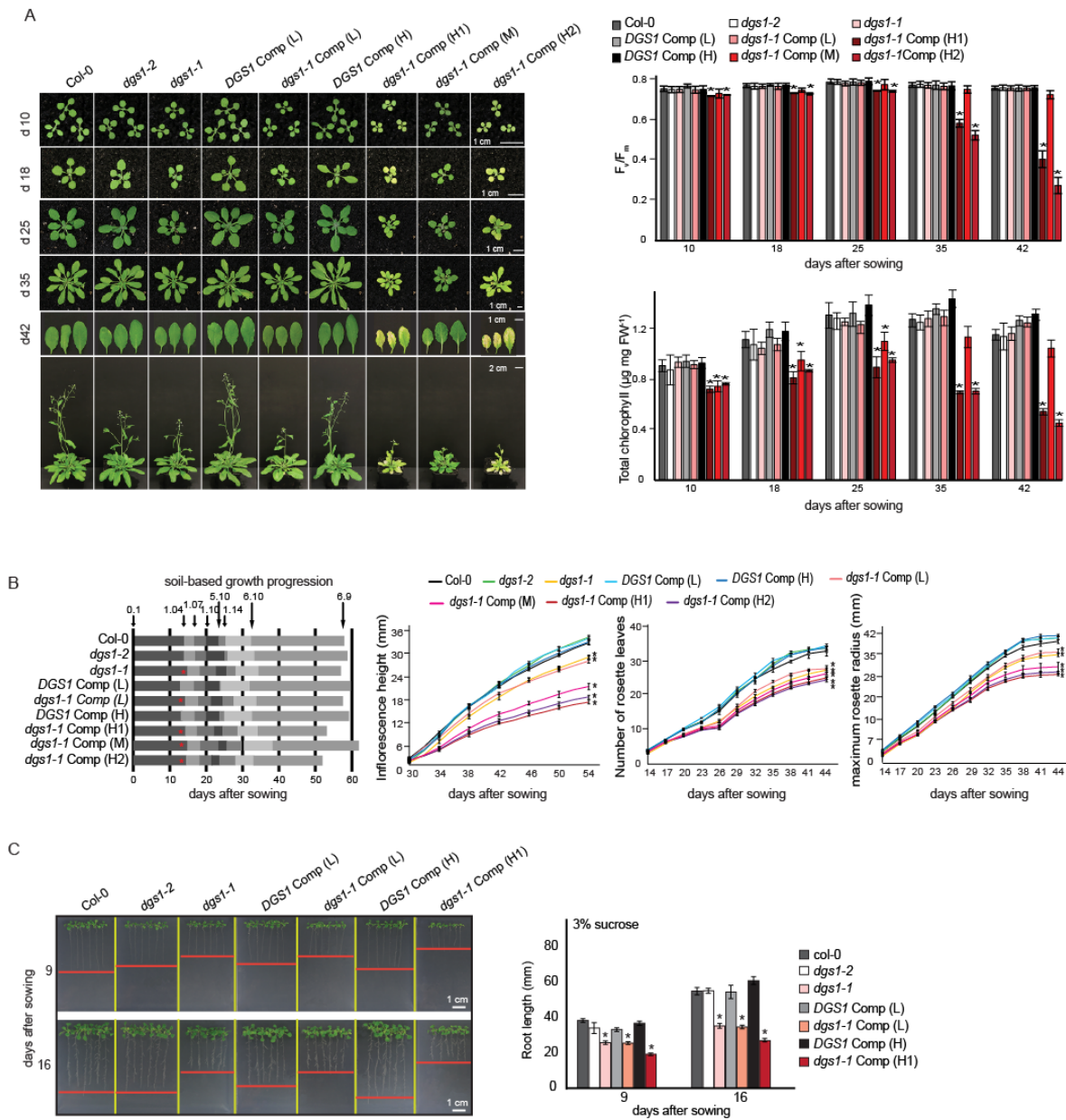


Figure 5.S3. The defective growth phenotype of mutants producing the DGS1-1 protein. Supports Figure 6A. A) Developmental progression of Col-0, *dgs1-2*, *dgs1-1*, DGS1 Comp and *dgs1-1* complemented lines grown under control condition was recorded. 20 individual plants for each genotype were grown and representative plants and detached rosette leaves are presented. Measurements of F_v/F_m and total

Figure 5.S3 (cont'd) chlorophyll content at time point as indicated. Averages were calculated based on three biological replicates for each measurement and significant differences are indicated by asterisks ($P \leq 0.05$, Student's t-test). B) Soil-based growth progression was recorded as described in Boyes et al. (2001): stage 1.04, 1.07, 1.10 and 1.14, maximum radius of 4, 7, 10 and 14 rosette leaves >1 mm; stage 5.10, first flower bud visible; stage 6.10, first flower opens and stage 6.9, flowering complete. Representative growth parameters inflorescence height (mm), number of rosette leaves more than 1 mm and maximum rosette radius (mm) across the growth period were measured. Averages and SE were calculated based on 20 plants with asterisks indicating the significant difference using a Student's t-test ($P \leq 0.05$). C) Root length analysis of Col-0, *dgs1* mutant lines grown on B5 media plate containing 2% (w/v) sucrose at 9 and 16 days after sowing. Averages and SE were determined based on data from 50 individual plants. The significant difference compared to wild-type (Col-0) was indicated by asterisks ($P \leq 0.05$, Student's t-test).

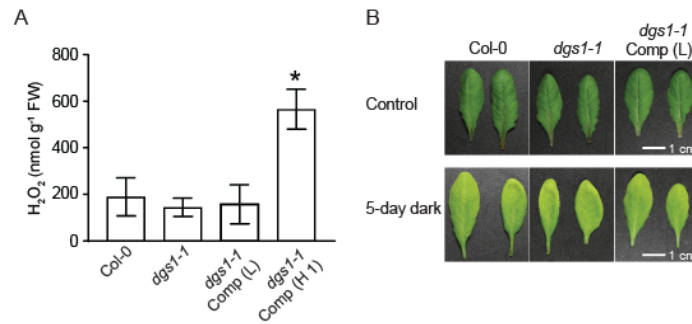


Figure 5.S4. Analyses of hydrogen peroxide in *dgs1-1* lines. Supports Figure 6A. A) Quantification of hydrogen peroxide in leaves extracts from Col-0, *dgs1-1*, *dgs1-1* Comp (L) and *dgs1-1* Comp (H1) plants. The significant difference compared to wild-type (Col-0) was indicated by asterisks ($P \leq 0.01$, Student's t-test). B) Dark-induced leaf senescence of Col-0, *dgs1-1*, *dgs1-1* Comp (L) leaves.

REFERENCES

REFERENCES

- Aaltonen, M.J., Friedman, J.R., Osman, C., Salin, B., di Rago, J.P., Nunnari, J., Langer, T. and Tatsuta, T.** (2016) MICOS and phospholipid transfer by Ups2-Mdm35 organize membrane lipid synthesis in mitochondria. *J Cell Biol*, **213**, 525-534.
- Altschul, S.F., Gish, W., Miller, W., Myers, E.W. and Lipman, D.J.** (1990) Basic local alignment search tool. *J Mol Biol*, **215**, 403-410.
- Awai, K., Marechal, E., Block, M.A., Brun, D., Masuda, T., Shimada, H., Takamiya, K., Ohta, H. and Joyard, J.** (2001) Two types of MGDG synthase genes, found widely in both 16:3 and 18:3 plants, differentially mediate galactolipid syntheses in photosynthetic and nonphotosynthetic tissues in *Arabidopsis thaliana*. *Proc Natl Acad Sci U S A*, **98**, 10960-10965.
- Benning, C. and Ohta, H.** (2005) Three enzyme systems for galactoglycerolipid biosynthesis are coordinately regulated in plants. *J Biol Chem*, **280**, 2397-2400.
- Beranek, A., Rechberger, G., Knauer, H., Wolinski, H., Kohlwein, S.D. and Leber, R.** (2009) Identification of a cardiolipin-specific phospholipase encoded by the gene CLD1 (YGR110W) in yeast. *J Biol Chem*, **284**, 11572-11578.
- Bessoule, J.J., Testet, E. and Cassagne, C.** (1995) Synthesis of phosphatidylcholine in the chloroplast envelope after import of lysophosphatidylcholine from endoplasmic reticulum membranes. *Eur J Biochem*, **228**, 490-497.
- Bindea, G., Mlecnik, B., Hackl, H., Charoentong, P., Tosolini, M., Kirilovsky, A., Fridman, W.-H., Pagès, F., Trajanoski, Z. and Galon, J.** (2009) ClueGO: a Cytoscape plug-in to decipher functionally grouped gene ontology and pathway annotation networks. *Bioinformatics*, **25**, 1091-1093.
- Braun, H.P., Emmermann, M., Kruff, V. and Schmitz, U.K.** (1992) The general mitochondrial processing peptidase from potato is an integral part of cytochrome c reductase of the respiratory chain. *EMBO J*, **11**, 3219-3227.
- Bray, N.L., Pimentel, H., Melsted, P. and Pachter, L.** (2016) Near-optimal probabilistic RNA-seq quantification. *Nature biotechnology*, **34**, 525.
- Bustillo-Zabalbeitia, I., Montessuit, S., Raemy, E., Basanez, G., Terrones, O. and Martinou, J.C.** (2014) Specific interaction with cardiolipin triggers functional activation of Dynamin-Related Protein 1. *PLoS One*, **9**, e102738.
- Camougrand, N., Pelissier, P., Velours, G. and Guerin, M.** (1995) NCA2, a second nuclear gene required for the control of mitochondrial synthesis of subunits 6 and 8 of ATP synthase in *Saccharomyces cerevisiae*. *J Mol Biol*, **247**, 588-596.

- Capella-Gutierrez, S., Silla-Martinez, J.M. and Gabaldon, T.** (2009) trimAl: a tool for automated alignment trimming in large-scale phylogenetic analyses. *Bioinformatics*, **25**, 1972-1973.
- Carrie, C., Giraud, E. and Whelan, J.** (2009) Protein transport in organelles: Dual targeting of proteins to mitochondria and chloroplasts. *FEBS J*, **276**, 1187-1195.
- Cheng, C.Y., Krishnakumar, V., Chan, A.P., Thibaud-Nissen, F., Schobel, S. and Town, C.D.** (2017) Araport11: a complete reannotation of the Arabidopsis thaliana reference genome. *Plant J*, **89**, 789-804.
- Cline, K., Andrews, J., Mersey, B., Newcomb, E.H. and Keegstra, K.** (1981) Separation and characterization of inner and outer envelope membranes of pea chloroplasts. *Proceedings of the National Academy of Sciences*, **78**, 3595-3599.
- Cox, J., Neuhauser, N., Michalski, A., Scheltema, R.A., Olsen, J.V. and Mann, M.** (2011) Andromeda: a peptide search engine integrated into the MaxQuant environment. *J Proteome Res*, **10**, 1794-1805.
- Cruz-Ramirez, A., Oropeza-Aburto, A., Razo-Hernandez, F., Ramirez-Chavez, E. and Herrera-Estrella, L.** (2006) Phospholipase DZ2 plays an important role in extraplastidic galactolipid biosynthesis and phosphate recycling in Arabidopsis roots. *Proc Natl Acad Sci U S A*, **103**, 6765-6770.
- Duchene, A.M., Giritch, A., Hoffmann, B., Cognat, V., Lancelin, D., Peeters, N.M., Zaepfel, M., Marechal-Drouard, L. and Small, I.D.** (2005) Dual targeting is the rule for organellar aminoacyl-tRNA synthetases in Arabidopsis thaliana. *Proc Natl Acad Sci U S A*, **102**, 16484-16489.
- Elo, A., Lyznik, A., Gonzalez, D.O., Kachman, S.D. and Mackenzie, S.A.** (2003) Nuclear genes that encode mitochondrial proteins for DNA and RNA metabolism are clustered in the Arabidopsis genome. *Plant Cell*, **15**, 1619-1631.
- Eom, S.H., Baek, S.A., Kim, J.K. and Hyun, T.K.** (2018) Transcriptome Analysis in Chinese Cabbage (*Brassica rapa* ssp. *pekinensis*) Provides the Role of Glucosinolate Metabolism in Response to Drought Stress. *Molecules*, **23**.
- Eubel, H., Braun, H.-P. and Millar, A.** (2005) Blue-native PAGE in plants: a tool in analysis of protein-protein interactions. *Plant methods*, **1**, 11.
- Förster, B., Osmond, C.B. and Pogson, B.J.** (2005) Improved survival of very high light and oxidative stress is conferred by spontaneous gain-of-function mutations in *Chlamydomonas*. *Biochimica et Biophysica Acta (BBA)-Bioenergetics*, **1709**, 45-57.
- Friedman, J.R., Lackner, L.L., West, M., DiBenedetto, J.R., Nunnari, J. and Voeltz, G.K.** (2011) ER tubules mark sites of mitochondrial division. *Science*, **334**, 358-362.

- Giraud, E., Ho, L.H., Clifton, R., Carroll, A., Estavillo, G., Tan, Y.F., Howell, K.A., Ivanova, A., Pogson, B.J., Millar, A.H. and Whelan, J.** (2008) The absence of ALTERNATIVE OXIDASE1a in Arabidopsis results in acute sensitivity to combined light and drought stress. *Plant Physiol*, **147**, 595-610.
- Glaser, E., Eriksson, A. and Sjoling, S.** (1994) Bifunctional role of the bc1 complex in plants. Mitochondrial bc1 complex catalyses both electron transport and protein processing. *FEBS Lett*, **346**, 83-87.
- Härtel, H., Dörmann, P. and Benning, C.** (2000) DGD1-independent biosynthesis of extraplasmidic galactolipids after phosphate deprivation in Arabidopsis. *Proc Natl Acad Sci U S A*, **97**, 10649-10654.
- Ho, L.H., Giraud, E., Uggalla, V., Lister, R., Clifton, R., Glen, A., Thirkettle-Watts, D., Van Aken, O. and Whelan, J.** (2008) Identification of regulatory pathways controlling gene expression of stress-responsive mitochondrial proteins in Arabidopsis. *Plant Physiol*, **147**, 1858-1873.
- Jacoby, R.P., Millar, A.H. and Taylor, N.L.** (2015) Assessment of respiration in isolated plant mitochondria using Clark-type electrodes. *Methods Mol Biol*, **1305**, 165-185.
- Jouhet, J., Marechal, E., Baldan, B., Bligny, R., Joyard, J. and Block, M.A.** (2004) Phosphate deprivation induces transfer of DGDG galactolipid from chloroplast to mitochondria. *J Cell Biol*, **167**, 863-874.
- Kelly, A.A. and Dormann, P.** (2002) DGD2, an arabidopsis gene encoding a UDP-galactose-dependent digalactosyldiacylglycerol synthase is expressed during growth under phosphate-limiting conditions. *J Biol Chem*, **277**, 1166-1173.
- Klecker, T., Wemmer, M., Haag, M., Weig, A., Bockler, S., Langer, T., Nunnari, J. and Westermann, B.** (2015) Interaction of MDM33 with mitochondrial inner membrane homeostasis pathways in yeast. *Sci Rep*, **5**, 18344.
- Kornmann, B., Currie, E., Collins, S.R., Schuldiner, M., Nunnari, J., Weissman, J.S. and Walter, P.** (2009) An ER-mitochondria tethering complex revealed by a synthetic biology screen. *Science*, **325**, 477-481.
- Kozjak-Pavlovic, V.** (2017) The MICOS complex of human mitochondria. *Cell Tissue Res*, **367**, 83-93.
- Kutik, S., Rissler, M., Guan, X.L., Guiard, B., Shui, G., Gebert, N., Heacock, P.N., Rehling, P., Dowhan, W., Wenk, M.R., Pfanner, N. and Wiedemann, N.** (2008) The translocator maintenance protein Tam41 is required for mitochondrial cardiolipin biosynthesis. *J Cell Biol*, **183**, 1213-1221.
- Larkin, R.M., Alonso, J.M., Ecker, J.R. and Chory, J.** (2003) GUN4, a regulator of chlorophyll synthesis and intracellular signaling. *Science*, **299**, 902-906.

- Li, L., Kubiszewski-Jakubiak, S., Radomiljac, J., Wang, Y., Law, S.R., Keech, O., Narsai, R., Berkowitz, O., Duncan, O., Murcha, M.W. and Whelan, J.** (2016) Characterization of a novel beta-barrel protein (AtOM47) from the mitochondrial outer membrane of *Arabidopsis thaliana*. *J Exp Bot*, **67**, 6061-6075.
- Li, W., Cowley, A., Uludag, M., Gur, T., McWilliam, H., Squizzato, S., Park, Y.M., Buso, N. and Lopez, R.** (2015) The EMBL-EBI bioinformatics web and programmatic tools framework. *Nucleic Acids Res*, **43**, W580-584.
- Li, X., Han, L., Zhao, Y., You, Z., Dong, H. and Zhang, C.** (2014) Hpa1 harpin needs nitroxyl terminus to promote vegetative growth and leaf photosynthesis in *Arabidopsis*. *Journal of biosciences*, **39**, 127-137.
- Lister, R., Carrie, C., Duncan, O., Ho, L.H., Howell, K.A., Murcha, M.W. and Whelan, J.** (2007) Functional definition of outer membrane proteins involved in preprotein import into mitochondria. *Plant Cell*, **19**, 3739-3759.
- Liu, Y., Ye, N., Liu, R., Chen, M. and Zhang, J.** (2010) H₂O₂ mediates the regulation of ABA catabolism and GA biosynthesis in *Arabidopsis* seed dormancy and germination. *J Exp Bot*, **61**, 2979-2990.
- Mehdipour, A.R. and Hummer, G.** (2016) Cardiolipin puts the seal on ATP synthase. *Proc Natl Acad Sci U S A*, **113**, 8568-8570.
- Mesmin, B.** (2016) Mitochondrial lipid transport and biosynthesis: A complex balance. *J Cell Biol*, **214**, 9-11.
- Michaud, M., Gros, V., Tardif, M., Brugière, S., Ferro, M., Prinz, W.A., Toulmay, A., Mathur, J., Wozny, M. and Falconet, D.** (2016) AtMic60 is involved in plant mitochondria lipid trafficking and is part of a large complex. *Current Biology*, **26**, 627-639.
- Michaud, M., Prinz, W.A. and Jouhet, J.** (2017) Glycerolipid synthesis and lipid trafficking in plant mitochondria. *FEBS J*, **284**, 376-390.
- Moellering, E.R. and Benning, C.** (2010) Phosphate regulation of lipid biosynthesis in *Arabidopsis* is independent of the mitochondrial outer membrane DGS1 complex. *Plant Physiol*, **152**, 1951-1959.
- Moellering, E.R. and Benning, C.** (2011) Galactoglycerolipid metabolism under stress: a time for remodeling. *Trends Plant Sci*, **16**, 98-107.
- Munoz-Gomez, S.A., Slamovits, C.H., Dacks, J.B., Baier, K.A., Spencer, K.D. and Wideman, J.G.** (2015a) Ancient homology of the mitochondrial contact site and cristae organizing system points to an endosymbiotic origin of mitochondrial cristae. *Curr Biol*, **25**, 1489-1495.

- Munoz-Gomez, S.A., Slamovits, C.H., Dacks, J.B. and Wideman, J.G.** (2015b) The evolution of MICOS: Ancestral and derived functions and interactions. *Commun Integr Biol*, **8**, e1094593.
- Murcha, M.W., Kmiec, B., Kubiszewski-Jakubiak, S., Teixeira, P.F., Glaser, E. and Whelan, J.** (2014) Protein import into plant mitochondria: signals, machinery, processing, and regulation. *J Exp Bot*, **65**, 6301-6335.
- Ng, S., De Clercq, I., Van Aken, O., Law, S.R., Ivanova, A., Willems, P., Giraud, E., Van Breusegem, F. and Whelan, J.** (2014) Anterograde and retrograde regulation of nuclear genes encoding mitochondrial proteins during growth, development, and stress. *Mol Plant*, **7**, 1075-1093.
- Nguyen, L.T., Schmidt, H.A., von Haeseler, A. and Minh, B.Q.** (2015) IQ-TREE: a fast and effective stochastic algorithm for estimating maximum-likelihood phylogenies. *Mol Biol Evol*, **32**, 268-274.
- Pan, R., Jones, A.D. and Hu, J.** (2014) Cardiolipin-mediated mitochondrial dynamics and stress response in Arabidopsis. *Plant Cell*, **26**, 391-409.
- Pelissier, P., Camougrand, N., Velours, G. and Guerin, M.** (1995) NCA3, a nuclear gene involved in the mitochondrial expression of subunits 6 and 8 of the Fo-F1 ATP synthase of *S. cerevisiae*. *Curr Genet*, **27**, 409-416.
- Rabl, R., Soubannier, V., Scholz, R., Vogel, F., Mendl, N., Vasiljev-Neumeyer, A., Korner, C., Jagasia, R., Keil, T., Baumeister, W., Cyrklaff, M., Neupert, W. and Reichert, A.S.** (2009) Formation of cristae and crista junctions in mitochondria depends on antagonism between Fcj1 and Su e/g. *J Cell Biol*, **185**, 1047-1063.
- Rhoads, D.M. and McIntosh, L.** (1992) Salicylic Acid Regulation of Respiration in Higher Plants: Alternative Oxidase Expression. *Plant Cell*, **4**, 1131-1139.
- Robinson, M.D., McCarthy, D.J. and Smyth, G.K.** (2010) edgeR: a Bioconductor package for differential expression analysis of digital gene expression data. *Bioinformatics*, **26**, 139-140.
- Rossel, J.B., Walter, P.B., Hendrickson, L., Chow, W.S., Poole, A., Mullineaux, P.M. and Pogson, B.J.** (2006) A mutation affecting ASCORBATE PEROXIDASE 2 gene expression reveals a link between responses to high light and drought tolerance. *Plant, Cell & Environment*, **29**, 269-281.
- Schneider, A.** (2011) Mitochondrial tRNA import and its consequences for mitochondrial translation. *Annu Rev Biochem*, **80**, 1033-1053.
- Schorr, S. and van der Laan, M.** (2018) Integrative functions of the mitochondrial contact site and cristae organizing system. *Semin Cell Dev Biol*, **76**, 191-200.

- Schuler, M.H., Di Bartolomeo, F., Martensson, C.U., Daum, G. and Becker, T.** (2016) Phosphatidylcholine Affects Inner Membrane Protein Translocases of Mitochondria. *J Biol Chem*, **291**, 18718-18729.
- Sedigheh, H.G., Mortazavian, M., Norouzi, D., Atyabi, M., Akbarzadeh, A., Hasanpoor, K. and Ghorbani, M.** (2011) Oxidative stress and leaf senescence. *BMC research notes*, **4**, 477.
- Thaler, J.S., Humphrey, P.T. and Whiteman, N.K.** (2012) Evolution of jasmonate and salicylate signal crosstalk. *Trends Plant Sci*, **17**, 260-270.
- van der Laan, M., Bohnert, M., Wiedemann, N. and Pfanner, N.** (2012) Role of MINOS in mitochondrial membrane architecture and biogenesis. *Trends Cell Biol*, **22**, 185-192.
- van der Laan, M., Horvath, S.E. and Pfanner, N.** (2016) Mitochondrial contact site and cristae organizing system. *Curr Opin Cell Biol*, **41**, 33-42.
- Wang, Y., Carrie, C., Giraud, E., Elhafez, D., Narsai, R., Duncan, O., Whelan, J. and Murcha, M.W.** (2012) Dual location of the mitochondrial preprotein transporters B14. 7 and Tim23-2 in complex I and the TIM17: 23 complex in Arabidopsis links mitochondrial activity and biogenesis. *The Plant Cell*, **24**, 2675-2695.
- Wang, Z. and Benning, C.** (2011) Arabidopsis thaliana polar glycerolipid profiling by thin layer chromatography (TLC) coupled with gas-liquid chromatography (GLC). *Journal of visualized experiments: JoVE*.
- Wideman, J.G. and Munoz-Gomez, S.A.** (2016) The evolution of ERMIONE in mitochondrial biogenesis and lipid homeostasis: An evolutionary view from comparative cell biology. *Biochim Biophys Acta*, **1861**, 900-912.
- Wiedemann, N. and Pfanner, N.** (2017) Mitochondrial Machineries for Protein Import and Assembly. *Annu Rev Biochem*, **86**, 685-714.
- Wu, F.-H., Shen, S.-C., Lee, L.-Y., Lee, S.-H., Chan, M.-T. and Lin, C.-S.** (2009) Tape-Arabidopsis Sandwich-a simpler Arabidopsis protoplast isolation method. *Plant methods*, **5**, 16.
- Xu, C., Fan, J., Riekhof, W., Froehlich, J.E. and Benning, C.** (2003) A permease-like protein involved in ER to thylakoid lipid transfer in Arabidopsis. *The EMBO Journal*, **22**, 2370-2379.
- Xu, C., Moellering, E.R., Fan, J. and Benning, C.** (2008) Mutation of a mitochondrial outer membrane protein affects chloroplast lipid biosynthesis. *Plant J*, **54**, 163-175.

- Yamaoka, S. and Leaver, C.J.** (2008) EMB2473/MIRO1, an Arabidopsis Miro GTPase, is required for embryogenesis and influences mitochondrial morphology in pollen. *Plant Cell*, **20**, 589-601.
- Zahedi, R.P., Sickmann, A., Boehm, A.M., Winkler, C., Zufall, N., Schonfisch, B., Guiard, B., Pfanner, N. and Meisinger, C.** (2006) Proteomic analysis of the yeast mitochondrial outer membrane reveals accumulation of a subclass of preproteins. *Mol Biol Cell*, **17**, 1436-1450.
- Zhang, X., Ivanova, A., Vandepoele, K., Radomiljac, J., Van de Velde, J., Berkowitz, O., Willems, P., Xu, Y., Ng, S., Van Aken, O., Duncan, O., Zhang, B., Storme, V., Chan, K.X., Vaneechoutte, D., Pogson, B.J., Van Breusegem, F., Whelan, J. and De Clercq, I.** (2017) The Transcription Factor MYB29 Is a Regulator of ALTERNATIVE OXIDASE1a. *Plant Physiol*, **173**, 1824-1843.

CHAPTER 6

Future Perspectives

Introduction

Glycerolipid biosynthesis is a dynamic and essential process in plants, the regulation of which is yet to be fully understood. Cellular metabolism demands the maintenance of membranes not only for the chemical composition of the membrane lipid bilayer, but also for membrane biophysical properties like curvature. The thylakoid membranes in the chloroplast, have a unique galactolipid composition, predominately monogalactosyldiacylglycerol (MGDG) and digalactosyldiacylglycerol (DGDG). The highly curved grana stacks of the thylakoids house the photosynthetic machinery. Proteins embedded in and associated with the membrane often depend on the lipid environment to perform their biochemical roles as well as interact with other proteins and substrates. To meet the cellular needs, there must be tight regulation of lipid synthesis and turnover. Some of this regulation occurs at the transcriptional level, where the transcript levels dictate the amount of protein produced for lipid biosynthesis. Transcription itself can be regulated through the action of transcription factors that respond to stimuli from within the cell as well as outside the cell. Some transcription factors, such as WRINKLED1, have already been identified as regulators of basal lipid metabolism. There are also genes that get transcribed due to stress signals, such as those encoding the PLIP lipases. In addition to transcriptional regulation, it seems that there must be post-translational regulation of the lipid biosynthetic enzymes.

Role of Proteolysis in Lipid Homeostasis

The characterization of the lipid phenotype exhibited by knock-out mutants of RBL10, a rhomboid-like protease, introduces the potential for regulated intramembrane proteolysis

(RIP) as a means to modulate lipid metabolism in Arabidopsis. In mammals, RIP has been shown to be involved in lipid homeostasis through processing of the amyloid precursor protein (APP), which is implicated in Alzheimer's Disease (AD). Cleavage of APP can be controlled by levels of cholesterol and other lipids in the cell, at the same time, lipid homeostasis also seems to be controlled by the APP cleavage products (Grimm *et al.*, 2012a, Grimm *et al.*, 2012b). Another example of RIP controlled lipid metabolism comes from cholesterol feedback regulation, where the sterol regulatory element binding protein (SREBP) is dually processed by site-1-protease and site-2-protease respectively, freeing SREBP from the membrane of the ER under low cholesterol levels (Brown and Goldstein, 2009). As described in Chapter 3, it seems that the presence of RBL10 enables the flipping of phosphatidic acid (PA) across the inner envelope membrane, thereby allowing the biosynthesis of galactolipids such as MGDG and DGDG from chloroplast-derived precursors. The identity of the protein responsible for the translocation of PA is not yet known and adds another facet to the multistep lipid biosynthetic pathway in plastids. Searching for this protein presents a big challenge as it may or may not be the direct protein substrate for RBL10. Rhomboids have been shown to activate signaling ligands (Lee *et al.*, 2001, Urban *et al.*, 2002), raising the possibility that additional protein participants coordinate the expression, localization, or activation of this PA transporter. One traditional approach to identifying participants is to perform a suppressor screen in the *rb10* mutant background. However, since RBL10 seems to have an activating role in a sense it is unlikely that removing downstream participants will rescue the lipid phenotype. However, in the case that the regulatory mechanism is transcriptional repression of the gene encoding the PA transporter, a suppressor screen could reveal

such a participant through a rescued lipid phenotype. Screening for recovered MGDG acyl composition would require the use of gas chromatography (GC) lipid analysis (Wang and Benning, 2011), but since the phenotype of *rb110-1* can be seen in the total acyl composition this would remove the need for the use of thin layer chromatography and enable direct analysis of leaf tissue, expediting screening. Aside from searching for loss-of-function (LOF) mutants, it's possible to discover a gain-of-function (GOF) mutant as there is an increasing number of examples of GOF in the literature (Li *et al.*, 2019). In the event that LOF or GOF mutants cannot be isolated, analyzing changes in transcript abundance between WT and *rb110* mutant would be an approach which could reveal downstream signaling activated by RBL10 proteolytic activity.

RBL10 and its Protein Interactome

Chapter 4 describes the discovery of RBL10's oligomeric state and raises the question of how RBL10 performs its function in the context of a large molecular weight complex. Rhomboids have been implicated in enabling the oligomerization of complexes (Stevenson *et al.*, 2007) and few have been reported to interact with other non-substrate proteins (Jeyaraju *et al.*, 2006, Hwang *et al.*, 2016). However, little is known about rhomboids participating in stable complexes. Identifying the residents of the RBL10 complex would be an important first step in understanding the role of this association. Through co-immunoprecipitation (Co-IP) experiments described in Chapter 4, a list of potential complex denizens has been provided. At first glance, the information currently published about the identified candidates provides little explanation on how they might enable RBL10 to regulate PA trafficking. However, some of the candidates likely are

involved in photosynthesis and photosystem repair mechanisms. Another set of proteins is involved in carbohydrate metabolism and ATP synthesis. In addition, some proteins seem to be either involved in protein translation or act as chaperones. Taken together these general functions hint at a potential interconnectivity between them. It has been well established that carbohydrate metabolism and lipid biosynthesis are closely linked and altering the balance of one can influence the other (Zale *et al.*, 2016, Zhai *et al.*, 2017) though the mechanism is not exactly understood. Photosynthetically derived sugars provide the carbon for lipid biosynthesis, and ultimately there must be some feedback regulation mechanism tuning photosynthetic flux. How all these proteins would come to interact with RBL10 or each other is not clear, but it is possible that RBL10 could be mediating the signal from carbohydrate synthesis and altering the balance of lipid biosynthesis through the plastid and ER pathways.

The immunoprecipitated proteins could also be substrates for RBL10 cleavage since there are a few with transmembrane domains. It is likely that discovering the direct substrate for an active protease will not be trivial, and a more stringent method, such as biotin proximity labeling BiOLD (Roux *et al.*, 2013), for detecting protein interactors could be used. Detecting protein substrates that are released from the chloroplast membrane and travel to the nucleus would not be detected with the approach used in Chapter 4, however the BiOLD approach in whole leaf tissues should capture any proteins that came into close proximity to RBL10. Any protein candidate that is identified by Co-IP or BiOLD labeling, should be further corroborated through another method such as split-ubiquitin yeast two-hybrid (Obrdlik *et al.*, 2004).

Role for Autocatalysis of RBL10

Another discovery described in Chapter 4 is that RBL10 exhibits proteolytic activity towards its own carboxy-terminal domain (CTD). A similar finding has been previously reported for the human Presenilin-associated rhomboid-like (PARL) protein, which cleaves its own amino-terminal domain (NTD) based on phosphorylation status at the NTD (Jeyaraju *et al.*, 2006). This mechanism is a form of regulation of the proteolytic activity of PARL, as the NTD processed form PACT is less active towards its substrate Pink1 (Meissner *et al.*, 2015, Shi and McQuibban, 2017). The self-processing of RBL10 is evidence for its proteolytic activity and also might explain why proteolytic assays have been challenging with purified RBL10 protein. It seems that within the plastid, the intact protein can be detected as well as the cleaved form, however, when RBL10 is heterologously produced in *E. coli* it immediately undergoes self-processing. The mechanism by which self-processing is triggered or blocked could be due to association with protein interactors in the plastid or post-translational modification. We know that RBL10 is part of a large molecular weight complex; so perhaps the association/dissociation with the complex components coordinates autocatalysis. If the amino acid sequence of RBL10 is analyzed using NetPhos3.1 prediction software (<http://www.cbs.dtu.dk/services/NetPhos>), 5 phosphorylation sites are predicted at the NTD (serine 49, 81, 88, 114, 119) and 2 closer to the CTD (serine 236, threonine 316) with a confidence above 0.9 (1.0 being the highest likelihood). Though these sites are predicted, it would be instructive to experimentally confirm the phosphorylation status of RBL10 by labeling the protein using ³²P-adenosine triphosphate (ATP). Understanding

the mechanism which controls the autocatalytic activity of RBL10 would further our understanding of how it can positively affect PA trafficking at the molecular level.

In the case of PARL's self-processing, it was also discovered that the NTD fragment was not degraded after cleavage, but exported from the mitochondria to the nucleus (Sik *et al.*, 2004). In this manner, PARL is able to sense the ATP status of the mitochondrion through phosphorylation and upon reduced ATP levels, send a signal to the nucleus. The discovery that the CTD fragment of RBL10 is present in isolated chloroplasts in addition to the full-length protein begged the question of whether this fragment remains in the chloroplast or is exported outside the plastid. If the fragment remains inside the chloroplast, what is its role? Perhaps, it is simply degraded. It is possible that the autocatalytic cleavage of RBL10 provides a potential mechanism for retrograde signaling from the chloroplast to the nucleus. Identifying the exact cleavage site and amino acid sequence of the CTD fragment would allow a better understanding of its potential role. For example, in the *rb110* mutant, the entire protein is gone and can be complemented by the WT gene. What if only the CTD fragment would be sufficient to complement the mutant lipid phenotype? Conversely, would the protein segment without the cleaved fragment sequence have a different phenotype when used to complement the mutant than just the CTD? These experiments could tease apart the role of each fragment. If the CTD travels to the nucleus, we could in essence capture the signal's downstream effects, observe any changes in lipid metabolism as well as overall phenotypes. Additionally, understanding the role of proteolysis in RBL10's molecular mechanism could in part explain why there is embryo lethality when the catalytic residues of RBL10 are mutated to alanine and the *rb110* mutant is complemented with those gene

variants. The ability of RBL10 to self-cleave, when it is present in the complex, may be an important step to the function of the chloroplast lipid biosynthetic pathway.

On the whole, RBL10 appears to be a multifaceted protein with the potential to relay signals from the chloroplast, affecting changes in lipid metabolism. Understanding the mechanism by which RBL10 acts, may identify a sensing mechanism in the chloroplast, add to our knowledge on retrograde signaling from the plastid, and ultimately further our efforts of understanding lipid regulation in plants.

Responses to Stress and Lipid Remodeling

Plants utilize phosphate for synthesizing numerous biomolecules and biochemical processes. In most organisms, phospholipids dominate the compositional makeup of membranes. Plants however, due to the abundance of thylakoid membranes in green tissues, reduce their phosphate dependence by using galactolipids for their photosynthetic membranes. As sessile organisms, under low phosphate conditions, plants must re-prioritize the use of phosphate for generating membranes and save them for nucleic acids and other essential macromolecules. Under phosphate starvation, plastid galactolipids are exported to extraplastidic membranes to replace phospholipids (Härtel *et al.*, 2000). Galactolipids come into play again during freezing stress response, when the plastid outer envelope protein SENSITIVE TO FREEZING2 (SFR2) protects the chloroplast from dehydration by transferring additional galactose units onto MGDG, creating oligogalactolipids (Moellering *et al.*, 2010, Moellering and Benning, 2011). In Chapter 5 I discuss how the mitochondrial protein DGS1 influences lipid composition not only in the mitochondria, but also the chloroplast. Initially discovered as a suppressor of

the *dgd1* mutation (Xu *et al.*, 2008, Moellering and Benning, 2010), DGS1 seems to be a part of the mitochondrial contact site and cristae organizing system (MICOS) complex. While the knock-out mutants of WT DGS1 protein do not seem to change lipid metabolism, the gain-of-function point mutation in *dgs1-1* seems to initiate changes in lipid transport between the chloroplast, ER, and mitochondria. Plants expressing the *dgs1-1* mutant gene also are more drought tolerant compared to WT plants. It seems that the DGS1 protein could be involved in the response to stress in the mitochondrion, and the MICOS complex is important in proper lipid transport between mitochondria and other organelles. How does a mutant DGS1 protein affect lipid transport? There is the possibility that retrograde signaling from the mitochondrion is the mechanism by which the *dgs1-1* overexpressing plants mount a stress response. Additional analysis of the single amino acid change from aspartic acid to asparagine at position 457 near the predicted transmembrane region of DGS1 could give insight on how the change could affect the way DGS1 interacts with components of the MICOS complex.

Concluding Remarks

Overall, plant cells sense and respond to stress through many mechanisms. Some stresses are detected through organelles like the chloroplast and the mitochondrion. Preliminary evidence for retrograde signals being sent from these compartments, as suggested by findings in the chapters of this dissertation, provides an opportunity to further study the role of the investigated proteins on novel mechanisms for sensing the metabolic status or stress condition of the plant.

REFERENCES

REFERENCES

- Brown, M.S. and Goldstein, J.L.** (2009) Cholesterol feedback: from Schoenheimer's bottle to Scap's MELADL. *J Lipid Res*, **50 Suppl**, S15-27.
- Grimm, M.O., Rothhaar, T.L., Grosgen, S., Burg, V.K., Hundsdorfer, B., Hauptenthal, V.J., Friess, P., Kins, S., Grimm, H.S. and Hartmann, T.** (2012a) Trans fatty acids enhance amyloidogenic processing of the Alzheimer amyloid precursor protein (APP). *J Nutr Biochem*, **23**, 1214-1223.
- Grimm, M.O., Rothhaar, T.L. and Hartmann, T.** (2012b) The role of APP proteolytic processing in lipid metabolism. *Exp Brain Res*, **217**, 365-375.
- Härtel, H., Dörmann, P. and Benning, C.** (2000) DGD1-independent biosynthesis of extraplastidic galactolipids after phosphate deprivation in Arabidopsis. *Proc Natl Acad Sci U S A*, **97**, 10649-10654.
- Hwang, J., Ribbens, D., Raychaudhuri, S., Cairns, L., Gu, H., Frost, A., Urban, S. and Espenshade, P.J.** (2016) A Golgi rhomboid protease Rbd2 recruits Cdc48 to cleave yeast SREBP. *EMBO J*, **35**, 2332-2349.
- Jeyaraju, D.V., Xu, L., Letellier, M.C., Bandaru, S., Zunino, R., Berg, E.A., McBride, H.M. and Pellegrini, L.** (2006) Phosphorylation and cleavage of presenilin-associated rhomboid-like protein (PARL) promotes changes in mitochondrial morphology. *Proc Natl Acad Sci U S A*, **103**, 18562-18567.
- Lee, J.R., Urban, S., Garvey, C.F. and Freeman, M.** (2001) Regulated intracellular ligand transport and proteolysis control EGF signal activation in Drosophila. *Cell*, **107**, 161-171.
- Li, Y., Zhang, Y., Li, X., Yi, S. and Xu, J.** (2019) Gain-of-Function Mutations: An Emerging Advantage for Cancer Biology. *Trends Biochem Sci*, **44**, 659-674.
- Meissner, C., Lorenz, H., Hehn, B. and Lemberg, M.K.** (2015) Intramembrane protease PARL defines a negative regulator of PINK1-and PARK2/Parkin-dependent mitophagy. *Autophagy*, **11**, 1484-1498.
- Moellering, E.R. and Benning, C.** (2010) Phosphate regulation of lipid biosynthesis in Arabidopsis is independent of the mitochondrial outer membrane DGS1 complex. *Plant Physiol*, **152**, 1951-1959.
- Moellering, E.R. and Benning, C.** (2011) Galactoglycerolipid metabolism under stress: a time for remodeling. *Trends Plant Sci*, **16**, 98-107.

- Moellering, E.R., Muthan, B. and Benning, C.** (2010) Freezing Tolerance in Plants Requires Lipid Remodeling at the Outer Chloroplast Membrane. *Science*, **330**, 226-228.
- Obrdlik, P., El-Bakkoury, M., Hamacher, T., Cappellaro, C., Vilarino, C., Fleischer, C., Ellerbrok, H., Kamuzinzi, R., Ledent, V., Blaudez, D., Sanders, D., Revuelta, J.L., Boles, E., Andre, B. and Frommer, W.B.** (2004) K⁺ channel interactions detected by a genetic system optimized for systematic studies of membrane protein interactions. *Proc Natl Acad Sci U S A*, **101**, 12242-12247.
- Roux, K.J., Kim, D.I. and Burke, B.** (2013) Biold: a screen for protein-protein interactions. *Curr Protoc Protein Sci*, **74**, Unit 19 23.
- Shi, G. and McQuibban, G.A.** (2017) The Mitochondrial Rhomboid Protease PARL Is Regulated by PDK2 to Integrate Mitochondrial Quality Control and Metabolism. *Cell Rep*, **18**, 1458-1472.
- Sik, A., Passer, B.J., Koonin, E.V. and Pellegrini, L.** (2004) Self-regulated cleavage of the mitochondrial intramembrane-cleaving protease PARL yields Pbeta, a nuclear-targeted peptide. *J Biol Chem*, **279**, 15323-15329.
- Stevenson, L.G., Strisovsky, K., Clemmer, K.M., Bhatt, S., Freeman, M. and Rafter, P.N.** (2007) Rhomboid protease AarA mediates quorum-sensing in *Providencia stuartii* by activating TatA of the twin-arginine translocase. *Proc Natl Acad Sci U S A*, **104**, 1003-1008.
- Urban, S., Lee, J.R. and Freeman, M.** (2002) A family of Rhomboid intramembrane proteases activates all *Drosophila* membrane-tethered EGF ligands. *EMBO J*, **21**, 4277-4286.
- Wang, Z. and Benning, C.** (2011) Arabidopsis thaliana polar glycerolipid profiling by thin layer chromatography (TLC) coupled with gas-liquid chromatography (GLC). *J Vis Exp*, 1-6.
- Xu, C., Moellering, E.R., Fan, J. and Benning, C.** (2008) Mutation of a mitochondrial outer membrane protein affects chloroplast lipid biosynthesis. *Plant J*, **54**, 163-175.
- Zale, J., Jung, J.H., Kim, J.Y., Pathak, B., Karan, R., Liu, H., Chen, X., Wu, H., Candreva, J., Zhai, Z., Shanklin, J. and Altpeter, F.** (2016) Metabolic engineering of sugarcane to accumulate energy-dense triacylglycerols in vegetative biomass. *Plant Biotechnol J*, **14**, 661-669.
- Zhai, Z.Y., Liu, H., Xu, C.C. and Shanklin, J.** (2017) Sugar Potentiation of Fatty Acid and Triacylglycerol Accumulation. *Plant Physiol*, **175**, 696-707.